

Theoretical Study on Reaction Pathway and Ligand Design for Nitrogen Fixation Catalyzed by Molybdenum Complexes

江木, 晃人

<https://hdl.handle.net/2324/6787560>

出版情報 : Kyushu University, 2022, 博士 (工学) , 課程博士
バージョン :
権利関係 :



**Theoretical Study on Reaction Pathway and
Ligand Design for Nitrogen Fixation
Catalyzed by Molybdenum Complexes**

Akihito Egi

Department of Chemistry and Biochemistry

Graduate School of Engineering

Kyushu University

2022

Table of Contents

Chapter 1	General Introduction	5
1.1.	About Nitrogen Fixation	5
1.2.	Metal–N ₂ Complexes	7
1.3.	Nitrogen Fixation Catalyzed by Metal Complexes	9
1.4.	Survey of This Thesis	12
	References	14
Chapter 2	Nitrogen Fixation Catalyzed by Dimolybdenum Complexes Bearing PCP- and PNP-Type Pincer Ligands	19
2.1	Introduction	19
2.2	Computational Methods	24
2.3	Results and Discussion	27
2.3.1	Proposed catalytic cycle	27
2.3.2	Free energy profiles of catalytic cycle	30
2.3.3	Relationship between electronic structure and reactivity for protonation of dimolybdenum–N ₂ complexes	34
2.4	Conclusions	40
	References	42
	Supporting Information	49
Chapter 3	Relationship between Electronic Structure and Nitrogen Fixation Reaction Pathway of Dimolybdenum Complexes	57
3.1	Introduction	57

3.2	Molecular Orbital of N₂	64
3.3	Orbital Interactions between Terminal N₂ Ligand and Mo Center	65
3.4	Orbital Interactions between Bridging N₂ Ligand and Two Mo Centers	67
3.5	Conversion of Terminal N₂ Ligand of Dimolybdenum Complex to NH₃	69
3.6	Conversion of Bridging N₂ Ligand of Dimolybdenum Complex to NH₃	74
3.7	Conclusions	79
	References	80

Chapter 4 Computational Design of Pincer Ligand for Mo-Catalyzed Nitrogen Fixation

85

4.1	Introduction	85
4.2	Computational Methods	90
4.3	Results and Discussion	92
4.3.1	Effect on LUMO energy of Mo-nitride complex	92
4.3.2	Effect on π -accepting ability of PCP ligand	97
4.3.3	Thermodynamic strength of N-H bond for prediction of the catalytic activity	101
4.3.4	New design of PCP ligand with fused benzene rings	106
4.4	Conclusions	111
	References	112
	Supporting Information	118

Chapter 5 General Conclusions

119

Acknowledgments

123

List of Publications

125

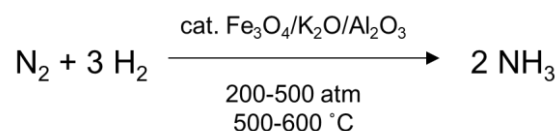
Chapter 1

General Introduction

1.1. About Nitrogen Fixation

Dinitrogen (N_2) is an abundant gas, accounting 78 % of the air. The N_2 is known as a chemically stable molecule because it has an $\text{N}\equiv\text{N}$ triple bond with a high dissociation energy of 911 kJ mol^{-1} ,¹ a large HOMO-LUMO gap, and nonpolarity. “Nitrogen fixation” is reductive conversion of N_2 toward subsequently reactive molecules such as ammonia (NH_3) or hydrazine (N_2H_4). The produced NH_3 is used for a nitrogen source of fertilizers, pharmaceuticals, and so on.² Recently, it has also attracted attention as a hydrogen carrier due to its features such as no carbon dioxide (CO_2) emissions after use.

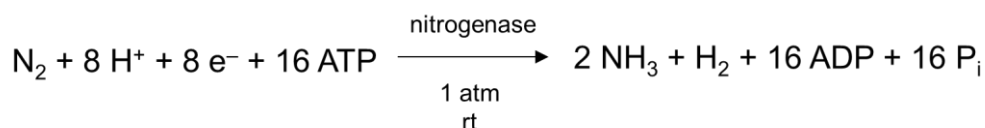
The Haber-Bosch process is an industrial process for nitrogen fixation, in which nitrogen and hydrogen gases (H_2) are converted to ammonia in the presence of solid iron catalysts under harsh reaction conditions such as high pressure (200–500 atm) and high temperature (500–600°C).² Therefore, ammonia production in this process is given as



The Haber-Bosch process was developed in 1913 and has been used for over 100 years. Thus, nitrogen fixation is a useful reaction to convert a chemically inert N_2 into reactive NH_3 , and has attracted much chemical and industrial attention.

In nature, Nitrogen fixation is a part of the nitrogen cycle and have attracted in the field of biology.³ The produced ammonia with the lowest oxidation number of the nitrogen atom -3 is oxidized stepwise to hydroxylamine (NH_2OH ; -1), nitrite (NO_2^- ; $+3$), and nitrate (NO_3^- ; $+5$). The NO_2^- is conversely reduced to nitric oxide (NO ; $+2$) and dinitrogen monoxide (N_2O ; $+1$), which are finally released into the atmosphere as nitrogen gas. Each of these reactions is catalyzed by appropriate enzymes. Active centers

containing transition metals are present in the enzyme proteins, which efficiently interact with small molecules to proceed the redox reactions. The reductive conversion of nitrogen molecule to ammonia is catalyzed by nitrogenases containing a double cubane-type molybdenum-iron-sulfur cluster $\text{MoFe}_7\text{S}_9\text{C}$ (FeMo-cofactor; Figure 1-1) as an active center.^{4,5} Therefore, ammonia production by nitrogenase is given as⁵



Although the details of the catalytic mechanism are not yet known, the eight-electron reduction of nitrogen gas yields two equivalents of ammonia and one equivalent amount of hydrogen.³ The enzymatic nitrogenase-catalyzed reaction is attractive because of mild reaction conditions of room temperature and atmospheric pressure.

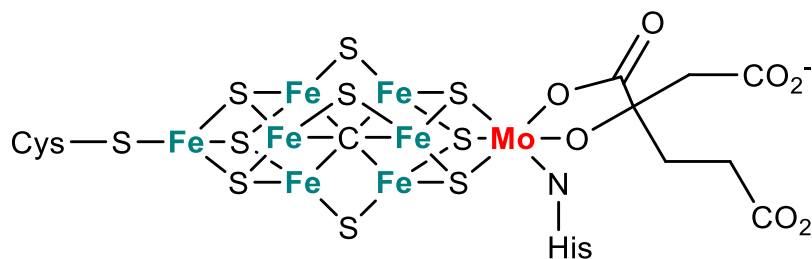


Figure 1-1. Schematic structure of FeMo-cofactor.
(Cys = Cysteine, His = Histidine)

1.2. Metal–N₂ Complexes

Owing to the lack of polarization of N₂ molecule, N₂ is more difficult to coordinate to metal centers than isoelectronic carbon monoxide (CO) molecule. However, in 1965, Allen and Senoff reported the first example of the metal–N₂ complex **1**, [N₂–Ru^{II}(NH₃)₅]²⁺ (Figure 1-2).⁶ In 1967, Yamamoto and coworkers reported a cobalt–N₂ complex **2**, [N₂–Co^IH(PPh₃)₃] (Figure 1-2) with the N₂ ligand derived from nitrogen gas.⁷ Hidai and coworkers discovered a molybdenum–N₂ complex **3**, [(N₂)₂–Mo⁰(dppe)₂] (dppe = bis(diphenylphosphino)ethane) in 1969 (Figure 1-2).⁸ This advance in the chemistry of metal–N₂ complexes derived from atmospheric N₂ provided a trigger for nitrogen fixation reactions using the metal complexes.

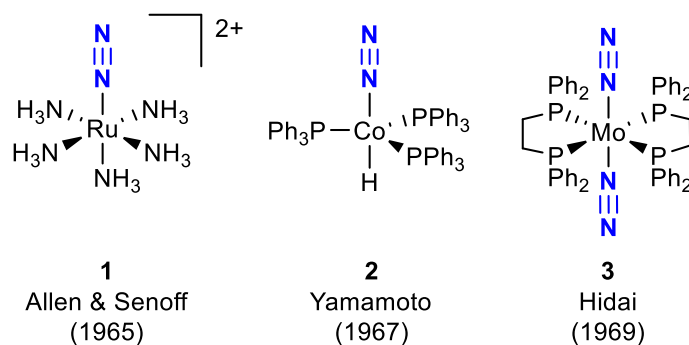


Figure 1-2. Metal–N₂ complexes.

Stoichiometric production of ammonia from some metal–N₂ complexes have been reported. In 1970, Chatt and coworkers demonstrated the first stoichiometric synthesis of ammonia using mononuclear molybdenum–N₂ or tungsten–N₂ complexes, *cis*-[(N₂)₂–M(PMe₂Ph)₄]⁹ **4** and *trans*-[(N₂)₂–M(PMePh₂)₄]¹⁰ **5** (M = Mo or W) (Figure 1-3) in presence of sulfuric acid H₂SO₄ as a strong acid.¹¹ In the case of *cis*-[(N₂)₂–W(PMe₂Ph)₄], up to 90 % of the N₂ ligands was converted to NH₃. Chatt and coworkers proposed an NH₃ conversion mechanism as shown in Scheme 1.1, which is called the “Chatt cycle” (Scheme 1-1), using a mononuclear molybdenum–N₂ complex bearing bidentate phosphines, dppe or depe (= 1,2-bis(diethylphosphino)ethane).¹² In the mechanism, an N₂ ligand is converted to NH₃ through alternating protonations and reductions. The nitrogen fixation using the metal complex is expressed by the following chemical equation: N₂ + 6 H⁺ + 6 e[–] → 2 NH₃, in which H⁺ and e[–] are provided by a

proton source and a reducing reagent, respectively.

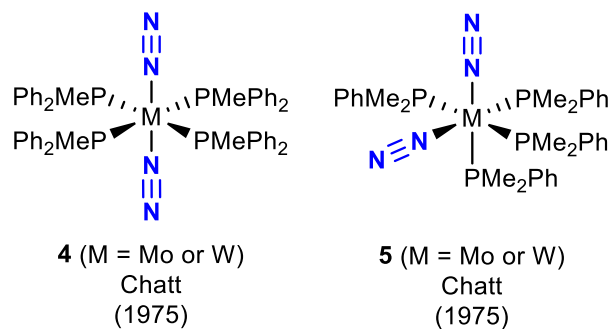
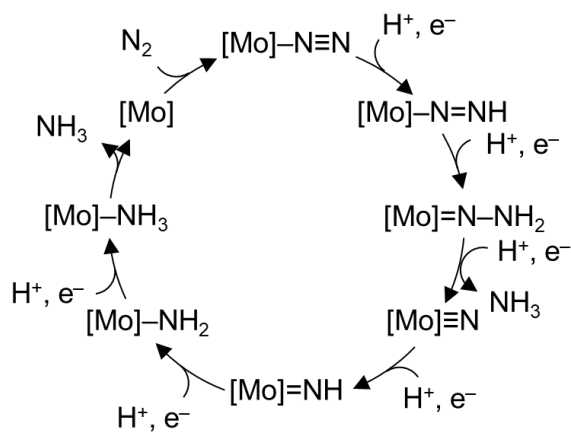


Figure 1-3. Dinitrogen-complexes enable stoichiometric ammonia formation.



Scheme 1-1. Chatt cycle.

1.3. Nitrogen Fixation Catalyzed by Metal Complexes

In 2003, Yandulov and Schrock reported the first example of a molecular metal–N₂ complex as a catalyst for NH₃ conversion from N₂ in the presence of proton and electron sources under ambient conditions.¹³ They synthesized monomolybdenum complex **6** bearing a cage type of tetradentate triamidoamine ligand and demonstrated catalytic NH₃ synthesis up to 8 equiv. per an Mo center (equiv./Mo) in the presence of [LutH]BAr^F₄ as a proton source and CrCp^{*}₂ as a reducing reagent (Lut = 2,6-dimethylpyridine, BAr^F₄ = B(3,5-(CF₃)₂C₆H₃)₄, Cp^{*} = η⁵-C₅(CH₃)₅). Since the report, transition metal complexes that contain titanium,¹⁴ vanadium,¹⁵ iron,¹⁶⁻²³ molybdenum,²⁵⁻³³ ruthenium,³⁴ osmium,³⁴ cobalt,³⁵ and rhenium³⁶ have been reported to catalyze the generation of NH₃. Among these complexes, molybdenum complexes have shown a higher catalytic activity.

In addition to the transition metal center in the complexes, ligands coordinating to the center is of course important for electronic state and spatial controls. Pincer ligands, which are meridional type tridentate ligands, provide good catalytic activity for nitrogen fixation. The pincer ligands with two phosphine side chains are often used for nitrogen-fixing molecular catalysts.^{23-27,29,31,32} For molybdenum complexes, we can see the pyridine-based PNP-type,^{23,26,31,32} the phosphine-based PPP-type,²⁴ and the *N*-heterocyclic carbene (NHC)-based PCP-type pincer ligands^{25,27,29,31} as shown in Figure 1-4.

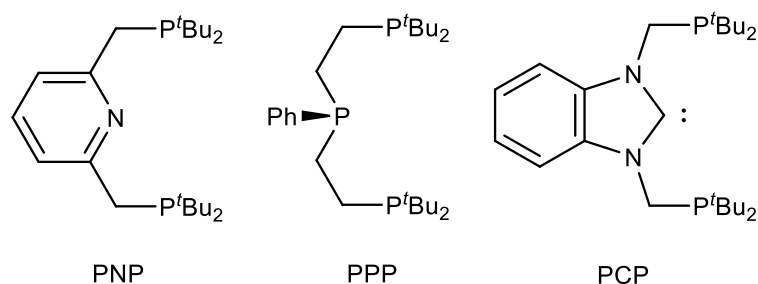


Figure 1-4. Pincer ligands used for molybdenum complexes.

Nishibayashi and coworkers have reported catalytic systems of nitrogen fixation using molybdenum complexes bearing the pincer ligands. In 2011, they synthesized N₂-

bridged dimolybdenum complex bearing PNP ligand [$\{\text{Mo}^0(\text{PNP})(\text{N}_2)_2\}_2(\mu\text{-N}_2)$] **7** (PNP = 2,6-bis(di-*tert*-butylphosphinomethyl)pyridine) as shown in Figure 1-5, and demonstrated the conversion up to 12 equiv/Mo of NH_3 from using **7** as a catalyst in the presence of [LutH]OTf as a proton source and CoCp_2 as a reducing reagent.²³ In addition, they next designed the NHC-based PCP ligand, and prepared N_2 -bridged dimolybdenum complexes bearing the PCP ligand [$\{\text{Mo}^0(\text{PCP})(\text{N}_2)_2\}_2(\mu\text{-N}_2)$] **8** (PCP = 1,3-((di-*tert*-butylphosphino)methyl)benzimidazole-2-ylidene) as shown in Figure 1-5.²⁵ The dimolybdenum complex **8** has higher catalytic activity (up to 100 equiv/Mo of NH_3) than complex **7** under ambient conditions in the presence of [LutH]OTf as a proton source and CrCp^*_2 as a reducing reagent. In later studies, they reported molybdenum-trihalide complex bearing the PNP (**9** as shown in Figure 1-5, up to 415 equiv./Mo of NH_3)²⁶ and PCP (**10** as shown in Figure 1-5, up to 4,350 equiv./Mo of NH_3)^{27,28,36} ligands as molecule catalysts with higher catalytic activity. Formation of a N_2 -bridged dimolybdenum intermediate formation and an N–N bond cleavage of the bridging N_2 ligand of the intermediate in the catalytic cycle using these complexes **9** and **10**.^{26,36} This reaction mechanism is different from the Chatt cycle, so complexes **8** and **9** represent the next generation of nitrogen fixation catalyzed by molecular catalysts. In summary, the Mo–PCP molecular catalysts are promising and remarkable due to their high catalytic activities.

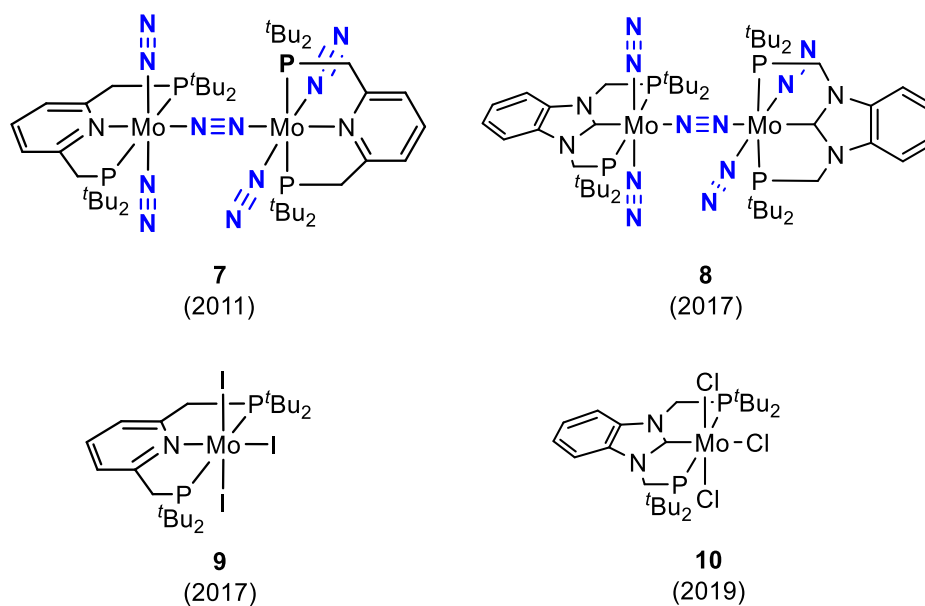


Figure 1-5. Dinitrogen-bridged dimolybdenum–dinitrogen complexes and molybdenum–trihalide complexes bearing PNP or PCP ligand.

1.4. Survey of This Thesis

Compared to the Haber-Bosch process currently in industrial use, the transition metal complex molecular catalysts have an attractive advantage of mild reaction conditions, but its disadvantage is its lower catalytic activity. Therefore, further enhancement of catalytic activity is required to achieve industrial applications in the future. Among the metal complexes, molybdenum complexes with PCP ligands are promising for industrial application because of their high catalytic activity. The author believes that it is effective to design highly active catalysts using the knowledge obtained from the reaction analysis to improve the catalytic activity. Although reaction pathways of catalytic reactions have been studied using DFT calculations for molybdenum complexes bearing a similar PNP ligand, that of the PCP ligand has not been done. The electronic structure of molybdenum complexes bearing the pincer ligands calculated by DFT calculations is useful for understanding the reaction mechanism and predicting the improvement of the catalytic activity.

In Chapter 2, reaction analysis of catalytic reactions using N_2 -bridged dimolybdenum- N_2 complexes bearing PNP (**7**) and PCP (**8**) ligands is presented. The author proposed that the $\text{Mo}-\text{N}\equiv\text{N}-\text{Mo}$ moiety of the complexes should be maintained during the entire of its catalytic cycle, and the reaction analysis of the entire catalytic cycle was performed by DFT calculations. The protonation of a terminal N_2 ligand is known to be the most difficult reaction step, but the newly discovered $\text{Mo}^{\text{I}}-\text{N}\equiv\text{N}-\text{Mo}^0$ moiety makes the protonation proceed more favorably than the $\text{Mo}^0-\text{N}\equiv\text{N}-\text{Mo}^0$ moiety of the initial N_2 -bridged dimolybdenum- N_2 complex. As a result, the author found a more active reaction pathway.

In the system using the molybdenum-trihalide complex bearing pincer ligands reported later, a N_2 -bridged dimolybdenum intermediate with a $\text{Mo}^{\text{I}}-\text{NN}-\text{Mo}^{\text{I}}$ moiety is formed, and direct N-N cleavage is considered to proceed. In Chapter 3, the author discusses the electronic structure of the $\text{Mo}-\text{NN}-\text{Mo}$ moiety of the N_2 -bridged dimolybdenum intermediates that switches between the catalytic cycle of Chapter 2 based on the Yandulov-Schrock cycle and the catalytic cycle involving the N-N bond cleavage.

The PCP-Mo-trihalide complex molecular catalyst is considered to follow a

different catalytic cycle from the catalytic system in Chapter 2, and its catalytic activity is also improved. In Chapter 4, the author designs PCP ligands to improve the catalytic activity of nitrogen fixation along the catalytic cycle. DFT calculations show that introducing electron-withdrawing groups into the PCP ligands enhances the catalytic activity because of the improvement of the π -accepting ability of the PCP ligand. In addition, the π -conjugate system of the PCP ligand is also found to improve the π -accepting ability.

References

1. Giddey, S.; Badwal, S. P. S.; Kulkarni, A. Review of Electrochemical Ammonia Production Technologies and Materials. *Int. J. Hydrog. Energy* **2013**, *38*, 14576–14594.
2. *Ammonia synthesis catalyst: Innovation and Practice*, ed. H. Liu, World Scientific, Beijing, 2013.
3. Hoffmann, B. M.; Lukoyanov, D.; Yang, Z.-Y., Dean, D. R.; Seefeldt, L. C. Mechanism of Nitrogen Fixation by Nitrogenase: The Next Stage. *Chem. Rev.* **2014**, *114*, 4041–4062.
4. Georgiadis, M. M.; Komiya, H.; Chakrabarti, P.; Woo, D.; Kornuc, J. J.; Rees, D. C. Crystallographic Structure of the Nitrogenase Iron Protein from *Azotobacter-Vinelandii*. *Science* **1992**, *257*, 1653–1659.
5. Maia, L. B.; Moura J. J. G. How Biology Handles Nitrite. *Chem. Rev.* **2014**, *114*, 5273–5357.
6. Allen A. D.; Senoff, C. V. Nitrogenopentaammineruthenium(II) Complexes. *Chem Commun.* **1965**, 621–622.
7. Yamamoto, A.; Kitazume, S.; Pu, L. S.; Ikeda, S. Study of the Fixation of Nitrogen. Isolation of tris(triophenylphosphine) Cobalt Complex Coordinated with molecular Nitrogen. *Chem. Commun.* **1967**, 79–80.
8. Hidai, M.; Tominari, K. Uchida, Y. Misono, A. A trans-dinitrogen Complex of Molybdenum. *Chem. Commun.* 1969, 1392-1392.
9. Chatt, J.; Wedd, A. G. Convenient Route to Lower Oxidation State Complexes of Molybdenum. *J. Organomet. Chem.* **1971**, *27*, C15–C16.
10. George, T. A.; Seibold, C. D. Bisdinitrogen Complexes of Molybdenum. *J. Organomet. Chem.* **1971**, *30*, C13–C14.

11. Chatt, J. The Reduction of Mono-Coordinated Molecular Nitrogen to Ammonia in a Protic Environment. *Nature* **1975**, 253, 39–40.
12. Chatt, J.; Dilworth, J. R.; Richard, R. L. Recent Advances in the Chemistry of Nitrogen Fixation. *Chem. Rev.* **1978**, 78, 589–625.
13. Doyle, L. R.; Wooles, A. J.; Jenkins, L. C.; Tuna, F.; McInnes, E. J. L.; Liddle, S. T. Catalytic Dinitrogen Reduction to Ammonia at a Triamideamine–Titanium Complex. *Angew. Chem. Int. Ed.* **2018**, 57, 6314–6318; *Angew. Chem.* **2018**, 130, 6422–6426.
14. Sekiguchi, Y.; Arashiba, K.; Tanaka, H.; Eizawa, A.; Nakajima, K.; Yoshizawa, K.; Nishibayashi, Y. Catalytic Reduction of Molecular Dinitrogen to Ammonia and Hydrazine Using Vanadium Complexes. *Angew. Chem. Int. Ed.* **2018**, 57, 9064–9068; *Angew. Chem.* **2018**, 130, 9202–9206.
15. Anderson, J. S.; Rittle, J.; Peters, J. C. Catalytic Conversion of nitrogen to ammonia by an iron model complex. *Nature* **2013**, 501, 84–87.
16. Creutz, S. E.; Peters, J. C. Catalytic Reduction of N₂ to NH₃ by an Fe–N₂ complex Featuring a C-Atom Anchor. *J. Am. Chem. Soc.* **2014**, 136, 1105–1115.
17. Ung, G.; Peters, J. C. Low-Temperature N₂ to Two-Coordinate L₂Fe⁰ Enables Reductive Trapping of L₂FeN₂[−] and NH₃ Generation. *Angew. Chem. Int. Ed.* **2015**, 54, 532–535; *Angew. Chem.* **2015**, 127, 542–545.
18. Del Castillo, T. J.; Thompson, N. B.; Peters, J. C. A Synthetic Single-Site Fe Nitrogenase: High Turnover, Freeze-Quench ⁵⁷Fe Mossbauer Data, and a Hydride Resting State. *J. Am. Chem. Soc.* **2016**, 138, 5341–5350.
19. Kuriyama, S.; Arashiba, K.; Nakajima, K.; Matsuo, Y.; Tanaka, H.; Ishii, K.; Yoshizawa, K.; Nishibayashi, Y. Catalytic Transformation of Dinitrogen into Ammonia and Hydrazine by Iron–Dinitrogen Complexes Bearing Pincer Ligand. *Nat. Commun.* **2016**, 7, 12181.
20. Hill, P. J.; Doyle, L. R.; Crawford, A. D.; Myers, W. K.; Ashley, A. E. Selective Catalytic Reduction of N₂ to N₂H₄ by a Simple Fe Complex. *J. Am. Chem. Soc.* **2016**, 138, 13521–13524.

21. Chalkley, M. J.; Del Castillo, T. J.; Matson, B. D.; Roddy, J. P.; Peters, J. C. Catalytic N₂-to-NH₃ Conversion by Fe at Lower Driving Force: A Proposed Role for Metallocene-Mediated PCET. *ACS Cent. Sci.* **2017**, *3*, 217–223.
22. Buscagan, T. M.; Oyala, P. H.; Peters, J. C. N₂-to-NH₃ Conversion by a Triphos–Iron Catalyst and Enhanced Turnover under Photolysis. *Angew. Chem. Int. Ed.* **2017**, *56*, 6921–6926; *Angew. Chem.* **2017**, *129*, 7025–7030.
23. Arashiba, K.; Miyake, Y.; Nishibayashi, Y. A Molybdenum Complex Bearing PNP-Type Pincer Ligands Leads to the Catalytic Reduction of Dinitrogen into Ammonia. *Nat. Chem.* **2011**, *3*, 120–125.
24. Arashiba, K.; Kinoshita, E.; Kuriyama, S.; Eizawa, A.; Nakajima, K.; Tanaka, H.; Yoshizawa, K.; Nishibayashi, Y. Catalytic Reduction of Dinitrogen to Ammonia by Use of Molybdenum–Nitride Complexes Bearing a Tridentate Triphosphine as Catalysts. *J. Am. Chem. Soc.* **2015**, *137*, 5666–5669.
25. Eizawa, A.; Arashiba, K.; Tanaka, H.; Kuriyama, S.; Matsuo, Y.; Nakajima, K.; Yoshizawa, K.; Nishibayashi, Y. Remarkable Catalytic Activity of Dinitrogen-Bridged Dimolybdenum Complexes Bearing NHC-Based PCP-Pincer Ligands toward Nitrogen Fixation. *Nat. Commun.* **2017**, *8*, 14874.
26. Arashiba, K.; Eizawa, A.; Tanaka, H.; Nakajima, K.; Yoshizawa, K.; Nishibayashi, Y. Catalytic Nitrogen Fixation via Direct Cleavage of Nitrogen–Nitrogen Triple Bond of Molecular Dinitrogen under Ambient Reactions. *Bull. Chem. Soc. Jpn.* **2017**, *90*, 1111–1118.
27. Eizawa, A.; Arashiba, K.; Egi, A.; Tanaka, H.; Nakajima, K.; Yoshizawa, K.; Nishibayashi, Y. Catalytic Reactivity of Molybdenum–Trihalide Complexes Bearing PCP-Type Pincer Ligands. *Chem. Asian J.* **2019**, *14*, 2091–2096.
28. Ashida, Y.; Arashiba, K.; Tanaka, H.; Egi, A.; Nakajima, K.; Yoshizawa, K.; Nishibayashi, Y. Molybdenum-Catalyzed Ammonia Formation Using Simple Monodentate and Bidentate Phosphines as Auxiliary Ligands. *Inorg. Chem.* **2019**, *58*, 8927–8932.

29. Ashida, Y.; Kondo, S.; Arashiba, K.; Kikuchi, T.; Nakajima, K.; Kakimoto, S.; Nishibayashi, Y. A Practical Synthesis of Ammonia from Nitrogen Gas, Samarium Diodide and Water Catalyzed by a Molybdenum–PCP Pincer Complex. *Synthesis* **2019**, *51*, 3792–3795.
30. Ashida, Y.; Arashiba, K.; Nakajima, K.; Nishibayashi, Y. Molybdenum-Catalyzed Ammonia Production with Samarium Diodide and Alcohols or Water. *Nature* **2019**, *568*, 536–540.
31. Egi, A.; Tanaka, H.; Konomi, A.; Nishibayashi, Y.; Yoshizawa, K. Nitrogen Fixation Catalyzed by Dinitrogen-Bridged Dimolybdenum Complexes Bearing PCP- and PNP-Type Pincer Ligands: A Shortcut Pathway Deduced from Free Energy Profile. *Eur. J. Inorg. Chem.* **2020**, 1490–1498.
32. Arashiba, K.; Tanaka, H.; Yoshizawa, K.; Nishibayashi, Y. Cycling between Molybdenum–Dinitrogen and –Nitride Complexes to Support the Reaction Pathway for Catalytic Formation of Ammonia from Dinitrogen. *Chem. Eur. J.* **2020**, *26*, 13383–13389.
33. Fajardo, Jr., J.; Peters, J. C. Catalytic Nitrogen-to-Ammonia Conversion by Osmium and Ruthenium Complexes. *J. Am. Chem. Soc.* **2017**, *139*, 16105–16108.
34. Kuriyama, S.; Arashiba, K.; Tanaka, H.; Matsuo, Y.; Nakajima, K.; Yoshizawa, K.; Nishibayashi, Y. Direct Transformation of Molecular Dinitrogen into Ammonia Catalyzed by Cobalt Dinitrogen Complexes Bearing Anionic PNP Pincer Ligands. *Angew. Chem. Int. Ed.* **2016**, *55*, 14291–14293; *Angew. Chem.* **2016**, *128*, 14503–14507.
35. Meng, F.; Kuriyama, S.; Tanaka, H.; Egi, A.; Yoshizawa, K.; Nishibayashi, Y. Ammonia Formation Catalyzed by a Dinitrogen-Bridged Ruthenium Complex Bearing PNP-Pincer Ligands under Mild Reaction Conditions. *Angew. Chem. Int. Ed.* **2021**, *60*, 13906–13912; *Angew. Chem.* **2021**, *133*, 14025–14031.

36. Ashida, Y.; Mizushima, T.; Arashiba, K.; Egi, A.; Tanaka, H.; Yoshizawa, K.; Nishibayashi, Y. Catalytic Production of Ammonia from Dinitrogen Employing Molybdenum Complexes Bearing N-Heterocyclic Carbene-Based PCP-type Pincer Ligands. *ChemRxiv* doi: 10.26434/chemrxiv-2022jp6hz.

Chapter 2

Nitrogen Fixation Catalyzed by Dimolybdenum Complexes Bearing PCP- and PNP-Type Pincer Ligands

2.1. Introduction

Biological nitrogen fixation, a catalytic conversion of atmospheric dinitrogen (N_2) to ammonia (NH_3), is efficiently achieved under mild reaction conditions by certain bacteria containing the enzyme nitrogenase.¹ In particular, molybdenum-containing nitrogenases have a double cubane-type molybdenum-iron-sulfur cluster $MoFe_7S_9C$, known as FeMo-cofactor, in their active site. Biological nitrogen fixation proceeds with protons and electrons on FeMo-cofactor.²⁻⁴ The structure and function of FeMo-cofactor may provide an attractive model for the design of molecular catalysts for nitrogen fixation under mild conditions.

Since the discovery of the first transition metal–dinitrogen complex by Allen and Senoff in 1965,⁵ much experimental and theoretical effort has been committed to the goal of artificial nitrogen fixation catalyzed by molecular catalysts beyond the industrial Haber-Bosch process.^{6,7} In 2003, Yandulov and Schrock reported the first successful example in a history of development of a distinct transition metal complexes for nitrogen fixation.⁸ Their Mo(III)–triamideamine complex catalyzes to convert N_2 to NH_3 using 2,6-lutidinium tetrakis[3,5-bis(trifluoromethyl)-phenyl]borate ($[LutH]BAr^F_4$) as a proton source and decamethylchromocene ($CrCp^*_2$) as an electron source, in which up to 8 equiv of NH_3 based on the Mo atom of the catalyst. Their results indicated that the presence of the molybdenum center in the metal complex is important to achieve artificial nitrogen fixation under mild conditions. At present, Mo(III)-trihalide complexes exhibits the highest catalytic activity,⁹ while titanium-,¹⁰ vanadium-,¹¹ iron-,¹²⁻¹⁹ molybdenum-,²⁰⁻²⁶ ruthenium-,²⁷ osmium-,²⁷ and cobalt-catalyzed²⁸ direct conversions of N_2 into NH_3 and

hydrazine (N_2H_4) have been accomplished as a result of intensive experimental works in this research field.

In 2011, the second example of nitrogen fixation catalyzed by transition-metal complexes was presented by Nishibayashi and coworkers. They synthesized an N_2 -bridged dimolybdenum complex with a tridentate phosphine- and puridine-based PNP-type pincer ligand [$\{\text{Mo}^0(\text{PNP})(\text{N}_2)_2\}_2(\mu\text{-N}_2)$] **1** (PNP = 2,6-bis((di-*tert*-butylphosphino)methyl)pyridine), in which the superscript number presents the oxidation number of the molybdenum atom. After that, they generated up to 12 equiv of NH_3 based on one Mo atom of **1** using complex **1** in the presence of 2,6-lutidinium trifluoromethanesulfonate ([LutH]OTf) as a proton source and cobaltocene (CoCp_2) as an electron source (Figure 2-1).²⁰ Modification of the PNP ligand is a promising way to enhance catalytic activity for nitrogen fixation. Introducing electron-donating groups at the 4-position of the pyridine ring of the PCP ligand enhanced the catalytic activity, in which up to 26 equiv. of NH_3 based on one Mo atom of **1** in the case of introducing a methoxy group.²⁹ Yoshizawa and Nishibayashi groups have proposed a possible catalytic mechanism of nitrogen fixation as shown in Figure 2-2 using **1** from a view point of synergetic experimental and theoretical works.^{30,31} In their works, they considered that the N_2 -bridged dimolybdenum ($\text{Mo-N}\equiv\text{N-Mo}$) structure is essential for the catalytic activity in this dimolybdenum system. Their DFT calculations revealed that the $\text{Mo-N}\equiv\text{N-Mo}$ structure must be maintained at the earliest stage of the catalytic cycle, especially at the first protonation of a terminal N_2 ligand. Batista and coworkers independently pointed out a remarkable role of the dinuclear molybdenum complex in the catalytic activity of **1** from a thermodynamic point of view.³²

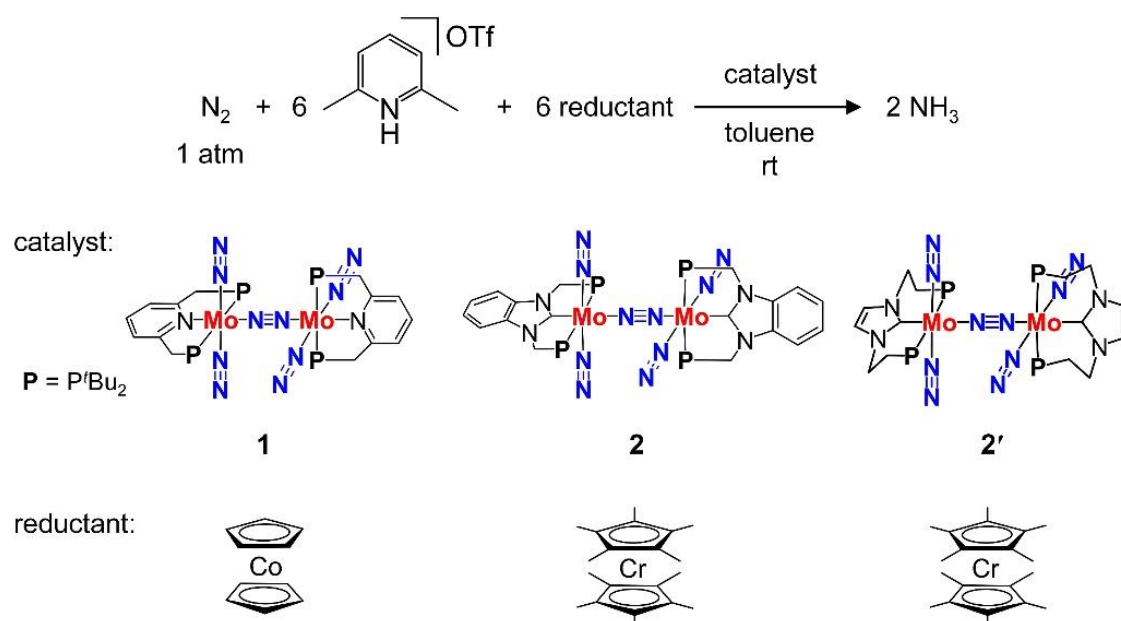


Figure 2-1. N₂-bridged dimolybdenum complex catalysts developed by Nishibayashi and coworkers.

Catalytic mechanism of conversion of N₂ to NH₃ shown in Figure 2-2 was theoretically proposed on the basis of some hypotheses supported by experimental results, and the entire catalytic cycle can be divided into four stages: (i) At first, protonation of a terminal N₂ ligand of **1**. After the protonation, the exchange of the N₂ ligand trans to the -NNH moiety for triflate (OTf⁻) that is the counter anion of LutH⁺ proceeds. As a result, this process gives a Mo(II)Mo(0)-diazene complex, [Mo^{II}(PNP)(OTf)(NNH)-N≡N-Mo⁰(PNP)(N₂)₂] **A**. (ii) Protonations and reductions of **A** yielding first NH₃ causes the separation of the Mo-N≡N-Mo structure to afford two mononuclear complexes, Mo(IV)-nitride, [Mo^{IV}(PNP)(OTf)(≡N)] **B** and six-coordinated Mo(0)-N₂, [Mo⁰(PNP)(N₂)₃] **C**. (iii) Complex **B** is gradually converted to a six-coordinated Mo(I)-ammine complex, [Mo^I(PNP)(OTf)(NH₃)(N₂)] **D**. (iv) Reduction of afforded complex **D** and regeneration of the Mo-N≡N-Mo structure with **C** resulted in a return to initial complex **1**.

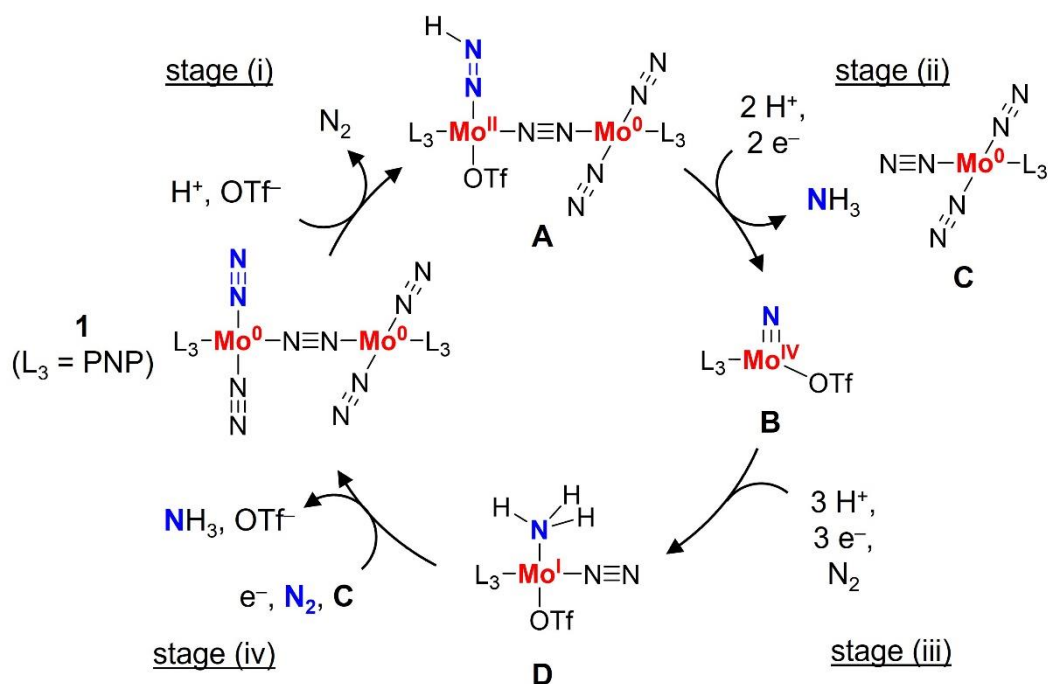


Figure 2-2. Catalytic cycle of nitrogen fixation using **1** proposed in ref 30.

Based on the mechanistic elucidation of the Mo–PNP system, they have newly designed and synthesized the N_2 -bridged dimolybdenum complex with *N*-heterocyclic carbene- (NHC-)based PCP-type pincer ligand, $[\{\text{Mo}(\text{PCP})(\text{N}_2)_2\}_2(\mu-\text{N}_2)]$ **2** (PCP = 1,3-bis((di-*tert*-butylphosphino)methyl)benzimidazole-2-ylidene).²² Complex **2** exhibited higher catalytic activity for nitrogen fixation and longer lifetime than that of complex **1**. 100 equiv. of NH_3 based on the Mo atom of **2** are generated in the presence of $[\text{LutH}]\text{OTf}$ as a proton source and dcamethylchromocene (CrCp^*_2) as an electron source. They also experimentally observed that a stable Mo– $\text{N}\equiv\text{N}$ –Mo structure is essential for the conversion of N_2 into NH_3 using Mo–PCP complexes; an N_2 -bridged dimolybdenum complex with another PCP-type pincer ligand, $[\{\text{Mo}(\text{PCP}')(\text{N}_2)_2\}_2(\mu-\text{N}_2)]$ **3** (PCP' = 1,3-bis(2-(di-*tert*-butylphosphino)ethyl)imidazole-2-ylidene), showed very low catalytic activity for nitrogen fixation. The length of the $(\text{CH}_2)_n$ linker connecting the NHC moiety to the phosphine group in the PCP ligands critically controls steric hindrance of N_2 -bridged dimolybdenum complexes, in which $n = 1$ for **2** and $n = 2$ for **3**. As a result, stability of chemical forms of **2** differs from that of **3** in solution. In fact, owing to the infrared spectra of **2** and **3** in tetrahydrofuran (THF), **2** maintained the Mo– $\text{N}\equiv\text{N}$ –Mo structure but **3** separated into mononuclear species. The catalytic activities of **2** and **3**

clearly highlight the importance of the Mo–N≡N–Mo structure of the Mo–PCP system. The author expects that this knowledge will be applicable to the Mo–PNP system.

In order to develop more effective molybdenum catalysts for nitrogen fixation, the origin of the high catalytic activity of **2** needs to be elucidated in detail. Despite Yoshizawa and Nishibayashi groups initially predicted that the terminal N₂ ligand of **2** is more activated reductively for protonation than that of **1**, preliminary DFT calculations contradicted this prediction.²² They found that PNP ligand serves as only a moderate σ -donor, but PCP ligand serves not only a strong σ -donor but a π -acceptor. A rigid Mo–C(carbene) bond is derived from σ -donation and π -backdonation between the Mo center and the carbene C atom of PCP ligand, resulting in the high catalytic activity and long lifetime of **2**. However, the author has not yet obtained detailed information on the entire catalytic cycle of the Mo–PCP system, because the previous DFT calculations focused only on the first protonation step (stage (i) in Figure 2-2). In this study, more detailed DFT calculations based on those reported for the Mo–PNP system were performed to evaluate the complete reaction pathway for nitrogen fixation catalyzed by **2**. The calculation of the free energy change for the separation of the Mo–N≡N–Mo structures of **2** and **1** strongly demands that the dispersion is properly treated in both the Mo–PNP and Mo–PCP systems. The calculation with B3LYP-D3³³ of free energy profiles for the revised catalytic cycle indicates that the Mo–N≡N–Mo structure should be maintained during the entire catalytic cycle. In addition, the author newly proposes a shortcut pathway via protonation of a terminal N₂ ligand on dinuclear Mo(I)Mo(0) core and reveals that the shortcut pathway is energetically more favorable than the previously proposed pathways.

2.2. Computational Methods

DFT calculations were performed to search all intermediates and transition structures on potential energy surfaces using the Gaussian 09 program (Rev. D.01).³⁴ Geometry optimizations were carried out with the B3LYP-D3 functional, which is the B3LYP hybrid functional³⁵⁻³⁸ combined with an empirical dispersion correction developed by Grimme.³³ As described later, the author found in the present study that an appropriate treatment of dispersion is strongly demanded in the evaluation of free energy changes at 298 K (ΔG_{298}) for the formation of the Mo–N≡N–Mo geometry in dinitrogen-bridged dimolybdenum complexes. The SDD (Stuttgart/Dresden pseudopotentials) basis set^{39,40} and 6-31G(d) basis sets⁴¹⁻⁴⁴ were employed for the Mo atoms and the other atoms, respectively. All stationary-point structures were confirmed to have the appropriate number of imaginary frequencies by vibrational analysis. To determine the free energy profiles of reaction pathways, the author performed single-point energy calculations at the optimized geometries using the SDD and 6-311+G(d,p) basis sets.⁴⁵⁻⁴⁷ In the single-point calculations, solvation effects of toluene were taken into account by using the polarizable continuum model (PCM).⁴⁸

All protonation steps using 2,6-lutidinium (LutH⁺) as a proton source were evaluated from the kinetic viewpoint by searching for the transition state of the proton transfer process. On the other hand, the free energy profiles of the reduction steps of the molybdenum complexes were simply evaluated by the difference in free energies between the protonated and reduced species. This is because molybdenum complexes with PCP and PNP ligands used different electron sources, CrCp*₂ and CoCp₂, respectively. One of our goals of this study is to compare the free energy profiles of newly-proposed reaction pathways in the Mo–PCP and Mo–PNP systems and to reveal the origin of the higher catalytic activity in the Mo–PCP system.

In the previously-proposed reaction pathways for nitrogen fixation catalyzed by [$\{\text{Mo}(\text{PNP})(\text{N}_2)_2\}_2(\mu\text{-N}_2)$] **1**,³⁰ the author evaluated the zero-point energy difference ΔE_0 for the separation of the Mo–N≡N–Mo moiety of **1** calculated at the B3LYP* level of theory, where the B3LYP* functional is a reparametrized version of the B3LYP hybrid functional developed by Reiher and coworkers.^{49,50} The author chose the B3LYP*

functional to estimate the relative energy of different spin states properly. Despite the author expected that the relative energy of different spin states, the lowest spin state such as the closed-shell singlet and doublet states of all intermediates and transition states in the proposed catalytic cycle were more stable than the other spin states. The calculations encourage more attention to be paid to the proper treatment of the dispersion in the Mo–PNP and Mo–PCP systems, i.e. attractive interactions between bulky organic substituents on phosphorus atoms in both pincer ligands.⁵¹ This consideration should be important because of the experimental and theoretical observation that the formation of the stable Mo–N≡N–Mo structure is essential for higher catalytic activity for nitrogen fixation of **2**.²²

In this study, the author has found that a dispersion-corrected functional must be employed for more realistic free energy profiles at 298 K (ΔG_{298}). Table 2-1 describes bond dissociation energies (BDE) at 0 K and bond dissociation free energies (BDFE) at 298 K of a Mo–N₂(bridging) bond in **1** and **2** calculated at the B3LYP* and B3LYP-D3 level of theory. BDE and BDFE of the Mo–N₂(bridging) bond are evaluated as ΔE_0 and ΔG_{298} , respectively, for the reaction $[\text{Mo}^0(\text{L}_3)(\text{N}_2)_2\text{--N}\equiv\text{N--Mo}^0(\text{L}_3)(\text{N}_2)_2] \rightarrow [\text{Mo}^0(\text{L}_3)(\text{N}_2)_3] + \text{trans-}[\text{Mo}^0(\text{L}_3)(\text{N}_2)_2]$, in which L₃ = PNP for **1** or PCP for **2**. As shown in Table 2-1, when dispersion correction is not applied, the values of both BDE and BDFE decrease significantly. In particular, the BDFE of **2** obtained with the B3LYP* functional is only +5.9 kcal mol⁻¹, which is inconsistent with the stability of **2** in THF solution due to spectroscopic observation at room temperature.²² Therefore, the author concluded that the B3LYP* functional is not suitable for the evaluation of free energy profiles in the Mo–PCP and Mo–PNP systems and employed the B3LYP-D3 functional in this study.

Table 2-1. BDEs (ΔE_0) and BDFEs (ΔG_{298}) of a Mo–N₂(bridging) bond in [$\{\text{Mo}^0(\text{L}_3)(\text{N}_2)_2\}_2(\mu\text{-N}_2)$] **1** ($\text{L}_3 = \text{PNP}$) and **2** ($\text{L}_3 = \text{PCP}$) calculated with the B3LYP* and B3LYP-D3 functionals

Functional	1 ($\text{L}_3 = \text{PNP}$)		2 ($\text{L}_3 = \text{PCP}$)	
	B3LYP*	B3LYP-D3	B3LYP*	B3LYP-D3
$\Delta E_0^{[\text{a}]}$ (kcal mol ^{−1})	24.8	43.5	19.0	33.9
$\Delta G_{298}^{[\text{a}]}$ (kcal mol ^{−1})	10.7	28.8	5.9	20.3

[a] Evaluated as (free) energy changes for reaction [$\{\text{Mo}^0(\text{L}_3)(\text{N}_2)_2\}_2(\mu\text{-N}_2)$] \rightarrow [$\text{Mo}^0(\text{L}_3)(\text{N}_2)_3$] + *trans*-[$\text{Mo}^0(\text{L}_3)(\text{N}_2)_2$].

2.3. Results and Discussion

2.3.1. Proposed catalytic cycle

Figure 2-3 describes a newly-proposed catalytic cycle for nitrogen fixation using Mo–PCP complex **2** and Mo–PNP complex **1**. In order to obtain a more energetically efficient catalytic cycle than the previously-proposed catalytic cycle shown in Figure 2-2,³⁰ the author discarded two old assumptions: (1) A dimolybdenum complex with the Mo–N≡N–Mo structure separates into two mononuclear Mo complexes at a certain stage of the catalytic cycle, and key Mo–nitride complex, [Mo(PNP)(≡N)(OTf)] **B**, is formed from the yielded mononuclear Mo complex. (2) The dinuclear complex **2** and **1** are regenerated and the next catalytic cycle is initiated. According to the revised catalytic cycle shown in Figure 2-3 based on the B3LYP-D3 results, the Mo–N≡N–Mo structure should be maintained during the entire catalytic cycle. The author has also found out that a terminal N₂ ligand on the Mo^I–N≡N–Mo⁰ moiety of [Mo^I(L₃)(N₂)(OTf)–Mo⁰(L₃)(N₂)₂] **XII** has higher reactivity with a proton donor than that on the Mo⁰–N≡N–Mo⁰ moiety of **2** and **1**.

The newly-proposed catalytic cycle shown in Figure 2-3 can be divided into four stages (i)-(iv). In stage (i), protonation of a terminal N₂ ligand of **2** and **1** leads to a ligand exchange of the N₂ ligand trans to the NNH moiety for OTf[–], which is the counter anion of LutH⁺. As a result, dinuclear Mo(II)–diazene complex, [Mo^{II}(L₃)(OTf)(NNH)–N≡N–Mo⁰(L₃)(N₂)₂] **IV**, is yielded. In stage (ii), two successive protonation/reduction reactions of **IV** produce the first molecule of NH₃ and dinuclear Mo(IV)–nitride complex, [Mo^{IV}(L₃)(OTf)(≡N)–N≡N–Mo⁰(L₃)(N₂)₂] **VII**. In stage (iii), three successive protonation/reduction reactions of **VII** afford dinuclear Mo(I)Mo(0)–ammine complex, [Mo^I(L₃)(OTf)(NH₃)–N≡N–Mo⁰(L₃)(N₂)₂] **X**. The protonation of **VII** occurs instead of the separation of **VII** into two mononuclear complexes, [Mo^{IV}(L₃)(OTf)(≡N)] and [Mo⁰(L₃)(N₂)₃]. In stage (iv), the ammine ligand in **X** is replaced by an incoming N₂ molecule to form Mo(I)Mo(0)–N₂ complex **XII**. Since **XII** exhibits higher reactivity with LutH⁺ than Mo(0)Mo(0)–N₂ complex **2** and **1**, alternating protonation and reduction of **XII** occurs to give **IV**. Thus, the regeneration of the initial Mo(0)Mo(0)–N₂ complex **2** or **1** is not required for closing the catalytic cycle. Based on the catalytic pathways

independently proposed by Batista³² and us, a nitrogen fixation pathway that maintains the Mo–N≡N–Mo structure with an OTf group of the Mo–PNP system, the so-called “combined” catalytic pathway, has been proposed by Mézailles.⁵² This is a basically similar mechanism to the newly-proposed one in Figure 2-3, although it does not require regeneration of Mo(0)Mo(0)–N₂ complex **1**. The author’s proposal differs from Batista’s mechanism mainly on the pathway of protonation/reduction of N₂. Batista considered a possibility of double protonation before the first reduction reaction. On the other hand, the author assumes alternating protonation/reduction to complexes **1** and **2** based on the Yandulov-Schrock mechanism proposed for the Mo(III)–triamideamine system.⁸

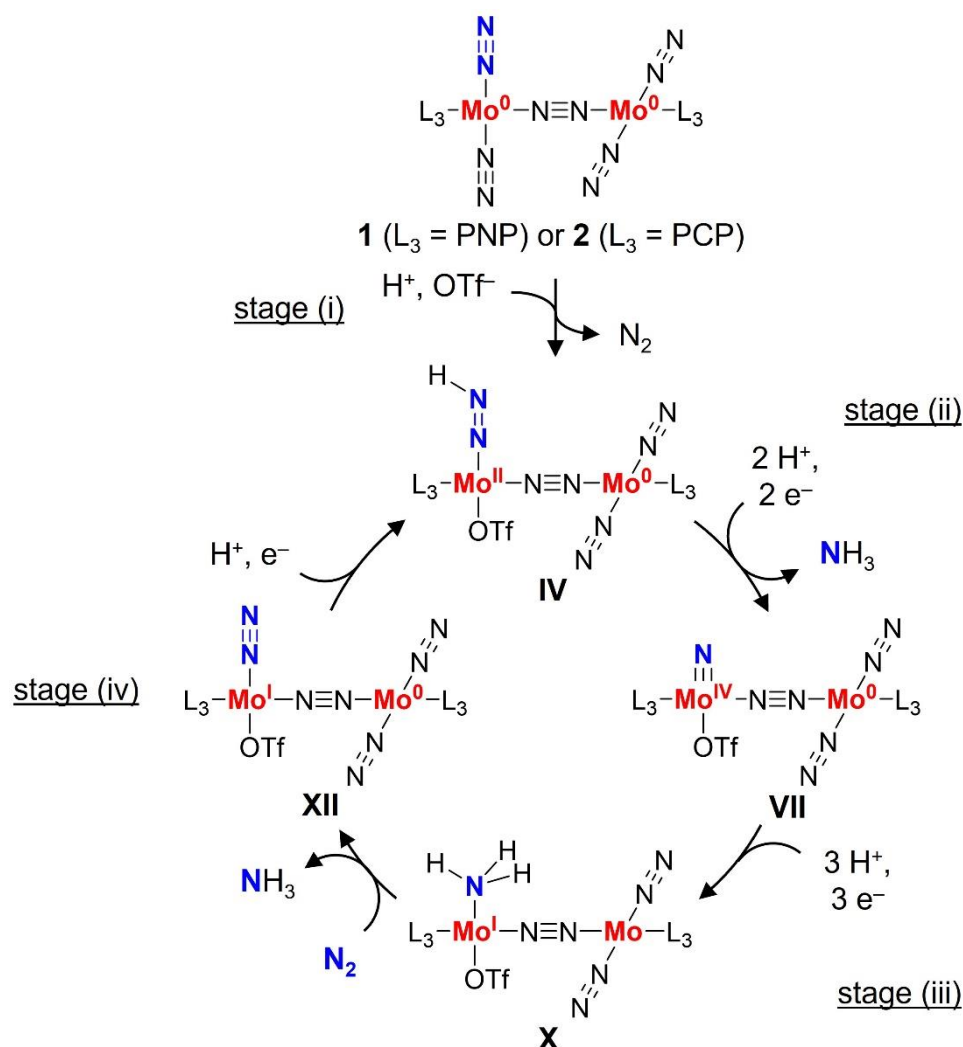


Figure 2-3. Newly-proposed catalytic cycle for nitrogen fixation using **2** (**1**). The numbers of complexes are also described in Figure 2-4.

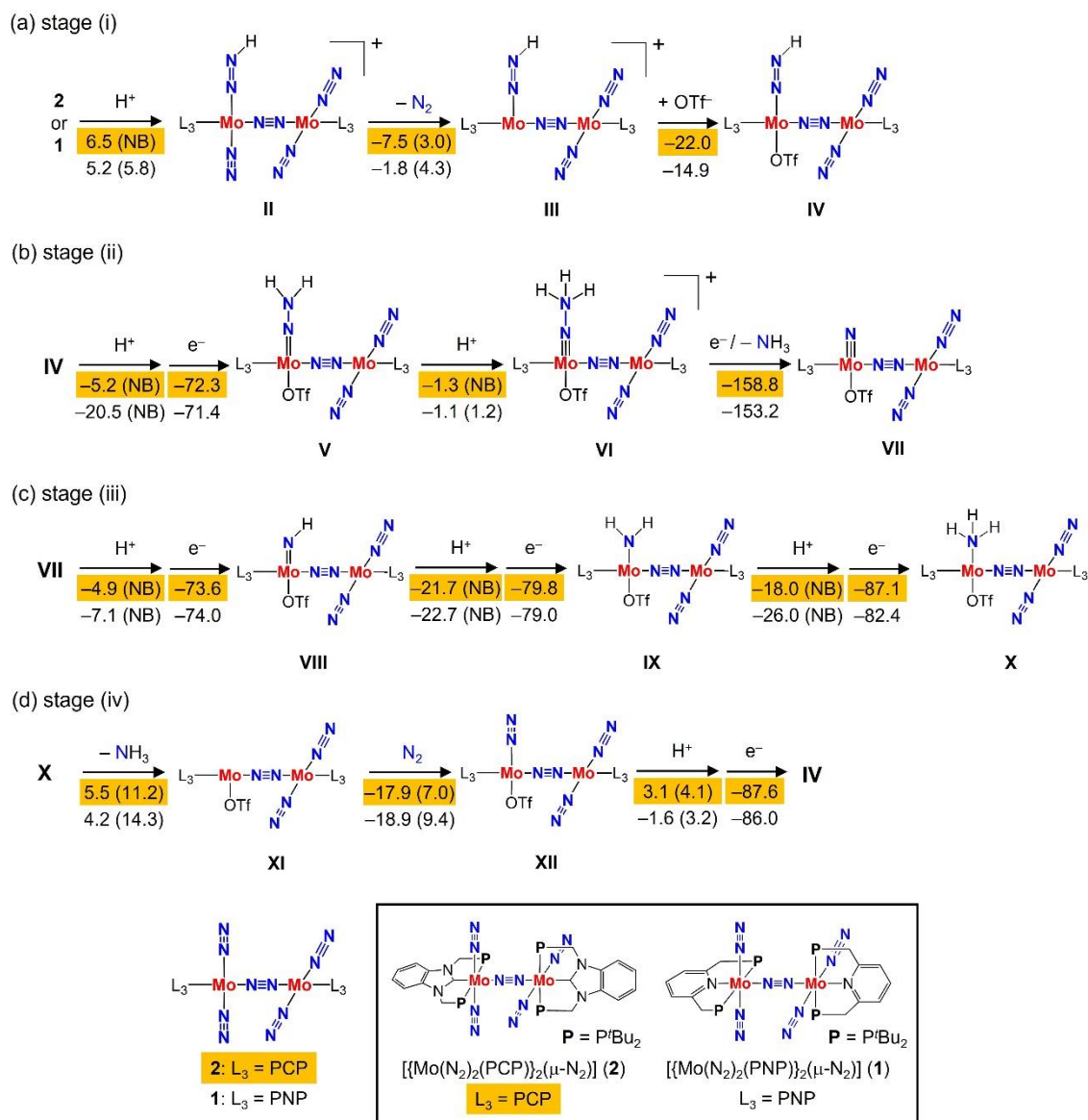


Figure 2-4. Entire reaction pathway and energy profiles of nitrogen fixation catalyzed by **2** (**1**). Free energy changes at 298 K and free energies of activation (in parenthesis) for individual steps were calculated at the B3LYP-D3 level of theory (units in kcal/mol). NB represents that the corresponding reaction has no activation barrier.

2.3.2. Free energy profiles of catalytic cycle

Figure 2-4(a) shows the free energy profile of the reaction steps in stage (i), which begins with the protonation of one of the four terminal N₂ ligands in **2** (**I**). The bridging N₂ ligand is sterically protected by the bulky *tert*-butyl groups of the pincer ligands. Therefore, protonation of it cannot proceed with the bulky LutH⁺.³⁰ Protonation of **2** (**I**) is endergonic by 6.5 kcal mol⁻¹ (L₃ = PCP) and 5.2 kcal mol⁻¹ (L₃ = PNP), yielding a cationic Mo(I)Mo(0)–diazene complex, [Mo^I(L₃)(N₂)(NNH)–N≡N–Mo⁰(L₃)(N₂)₂]⁺ **II**. Moreover, this step has virtually no activation barrier (L₃ = PCP) or a very low free energy of activation (L₃ = PNP, ΔG[‡] = +5.8 kcal mol⁻¹). Because the Mo–N₂(terminal) bond *trans* to the NNH group in **II** is significantly weakened, the liberation of the N₂ ligand from the Mo center can proceed to give a cationic five-coordinate Mo(I)Mo(0)–diazene complex, [Mo^I(L₃)(NNH)–N≡N–Mo⁰(L₃)(N₂)₂]⁺ **III**. The Mo center readily liberates the N₂ ligand at the *trans* position of the NNH group in an exergonic way by 7.5 kcal mol⁻¹ (L₃ = PCP) and 1.8 kcal mol⁻¹ (L₃ = PNP) with very low activation free energies, +3.0 kcal mol⁻¹ (L₃ = PCP) and +4.3 kcal mol⁻¹ (L₃ = PNP). The positive charge of **III** is quenched by the coordination of OTf⁻ with highly exergonicity of 22.0 kcal mol⁻¹ (L₃ = PCP) and 14.9 kcal mol⁻¹ (L₃ = PNP), resulting in six-coordinate [Mo^{II}(L₃)(OTf)(NNH)–N≡N–Mo⁰(L₃)(N₂)₂] **IV**. This ligand exchange step of N₂ for OTf⁻ is regarded as a vital step to stabilize the hydrazide species for the next protonation and reduction steps. Indeed, the stoichiometric reaction of **1** and 2 equiv. of [LutH]OTf in toluene led to the observation of a dimolybdenum complex [Mo(PNP)(≡N)(OTf)–N≡N–Mo(PNP)(N₂)] by mass spectrometry from.³⁰ To sum up, the free energy changes for stage (i) are calculated to be ΔG₂₉₈ = –23.0 kcal mol⁻¹ (L₃ = PCP) and –11.5 kcal mol⁻¹ (L₃ = PNP).

In stage (ii), the yielded Mo(II)Mo(0)–diazene complex **IV** undergoes two sequential protonation and reduction reactions to produce the first molecule of NH₃ and Mo(IV)Mo(0)–nitride complex, [Mo^{IV}(L₃)(OTf)(≡N)–N≡N–Mo⁰(L₃)(N₂)₂] **VII**. Figure 2-4(b) describes that protonation of **IV** proceeds exergonically by 5.2 kcal mol⁻¹ (L₃ = PCP) and 20.5 kcal mol⁻¹ (L₃ = PNP). The significant difference in the ΔG₂₉₈ values at this step is likely due to the relative lower thermodynamic stability of **IV** (L₃ = PNP) compared to **IV** (L₃ = PCP). As described above, the production of **IV** (L₃ = PNP) from

1 is +11.5 kcal mol⁻¹ less exergonic than that of **IV** (L₃ = PCP) from **2**. On the search of a transition state for the protonation of **IV** (L₃ = PNP) by LutH⁺ at the B3LYP-D3 level of theory, the author could not find either the corresponding reactant complex or transition state. Thus, in the evaluation of ΔG₂₉₈ for the protonation of **IV** (L₃ = PNP), the author regarded an optimized structure with the NN(H)···H⁺(Lut) distance of 5.0 Å as the reactant complex. The protonated **IV** (**V**⁺) is reduced to give the Mo(III)Mo(0)–hydrazide(2–) complex, [Mo^{III}(L₃)(OTf)(=NNH₂)–N≡N–Mo⁰(L₃)(N₂)₂] **V**, in which the free energy differences for reduction of **V**⁺ are –72.3 kcal mol⁻¹ (L₃ = PCP) and –71.4 kcal mol⁻¹ (L₃ = PNP).

Protonation of the NNH₂ group of **V** yields the cationic Mo(IV)Mo(0)–hydrazidium complex, [Mo^{IV}(L₃)(OTf)(=NNH₃)–N≡N–Mo⁰(L₃)(N₂)₂]⁺ **VI**, in a slightly exergonic way; ΔG₂₉₈ = –1.3 kcal mol⁻¹ (L₃ = PCP) and –1.1 kcal mol⁻¹ (L₃ = PNP). Next reduction of **VI** spontaneously cleaves N–N bond of the NNH₃ group to form the first molecule of NH₃ and [Mo^{IV}(L₃)(OTf)(≡N)–N≡N–Mo⁰(L₃)(N₂)₂] **VII**. This reduction process is highly exergonic (–158.8 kcal mol⁻¹ for L₃ = PCP and –153.2 kcal mol⁻¹ for L₃ = PNP) because of thermodynamically stability of the produced NH₃. Based on both experimental and computational results: isolation of a chloride analog of **B**, [Mo^{IV}(PNP)(Cl)(≡N)], and the small BDE value of a Mo–N₂(bridging) bond of **VII** (ΔE₀ = +4.4 kcal mol⁻¹) calculated with the B3LYP* functional, Yoshizawa group previously proposed that **VII** should separates into two mononuclear complexes, [Mo^{IV}(PNP)(OTf)(≡N)] **B** and [Mo⁰(PNP)(N₂)₃] **C**, as shown in Figure 2-2.³⁰ However, the BDFE values at 298 K (ΔG₂₉₈) were computed to be +11.8 kcal mol⁻¹ (L₃ = PCP) and +11.7 kcal mol⁻¹ (L₃ = PNP) at the dispersion-corrected B3LYP-D3 level of theory. Therefore, the author concluded that **VII** maintains the Mo–N≡N–Mo moiety because these BDFE of the Mo–Mo–N₂(bridging) bond in **VII** are large enough. Indeed, in stage (iii), protonation of **VII** yielding the corresponding Mo(IV)Mo(0)–imide complex, [Mo^{IV}(L₃)(OTf)(=NH)–N≡N–Mo⁰(L₃)(N₂)₂]⁺, is calculated to be an exergonic reaction with almost no activation barrier in both Mo–PCP and Mo–PNP systems.

In the newly-proposed catalytic mechanism shown in Figure 2-3, the second molecule of NH₃ is produced on the dimolybdenum platform [Mo(L₃)(OTf)–NN–Mo(L₃)(N₂)₂] instead of a monomolybdenum one [Mo(L₃)(OTf)] shown in Figure 2-2.

Figure 2-4(c) is the free energy profile of stage (iii), which describes the conversion of the nitride N atom of **VII** to NH_3 . In both the Mo–PCP and Mo–PNP systems, the three protonation steps for the formation of MoMo–imide (**VIII**), –amide (**IX**), and –ammine (**X**) complexes were found to proceed in an exergonic way. Moreover, these protonation steps do not require activation energy. The ΔG_{298} values calculated for the Mo–PCP system are $-4.9 \text{ kcal mol}^{-1}$ for **VII** \rightarrow **VIII**, $-21.7 \text{ kcal mol}^{-1}$ for **VIII** \rightarrow **IX**, and $-18.0 \text{ kcal mol}^{-1}$ for **IX** \rightarrow **X**. On the other hand, reduction steps proceed with free energy changes of about -80 to $-70 \text{ kcal mol}^{-1}$. The free energy profile of stage (iii) in the Mo–PNP system shows the same trend as that in the Mo–PCP system.

Stage (iv) shows the regeneration of an MoMo– N_2 species to start the next catalytic cycle. In the previously-proposed mechanism of the Mo–PNP system, the author assumed the regeneration of the initial Mo(0)Mo(0)– N_2 complex **1**.³⁰ However, in this study, Mo(I)Mo(0)– N_2 complex, $[\text{Mo}^{\text{I}}(\text{L}_3)(\text{OTf})(\text{N}_2)-\text{N}\equiv\text{N}-\text{Mo}^0(\text{L}_3)(\text{N}_2)_2]$ **XII**, is regenerated, and our calculations have revealed that an N_2 ligand coordinated to the $\text{Mo}^{\text{I}}-\text{N}\equiv\text{N}-\text{Mo}^0$ moiety appears to be more reactive with LutH^+ than that of the $\text{Mo}^0-\text{N}\equiv\text{N}-\text{Mo}^0$ moiety. This regeneration of **XII** in Figure 2-4(d) indicates that it is regarded as a “shortcut” reaction pathway.

In the newly-proposed reaction pathway, ligand exchange of the NH_3 ligand in $[\text{Mo}^{\text{I}}(\text{L}_3)(\text{OTf})(\text{NH}_3)-\text{N}\equiv\text{N}-\text{Mo}^0(\text{L}_3)(\text{N}_2)_2]$ **X** for an incoming N_2 molecule occurs. At first, the dissociation of the Mo– NH_3 bond in **X** leads to the five-coordinate Mo(I)Mo(0) complex, $[\text{Mo}^{\text{I}}(\text{L}_3)(\text{OTf})-\text{N}\equiv\text{N}-\text{Mo}^0(\text{L}_3)(\text{N}_2)_2]$ **XI**. This dissociation reaction is computed to be endergonic by $+5.0 \text{ kcal mol}^{-1}$ ($\text{L}_3 = \text{PCP}$) or $+4.2 \text{ kcal mol}^{-1}$ ($\text{L}_3 = \text{PNP}$) with the activation free energy of $+11.2 \text{ kcal mol}^{-1}$ ($\text{L}_3 = \text{PCP}$) and $+14.3 \text{ kcal mol}^{-1}$ ($\text{L}_3 = \text{PNP}$). Next, an N_2 molecule coordinates to the vacant site of the Mo(I) center of **XI**, resulting in the formation of Mo(I)Mo(0)– N_2 complex **XII**. The ΔG_{298} (ΔG^\ddagger) values for the coordination of N_2 are $+17.9$ ($+7.0$) kcal mol^{-1} for **XI** ($\text{L}_3 = \text{PCP}$) and $+18.9$ ($+9.4$) kcal mol^{-1} for **XI** ($\text{L}_3 = \text{PNP}$). This reaction free energy indicates that the ligand exchange will be attained under mild conditions because the $\text{Mo}^{\text{I}}-\text{N}_2$ bond is stronger than the $\text{Mo}^{\text{I}}-\text{NH}_3$ bond.

The final step of stage (iv) is the protonation step of **XII**, yielding **IV** and closing the catalytic cycle. In the newly-proposed pathway, the regeneration of Mo(0)Mo(0)– N_2

complex **2** (**1**) should not be required in catalytic cycle for the nitrogen fixation. The ΔG_{298} (ΔG^\ddagger) values calculated for the protonation of **XII** are +3.1 (+4.1) kcal mol⁻¹ (L_3 = PCP) and +1.7 (+4.0) kcal mol⁻¹ (L_3 = PNP). These values indicate that the terminal N₂ ligand at the *trans* position of the OTf group in **XII** should be more reactive than that in **2** (**1**).

Taken together, the free energy profiles in Figures 2-3 and 2-4 describe that the Mo^{I/0}-N≡N-Mo⁰ structure should be preserved throughout the catalytic cycle. This newly-proposed dinuclear mechanism is superior to the conventional mechanism in which **VII** separates into two certain monomeric complexes. The separation of the dinuclear structure may suppress the catalytic reaction rate because Mo^{I/0}-N≡N-Mo⁰ structures are essential for the first protonation of the N₂ ligand in both Mo-PCP and Mo-PNP systems. As described later, an N₂ ligand coordinated to monomeric Mo(I)-N₂ complex, [Mo^I(L₃)(OTf)(N₂)₂], is not reactive with the proton donor (LutH⁺) and the activation free energy of the protonation of the N₂ ligand can be efficiently lowered by intermetallic electron transfer in Mo^I-N≡N-Mo⁰ structure. Because of the very low catalyst of **1** or **2** concentration in the reaction solution, monomeric Mo complex such as **D** in Figure 2-2 seems to have difficulty meeting another monomeric Mo complex to rebuild the dinuclear molybdenum complex for the next catalytic cycle. In this study, B3LYP-D3 results provide support that Mo(I)Mo(0)-N₂ complex **VII** should be maintained until the next protonation reaction.

2.3.3. Relationship between electronic structure and reactivity for protonation of dimolybdenum–N₂ complexes

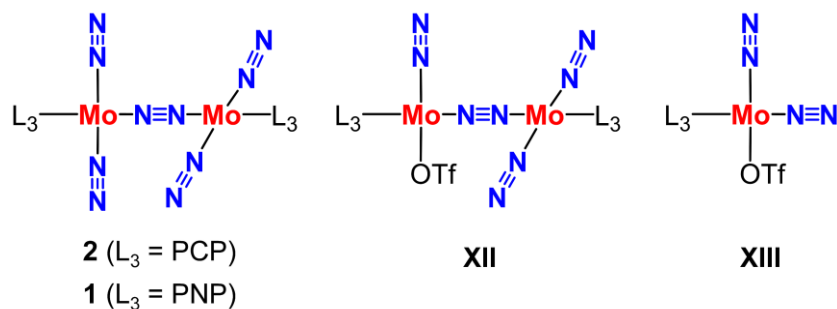
The dimolybdenum Mo–N≡N–Mo structure is essential for the protonation of a terminal N₂ ligand based on the previous DFT calculations on the catalytic mechanism for nitrogen fixation catalyzed by **1**. In other words, protonation of the N₂ ligands of [Mo⁰(PNP)(N₂)₃] **C** cannot proceed with LutH⁺. On the other hand, protonation of a terminal N₂ ligand in **1** can undergo endergonically with a lower activation energy.³⁰ In this study, a terminal N₂ ligand coordinated to the Mo^I–N≡N–Mo⁰ structure in **XII** was computed to be more reactive with LutH⁺ than **1** (**2**) with the Mo⁰–N≡N–Mo⁰ structure. In this section, the author compares the reactivity of the terminal N₂ ligand based on the geometric and electronic structures of dinuclear Mo(0)Mo(0)–N₂, Mo(I)Mo(0)–N₂, and monomeric Mo(I)–N₂ complexes **2**, **VII**, and **XIII** respectively. At first, the author examined the protonation of the axial N₂ ligand in Mo(I)–N₂ complex, *cis*-[Mo^I(L₃)(OTf)(N₂)₂] **XIII**, with LutH⁺. The reaction free energies of the proton transfer were endergonically computed to be +12.0 kcal mol⁻¹ (L₃ = PCP) and +9.8 kcal mol⁻¹ (L₃ = PNP), suggesting the axial N₂ ligand in the monomeric complex **XIII** is not easily protonated by LutH⁺. These DFT situations are very similar to the protonation of the corresting N₂ ligands of **1** and **C** (L₃ = PNP).³⁰

Table 2-2 presents a summary of the geometrical and electronic properties of **2** (**1**), **XII**, and **XIII** and reaction free energies of the protonation of them. Since the Mo–PCP and Mo–PNP systems showed nearly equal trends, the author focuses here on correlations among reactivity of N₂ ligand, geometry, and electronic structure about the Mo–PCP system. Comparing the N–N bond distance and Mayer bond order⁵³ of the terminal N₂ ligand between **2** and **XII**, it was found that the terminal N₂ ligand coordinated to the Mo(I) center is more reductively activated than that coordinated to the Mo(0) center, despite OTf⁻ in **XII** regarded as a strong electron-withdrawing group. The N–N bond distance of the N₂ ligand of **XII** is 0.010 Å longer, and the Mayer bond order is 0.12 lower than that in **2**. The fact that N₂ ligand of **XII** is significantly activated is supported by the charge of the N₂ ligand assigned by the natural population analysis (NPA).⁵⁴ The negative NPA charge on the N₂ ligand coordinated to a metal atom correlates well with the protonation reactivity of metal–N₂ complexes,⁵⁵⁻⁵⁷ since the N₂ ligand must

be protonated in the first step of nitrogen fixation. The N₂ ligand coordinated to the Mo(I) center in **XII** has a more negative NPA charge (−0.19) than that of the Mo(0) center in **2** (−0.09). This large difference in the NPA charge can be rationalized by shape of frontier orbitals of **C** and **XIII**. Figure 2-5 shows that the HOMO−1 of **C** and HOMO of **XIII** are assigned to π -backdonation from an out-of-plane *d* orbital of Mo center to a π^* orbital of the terminal N₂ ligand, activating the N≡N triple bond. The “excess” electrons on the Mo(0) center in **C** are shared to two axial N₂ ligands through the π -backdonation. On the other hand, the only one axial N₂ ligand in **XIII** can be provided a significant amount of the excess electrons because π -accepting capacity of the OTf group at the *trans* position to the axial N₂ ligand is almost nonexistent. The DFT computed results indicate that the electron-withdrawing OTf group plays as a weak π -acceptor and a positive factor in the activation of the terminal N₂ ligand.

The coordination of OTf[−] to the Mo(I) center can provide another advantage about the activation of coordinated N₂ when Mo(I)Mo(0)–N₂ complex **XII** with the imbalance between charges on the Mo centers is formed. Figure 2-6 describes the distribution of the NPA atomic charges in the optimized structures of **XII** and **XIII**. The total atomic charge of unit B (+0.23) in **XII** indicates electron (0.23 e[−]) transferring from unit B to unit A. The coordination of the electron-withdrawing OTf group to the Mo(I) center allows an electron-donating ability of the electron-rich Mo(0) unit in the Mo(I)Mo(0)–N₂ complex. The charges of the Mo^I(PCP)(N₂)₂ unit are assigned −0.36 for **XII** and −0.18 for **XIII**. Thus, the moving electrons (0.23 e[−]) to unit A in **XII** mainly locates on the Mo(I) center and N₂ ligands and utilized for further activation of the terminal N₂ ligand in unit A. The distribution of the moving electron can be relate to spatial distribution of the HOMO of **XII** shown in Figure 2-5.

Table 2-2. Free energy changes at 298 K (ΔG_{298}) for protonation of N₂ ligand in **2** (**1**), **XII**, and **XIII**, and their geometric and electronic properties



	PCP			PNP		
	2	XII	XIII	1	XII	XIII
ΔG_{298} for protonation of N ₂ /kcal mol ⁻¹ [a]	6.5	3.1 ^[b]	12.0	5.2	1.7 ^[b]	9.8
Mo–N ₂ distance /Å ^[a]	2.039	1.971 ^[b]	1.995	2.025	1.960 ^[b]	1.981
N–N distance /Å ^[a]	1.132	1.142 ^[b]	1.135	1.135	1.144 ^[b]	1.137
N–N bond order ^[a]	2.40	2.28 ^[b]	2.35	2.37	2.27 ^[b]	2.33
NPA charge on N ₂ /electrons ^[a]	-0.09	-0.19 ^[b]	-0.14	-0.10	-0.18 ^[b]	-0.15

[a] terminal or axial N₂ligand. [b] terminal N₂ ligand coordinated to the Mo(I) center.

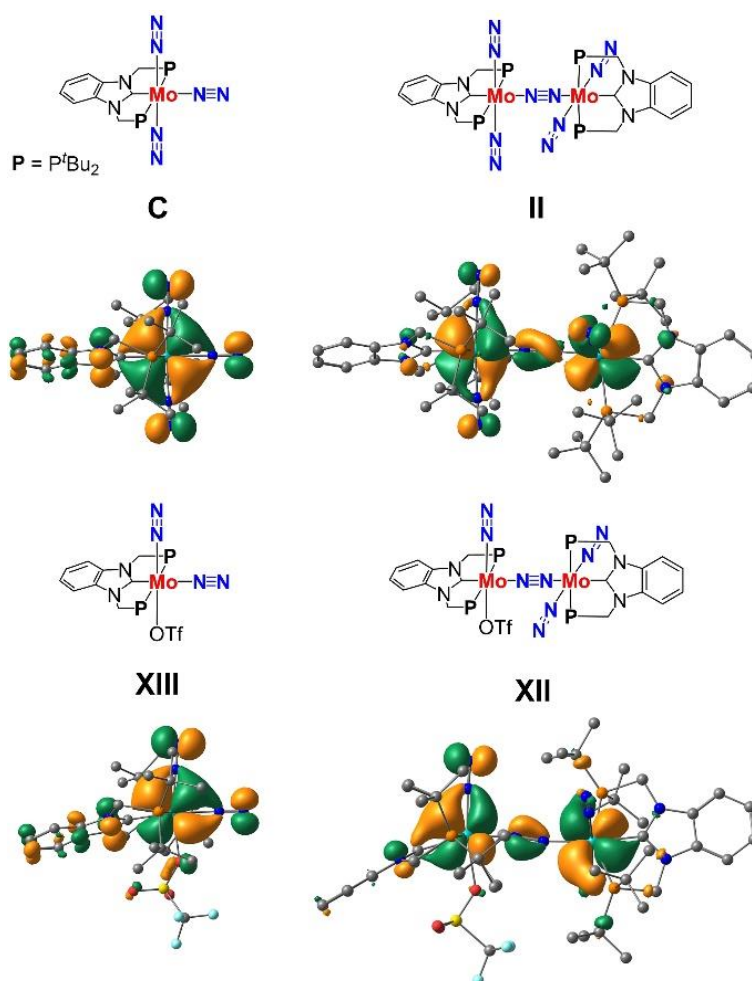


Figure 2-5. Spatial distribution of the HOMO-1 (C) and HOMO (2, XII, and XIII).

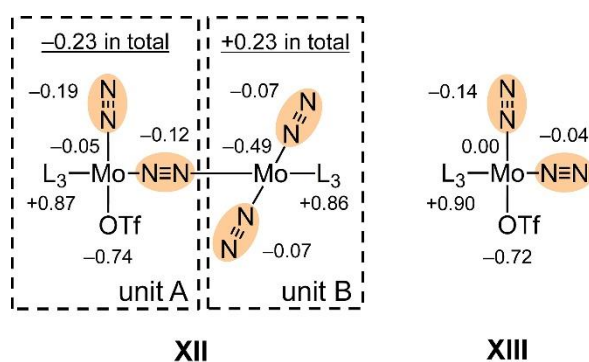
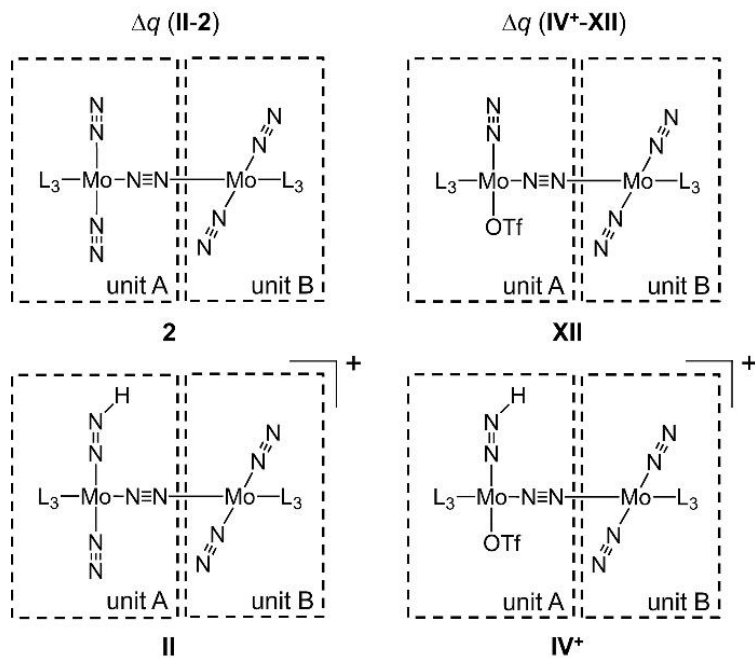


Figure 2-6. Distribution of the NPA charge in XII and XIII. The sum of atomic charges is separately obtained for the Mo atoms, the pincer ligand ($L_3 = PCP$), the OTf group, the terminal (axial) N_2 ligands, and the bridging (equatorial) N_2 ligands.

Yoshizawa group revealed that protonation of a terminal N₂ ligand in [$\{\text{Mo}^0(\text{PNP})(\text{N}_2)_2\}_2(\mu\text{-N}_2)$] **1** is caused by electron transfer between the $\text{Mo}^0\text{-N}\equiv\text{N-Mo}^0$ core via the bridging N₂ ligand, and thereby the terminal N₂ ligand is reductively activated for the protonation in the previous work.³⁰ This is the main reason why the $\text{Mo-N}\equiv\text{N-Mo}$ structure must be maintained at an early stage of the catalytic cycle in Figure 2-2. The author here discusses the synergetic effect of the two molybdenum centers in the protonation of $\text{PCP-Mo(0)Mo(0)-N}_2$ **2** and -Mo(I)Mo(0)-N_2 complexes **XII** from the viewpoint of the change in NPA charge of their MoMo-N_2 complexes and their protonated complexes, as well as the protonation of **1**.³⁰ Table 2-3 provides summaries of differences in the NPA charge (Δq) between the MoMo-N_2 complex and their protonated complexes. The difference in the total charge is +1 because one proton is added. Comparing the total charge between unit A and unit B provides insight into the role of the $\text{Mo}^0(\text{L}_3)(\text{N}_2)_2$ moiety as an electron-donating group driven by protonation with LutH^+ . In the protonation of the Mo(0)Mo(0)-N_2 complex **2**, the Δq in unit B (+0.40) implies that 0.40 electrons move from unit B to unit A during the protonation. On the other hand, in the protonation of **XII**, a more significant amount of electrons (0.48 e^-) is donated from unit B to unit A, despite 0.23 electrons have already relocated in **XII**. This extra electron donation during protonation can partially fix the formal charge imbalance between the Mo(II) and Mo(0) centers in **VI**⁺. Figure 2-5 describes that the HOMOs of **2** and **XII** are highly delocalized over *d* orbitals of the two Mo atoms and a distorted π orbital of the bridging N₂ ligand. This orbital delocalization would be responsible for the synergetic effect of the two Mo centers that boost the protonation reactivity of the terminal N₂ ligand.

Table 2-3. Differences in the NPA atomic charge (Δq) during the protonation of **II** and **XII** ($L_3 = \text{PCP}$)



	unit A	unit B	unit A	unit B
Mo	+0.38	+0.15	+0.25	+0.24
NNH	-0.06	—	+0.01	—
NN _{ter} ^a	+0.12	+0.05 ^c	—	+0.05 ^c
NN _{br} ^b	-0.11	—	-0.01	—
OTf	—	—	+0.03	—
L ₃	+0.27	+0.20	+0.24	+0.19
Total	+0.60	+0.40	+0.52	+0.48

^aterminal N₂ ligand. ^bbridging N₂ ligand. ^cthe sum of two N₂ ligands.

2.4. Conclusions

The author has performed DFT calculations to theoretically predict a plausible catalytic cycle for nitrogen fixation using dinitrogen-bridged dimolybdenum complexes bearing *N*-heterocyclic-carbene-based PCP (**2**) and pyridine-based PNP ligands (**1**). The author focused and computed the separation of the dimolybdenum structure of **2** (**1**) from a viewpoint of the reaction free energy. As a result, appropriate treatments of dispersion are strongly demanded to evaluate more realistic free energy profiles. The free energy profiles of the entire reaction pathway calculated at the B3LYP-D3 level of theory provided a more energetically efficient catalytic mechanism than the previous one proposed using **1** as a catalyst.³⁰ In the newly-proposed mechanism, the essential Mo–N≡N–Mo structure should be maintained during the entire catalytic cycle. Moreover, the author found the terminal N₂ ligand on the Mo(I) center is more reactive with a proton donor in Mo(I)Mo(0)–N₂ complex **XII** than that in the Mo(0)Mo(0)–N₂ complex **2** (**1**). Therefore, the author concluded that the newly-proposed reaction pathway does not require regeneration of **2** (**1**) for cycling the next catalytic cycle.

The terminal N₂ ligand on the Mo(I) center in Mo(I)Mo(0)–N₂ complex **XII** is more reductively activated than those in **2** (**1**) despite coordination of the strong electron-withdrawing OTf group to the Mo(I) center. The low π -accepting capability of the OTf group would be a key factor in the activation of N₂ ligand sharing the same metal center. The OTf group at the *trans* position to the terminal N₂ ligand does not weaken π -backdonation from Mo to N₂, which is essential for the coordination and activation of N₂. Moreover, the coordination of the OTf group at the Mo(I) center in the dimolybdenum complex **XII** brings out an electron-donating ability of the remaining Mo(0) center, resulting in further activation of N₂ at the Mo(I) center. The author has also observed intermetallic electron transfer between two Mo centers through the bridging N₂ ligand during the protonation of a terminal N₂ ligand. The approach of a proton to the terminal N₂ ligand in **2** (**1**) and **XII** induces electron donation from an Mo(0) center to the active site of the other Mo(0) or Mo(I) center, and thereby the protonation of N₂ is promoted as long as the Mo–N≡N–Mo structure is maintained.

The author wants to discuss here the origin of the high catalytic activity and long-

lived operation of the Mo–PCP complex **2** as a catalyst for nitrogen fixation. The free energy profiles of the entire reaction pathways starting from **2** and **1** showed almost the same trends, and thus the difference in catalytic performance between the Mo–PCP and Mo–PNP systems cannot be distinguished in the present mechanistic study. The author now concludes that the high catalytic activity of **2** is stemmed from the solid connection between the pincer ligand with the Mo center that prevents the catalyst from decomposition during the catalytic reaction, as previously proposed.²²

In further improvement of the catalytic performance of dimolybdenum complexes, there is a problem on the catalytic mechanism of nitrogen fixation using **1** and **2** as catalysts. The coordinated N₂ must be first protonated, although the protonation reaction is endergonic. A possible way to avoid this problem is to find a new catalytic system that realizes direct N≡N bond cleavage of the Mo–N≡N–Mo structure yielding two molecules of molybdenum-nitride complexes. Very recently, Yoshizawa and Nishibayashi groups have reported that Mo–trihalide complexes bearing PNP and PCP ligands such as [Mo^{III}I₃(PNP)] and [Mo^{III}Cl₃(PCP)] exhibited significantly high catalytic activity.^{9,24,25} In order to explain the high catalytic performance, the dimolybdenum Mo^IMo^I–halide species [Mo^I(PNP)X–N≡N–Mo^I(PNP)X] (X = halide) is considered to be a key intermediate that enables the direct N≡N bond cleavage. The author believes that synergetic experimental and computational investigations on the reactivity of dinitrogen-bridged dimolybdenum complexes will open a new way to the development of more effective catalysts for nitrogen fixation working under ambient reaction conditions.

References

1. Burgess, B. K.; Lowe, D. V. Mechanism of Molybdenum Nitrogenase. *Chem. Rev.* **1996**, *96*, 2983–3011.
2. Einsle, O.; Tezcan, F. A.; Andrade, S. L. S.; Schmid, B.; Yoshida, M.; Howard, J. B.; Rees, D. C. Nitrogenase MoFe-Protein at 1.16 Å Resolution: A Central Ligand in the FeMo-Cofactor. *Science* **2002**, *297*, 1696–1700.
3. Lancaster, K. M.; Roemelt, M.; Ettenhuber, P.; Hu, Y.; Ribbe, M. W.; Neese, F.; Bergmann, U.; DeBeer, S. X-ray Emission Spectroscopy Evidences a Central Carbon in the Nitrogenase Iron-Molybdenum Cofactor. *Science* **2011**, *334*, 974–977.
4. Hoffman, B. M.; Lukoyanov, D.; Yang, Z.-Y.; Dean, D. R.; Seefeldt, L. C. Mechanism of Nitrogen Fixation by Nitrogenase: The Next Stage. *Chem. Rev.* **2014**, *114*, 4041–4062.
5. Allen, A. D.; Senoff, C. V. Nitrogenopentammineruthenium(II) complexes. *Chem. Commun.* **1965**, *24*, 621–622.
6. H. Liu, *Ammonia Synthesis Catalyst: Innovation and Practice*, Chemical Industry Press & World Scientific, Singapore, **2013**.
7. For a recent review on transition metal-catalyzed formation of ammonia from dinitrogen, see Nishibayashi, Y. Development of catalytic nitrogen fixation using transition metal-dinitrogen complexes under mild reaction conditions. *Dalton Trans.* **2018**, *47*, 11290–11297.
8. Yandulov, D. V.; Schrock, R. R. Catalytic Reduction of Dinitrogen to Ammonia at a Single Molybdenum Center. *Science* **2003**, *301*, 76–78.
9. Ashida, Y.; Arashiba, K.; Nakajima, K.; Nishibayashi, Y. Molybdenum-Catalyzed Ammonia Production with Samarium Diiodide and Alcohols or Water. *Nature* **2019**, *568*, 536–540.

10. Doyle, L. R.; Wooles, A. J.; Jenkins, L. C.; Tuna, F.; McInnes, E. J. L.; Liddle, S. T. Catalytic Dinitrogen Reduction to Ammonia at a Triamideamine–Titanium Complex. *Angew. Chem. Int. Ed.* **2018**, *57*, 6314–6318; *Angew. Chem.* **2018**, *130*, 6422–6426.
11. Sekiguchi, Y.; Arashiba, K.; Tanaka, H.; Eizawa, A.; Nakajima, K.; Yoshizawa, K.; Nishibayashi, Y. Catalytic Reduction of Molecular Dinitrogen to Ammonia and Hydrazine Using Vanadium Complexes. *Angew. Chem. Int. Ed.* **2018**, *57*, 9064–9068; *Angew. Chem.* **2018**, *130*, 9202–9206.
12. Anderson, J. S.; Rittle, J.; Peters, J. C. Catalytic Conversion of nitrogen to ammonia by an iron model complex. *Nature* **2013**, *501*, 84–87.
13. Creutz, S. E.; Peters, J. C. Catalytic Reduction of N₂ to NH₃ by an Fe–N₂ Complex Featuring a C-Atom Anchor. *J. Am. Chem. Soc.* **2014**, *136*, 1105–1115.
14. Ung, G.; Peters, J. C. Low-Temperature N₂ to Two-Coordinate L₂Fe⁰ Enables Reductive Trapping of L₂FeN₂[−] and NH₃ Generation. *Angew. Chem. Int. Ed.* **2015**, *54*, 532–535; *Angew. Chem.* **2015**, *127*, 542–545.
15. Del Castillo, T. J.; Thompson, N. B.; Peters, J. C. A Synthetic Single-Site Fe Nitrogenase: High Turnover, Freeze-Quench ⁵⁷Fe Mossbauer Data, and a Hydride Resting State. *J. Am. Chem. Soc.* **2016**, *138*, 5341–5350.
16. Kuriyama, S.; Arashiba, K.; Nakajima, K.; Matsuo, Y.; Tanaka, H.; Ishii, K.; Yoshizawa, K.; Nishibayashi, Y. Catalytic Transformation of Dinitrogen into Ammonia and Hydrazine by Iron–Dinitrogen Complexes Bearing Pincer Ligand. *Nat. Commun.* **2016**, *7*, 12181.
17. Hill, P. J.; Doyle, L. R.; Crawford, A. D.; Myers, W. K.; Ashley, A. E. Selective Catalytic Reduction of N₂ to N₂H₄ by a Simple Fe Complex. *J. Am. Chem. Soc.* **2016**, *138*, 13521–13524.
18. Chalkley, M. J.; Del Castillo, T. J.; Matson, B. D.; Roddy, J. P.; Peters, J. C. Catalytic N₂-to-NH₃ Conversion by Fe at Lower Driving Force: A Proposed Role for Metallocene-Mediated PCET. *ACS Cent. Sci.* **2017**, *3*, 217–223.

19. Buscagan, T. M.; Oyala, P. H.; Peters, J. C. N₂-to-NH₃ Conversion by a Triphos–Iron Catalyst and Enhanced Turnover under Photolysis. *Angew. Chem. Int. Ed.* **2017**, *56*, 6921–6926; *Angew. Chem.* **2017**, *129*, 7025–7030.
20. Arashiba, K.; Miyake, Y.; Nishibayashi, Y. A Molybdenum Complex Bearing PNP-Type Pincer Ligands Leads to the Catalytic Reduction of Dinitrogen into Ammonia. *Nat. Chem.* **2011**, *3*, 120–125.
21. Arashiba, K.; Kinoshita, E.; Kuriyama, S.; Eizawa, A.; Nakajima, K.; Tanaka, H.; Yoshizawa, K.; Nishibayashi, Y. Catalytic Reduction of Dinitrogen to Ammonia by Use of Molybdenum–Nitride Complexes Bearing a Tridentate Triphosphine as Catalysts. *J. Am. Chem. Soc.* **2015**, *137*, 5666–5669.
22. Eizawa, A.; Arashiba, K.; Tanaka, H.; Kuriyama, S.; Matsuo, Y.; Nakajima, K.; Yoshizawa, K.; Nishibayashi, Y. Remarkable Catalytic Activity of Dinitrogen-Bridged Dimolybdenum Complexes Bearing NHC-Based PCP-Pincer Ligands toward Nitrogen Fixation. *Nat. Commun.* **2017**, *8*, 14874.
23. Arashiba, K.; Eizawa, A.; Tanaka, H.; Nakajima, K.; Yoshizawa, K.; Nishibayashi, Y. Catalytic Nitrogen Fixation via Direct Cleavage of Nitrogen–Nitrogen Triple Bond of Molecular Dinitrogen under Ambient Reactions. *Bull. Chem. Soc. Jpn.* **2017**, *90*, 1111–1118.
24. Eizawa, A.; Arashiba, K.; Egi, A.; Tanaka, H.; Nakajima, K.; Yoshizawa, K.; Nishibayashi, Y. Catalytic Reactivity of Molybdenum–Trihalide Complexes Bearing PCP-Type Pincer Ligands. *Chem. Asian J.* **2019**, *14*, 2091–2096.
25. Ashida, Y.; Arashiba, K.; Tanaka, H.; Egi, A.; Nakajima, K.; Yoshizawa, K.; Nishibayashi, Y. Molybdenum-Catalyzed Ammonia Formation Using Simple Monodentate and Bidentate Phosphines as Auxiliary Ligands. *Inorg. Chem.* **2019**, *58*, 8927–8932.

26. Ashida, Y.; Kondo, S.; Arashiba, K.; Kikuchi, T.; Nakajima, K.; Kakimoto, S.; Nishibayashi, Y. A Practical Synthesis of Ammonia from Nitrogen Gas, Samarium Dioxide and Water Catalyzed by a Molybdenum–PCP Pincer Complex. *Synthesis* **2019**, *51*, 3792–3795.
27. Fajardo, Jr., J.; Peters, J. C. Catalytic Nitrogen-to-Ammonia Conversion by Osmium and Ruthenium Complexes. *J. Am. Chem. Soc.* **2017**, *139*, 16105–16108.
28. Kuriyama, S.; Arashiba, K.; Tanaka, H.; Matsuo, Y.; Nakajima, K.; Yoshizawa, K.; Nishibayashi, Y. Direct Transformation of Molecular Dinitrogen into Ammonia Catalyzed by Cobalt Dinitrogen Complexes Bearing Anionic PNP Pincer Ligands. *Angew. Chem. Int. Ed.* **2016**, *55*, 14291–14293; *Angew. Chem.* **2016**, *128*, 14503–14507.
29. Kuriyama, S.; Arashiba, K.; Nakajima, K.; Tanaka, H.; Kamaru, N.; Yoshizawa, K.; Nishibayashi, Y. Catalytic Formation of Ammonia from Molecular Dinitrogen by Use of Dinitrogen-Bridged Dimolybdenum–Dinitrogen Complexes Bearing PNP-Pincer Ligands: Remarkable Effect of Substituent at PNP-Pincer Ligand. *J. Am. Chem. Soc.* **2014**, *136*, 9716–9731.
30. Tanaka, H.; Arashiba, K.; Kuriyama, S.; Sasada, A.; Nakajima, K.; Yoshizawa, K.; Nishibayashi, Y. Unique Behaviour of Dinitrogen-Bridged Dimolybdenum Complexes Bearing Pincer Ligand Towards Catalytic Formation of Ammonia *Nat. Commun.* **2014**, *5*, 3737.
31. Tanaka, H.; Nishibayashi, Y.; Yoshizawa, K. Interplay between Theory and Experiment for Ammonia Synthesis Catalyzed by Transition Metal Complexes. *Acc. Chem. Res.* **2016**, *49*, 987–995.
32. Tian, Y.-H.; Pierpont, A. W.; Batista, E. R. How Does Nishibayashi’s Molybdenum Complex Catalyze Dinitrogen Reduction to Ammonia? *Inorg. Chem.* **2014**, *53*, 4177–4183.

33. Grimme, S.; Antony, J.; Ehrlich, S.; Krieg, H. A Consistent and Accurate *Ab Initio* Parameterization of Density Functional Dispersion Correlation (DFT-D) for the 94 Elements H-Pu. *J. Chem. Phys.* **2010**, *132*, 154104.
34. M. J. Frisch *et al.* *Gaussian 09, Revision D.01*, Gaussian Inc., 2009.
35. Becke, A. D. Density-Functional Exchange-Energy Approximation with Correct Asymptotic Behavior. *Phys. Rev. A* **1988**, *38*, 3098–3100.
36. Becke, A. D. Density-Functional Thermochemistry. III. The Role of Exact Exchange. *J. Chem. Phys.* **1993**, *98*, 5648–5652.
37. Lee, C.; Yang, W.; Parr, R. G. Development of the Colle-Salvetti Correlation-Energy Formula into a Functional of the Electron Density. *Phys. Rev. B* **1988**, *37*, 785–789.
38. Vosko, S. H.; Wilk, L.; Nusair, M. Accurate Spin-Dependent Electron Liquid Correlation Energies for Local Spin Density Calculation: A Critical Analysis. *Can. J. Phys.* **1980**, *58*, 1200–1211.
39. Dolg, M.; Wedig, U.; Stoll, H.; Preuß, H. Energy-Adjusted *Ab Initio* Pseudopotentials for the First Row Transition Elements. *J. Chem. Phys.* **1987**, *86*, 866–872.
40. Andrae, D.; Häußermann, U.; Dolg, M.; Stoll, H.; Preuß, H. Energy-Adjusted *Ab Initio* Pseudopotentials for the Second and Third Row Transition Elements. *Theor. Chim. Acta* **1990**, *77*, 123–141.
41. Ditchfield, R.; Hehre, W. J.; Pople, J. A. Self-Consistent Molecular-Orbital Methods. IX. An Extended Gaussian-Type Basis for Molecular-Orbital Studies of Organic Molecules. *J. Chem. Phys.* **1971**, *54*, 724–728.
42. Hehre, W. J.; Ditchfield, R.; Pople, J. A. Self-Consistent Molecular-Orbital Methods. XII. Further Extensions of Gaussian-Type Basis Sets for Use in Molecular Orbital Studies of Organic Molecules. *J. Chem. Phys.* **1972**, *56*, 2257–2261.
43. Hariharan, P. C.; Pople, J. A. The Influence of Polarizations on Molecular Orbital Hydrogenation Energies. *Theor. Chim. Acta* **1973**, *28*, 213–222.

44. Francel, M. M.; Pietro, W. J.; Hehre, W. J.; Binkley, J. S.; Gordon, M. S.; DeFrees, D. J.; Pople, J. A. Self-consistent molecular orbital methods. XXIII. A polarization-type basis set for second-row elements. *J. Chem. Phys.* **1982**, *77*, 3654–3665.
45. Krishnan, R.; Binkley, J. S.; Seeger, R.; Pople, J. A. Self-consistent molecular orbital methods. XX. A basis set for correlated wave functions. *J. Chem. Phys.* **1980**, *72*, 650–654.
46. McLean, A. D.; Chandler, G. S. Contracted Gaussian basis sets for molecular calculations. I. Second row atoms, Z=11–18. *J. Chem. Phys.* **1980**, *72*, 5639–5648.
47. Clark, T.; Chandrasekhar, J.; Spitznagel, G. W.; Schleyer, P. V. R. Efficient Diffuse Function-Augmented Basis Sets for Anion Calculations. III. The 3-21G Basis Set for First-Row Elements, Li-F. *J. Comput. Chem.* **1983**, *4*, 294–301.
48. Tomasi, J.; Mennucci, B.; Cammi, R. Quantum Mechanical Continuum Solvation Models. *Chem. Rev.* **2005**, *105*, 2999–3094.
49. Reiher, M.; Salomon, O.; Hess, B. A. Reparameterization of Hybrid Functionals Based on Energy Differences of States of Different Multiplicity. *Theor. Chem. Acc.* **2001**, *107*, 48–55.
50. Reiher, M. Theoretical Study of the Fe(phen)₂(NCS)₂ Spin-Crossover Complex with Reparameterized Density Functionals. *Inorg. Chem.* **2002**, *41*, 6028–6935.
51. Grimme, S. Density Functional Theory with London Dispersion Corrections. *WIREs Comput. Mol. Sci.* **2011**, *1*, 211–228.
52. N. Mézailles in *Transition Metal-Dinitrogen Complexes* (Ed.: Y. Nishibayashi), Wiley-VCH, Weinheim, **2019**, pp. 221–269.
53. Mayer, I. Charge, Bond Order and Valence in the *Ab Initio* SCF Theory. *Chem. Phys. Lett.* **1983**, *97*, 270–274.
54. D. Glendening, J. K. Badenhoop, A. E. Reed, J. E. Carpenter, J. A. Bohmann, C. M. Morales, C. R. Landis, F. Weinhold, *NBO 6.0*, Theoretical Chemistry Institute, University of Wisconsin, Madison, 2013.

55. Studt, F.; Tuzek, F. Theoretical, Spectroscopic, and Mechanistic Studies on Transition-Metal Dinitrogen Complexes: Implications to Reactivity and Relevance to the Nitrogenase Problem. *J. Comput. Chem.* **2006**, *27*, 1278–1291.
56. Habeck, C. M.; Lehnert, N.; Näther, C.; Tuzek, F. Mo/W–N₂ and –N₂H₂ Complexes with *trans* Nitrile Ligands: Electronic Structure, Spectroscopic Properties and Relevance to Nitrogen Fixation. *Inorg. Chim. Acta* **2002**, *337*, 11–31.
57. Tanaka, H.; Ohsako, F.; Seino, H.; Mizobe, Y.; Yoshizawa, K. Theoretical Study on Activation and Protonation of Dinitrogen on Cubane-Type M₃S₄ Cluster. (M = V, Cr, Mn, Fe, Co, Ni, Cu, Mo, Ru, and W) *Inorg. Chem.* **2010**, *49*, 2464–2470.

Supporting Information

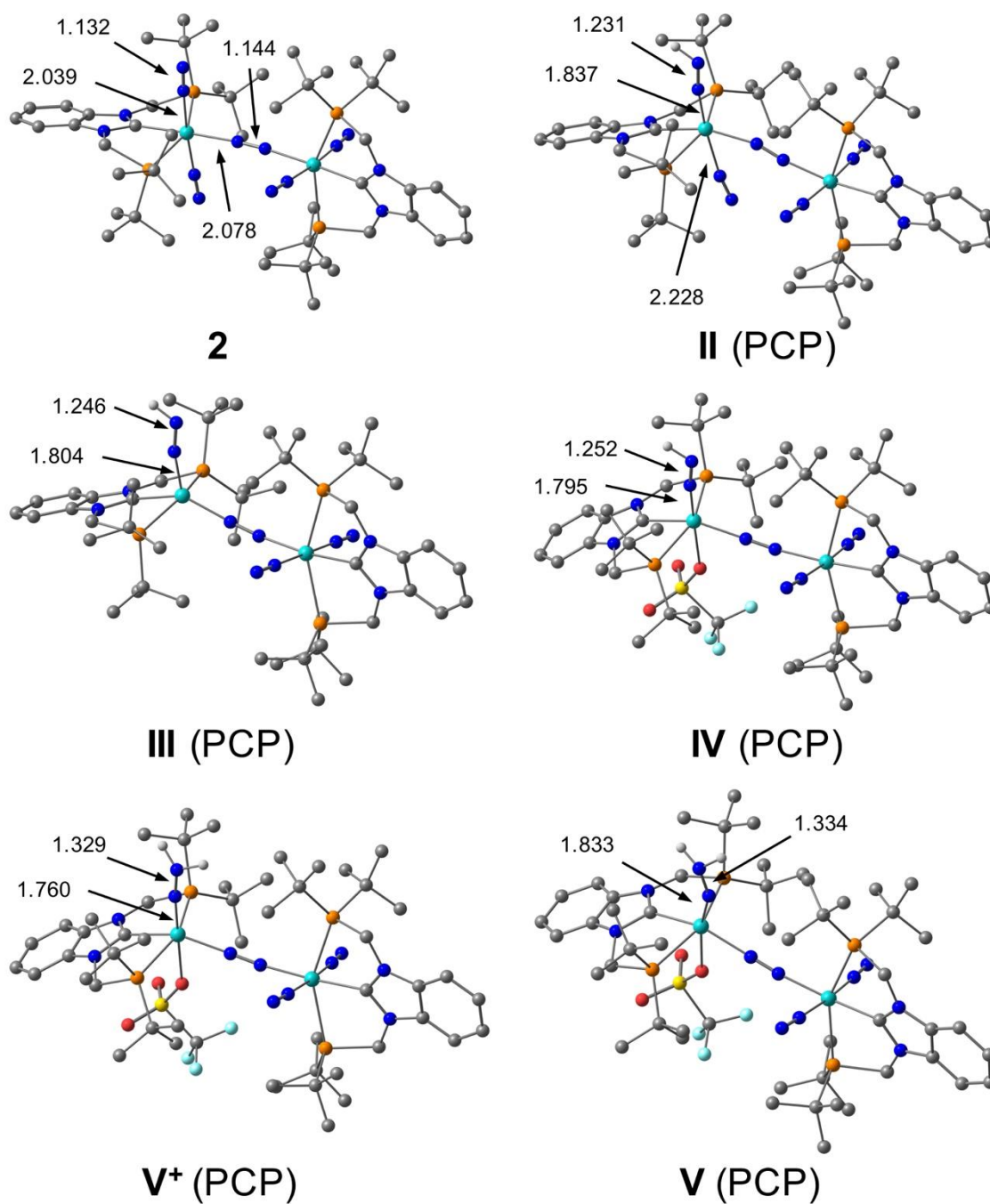
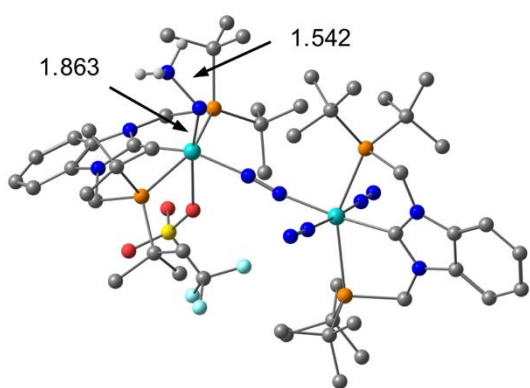
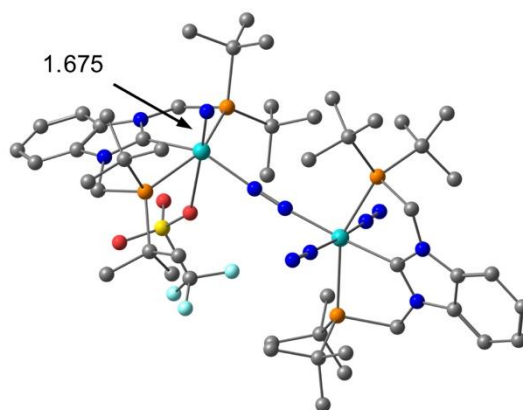


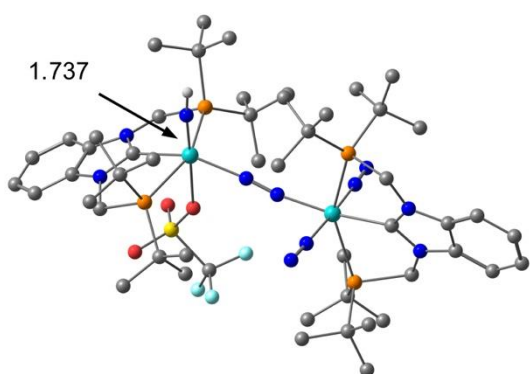
Figure S2-1. Optimized structures and selected geometric parameters of dinitrogen complex **2** and intermediates **II-XIII** (PCP). All hydrogen atoms attached to carbon atoms are omitted for clarity.



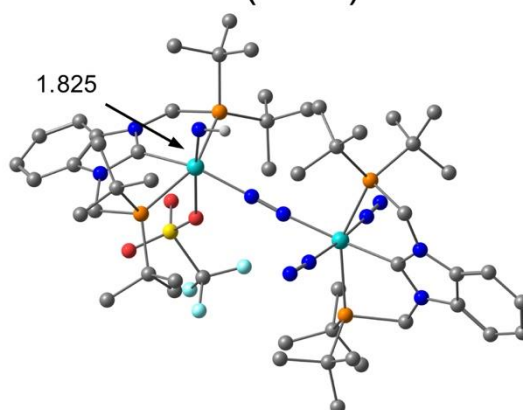
VI (PCP)



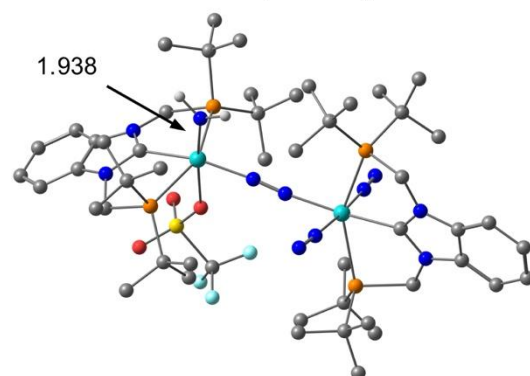
VII (PCP)



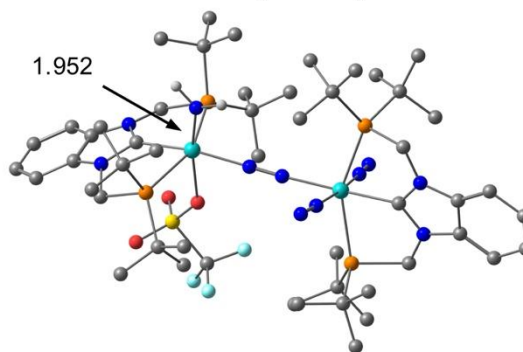
VIII⁺ (PCP)



VIII (PCP)

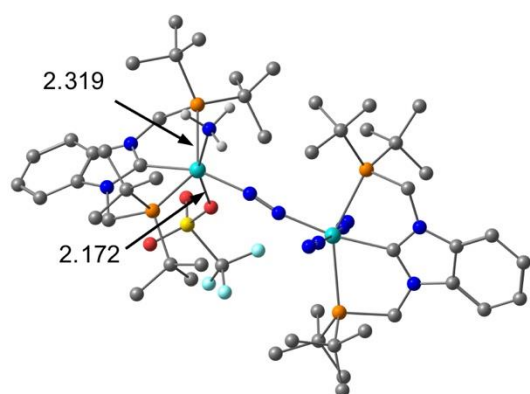


IX⁺ (PCP)

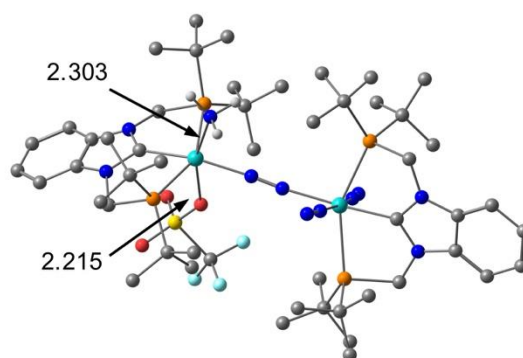


IX (PCP)

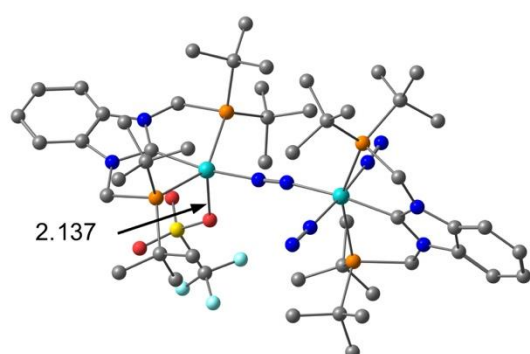
Figure S2-1. (Continued)



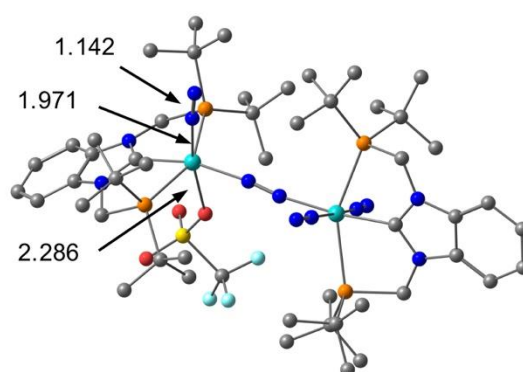
X⁺ (PCP)



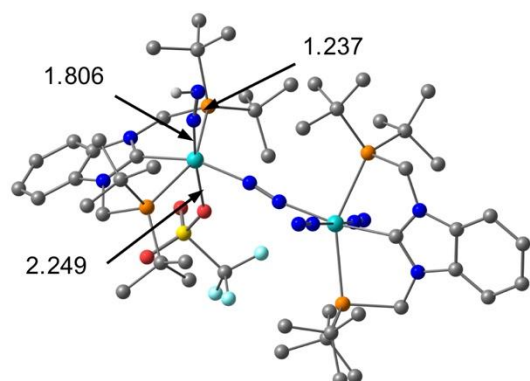
X (PCP)



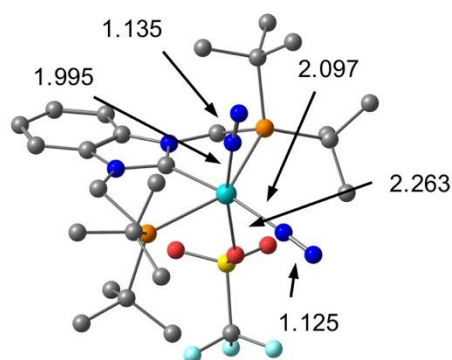
XI (PCP)



XII (PCP)



IV⁺ (PCP)



XIII (PCP)

Figure S2-1. (Continued)

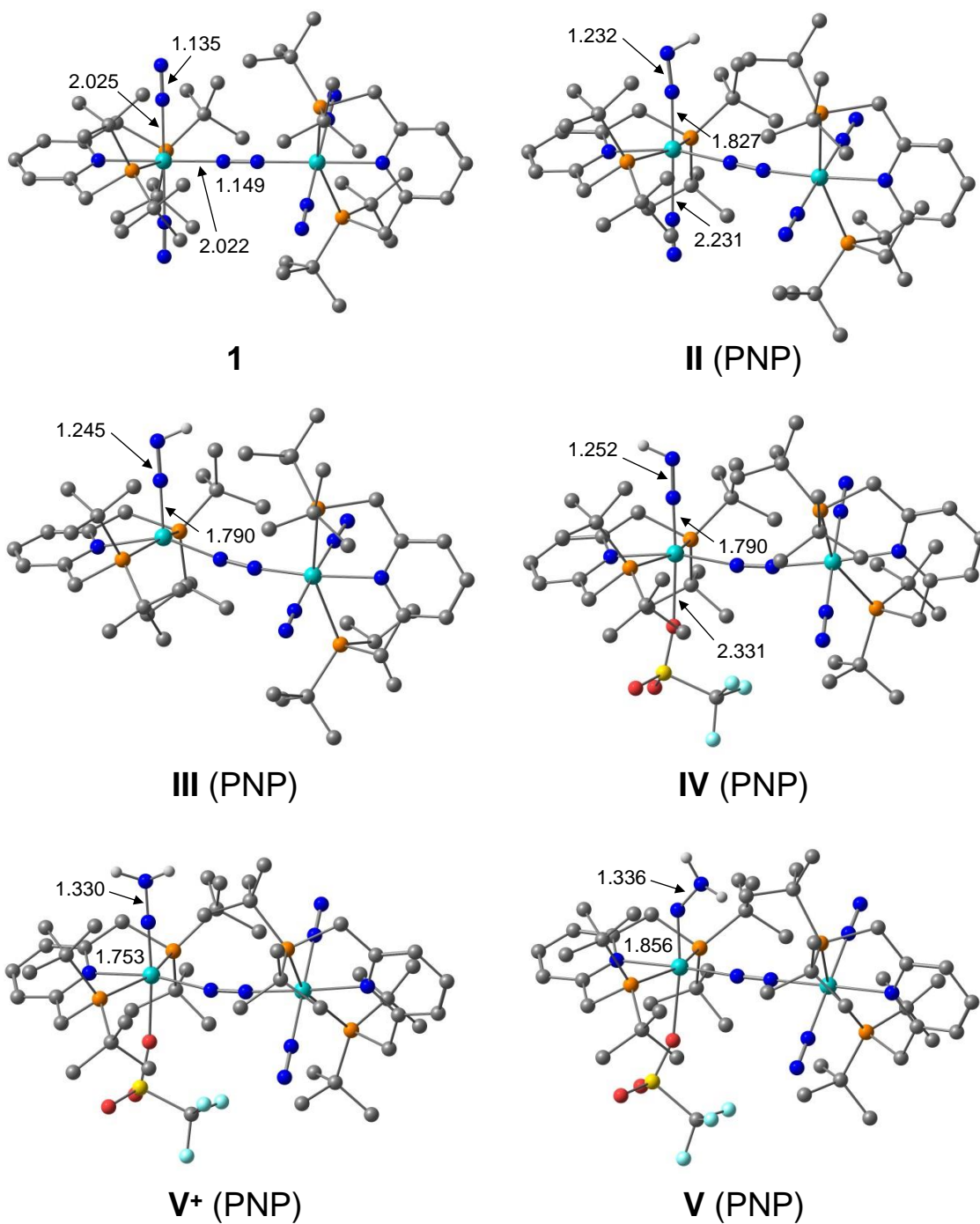
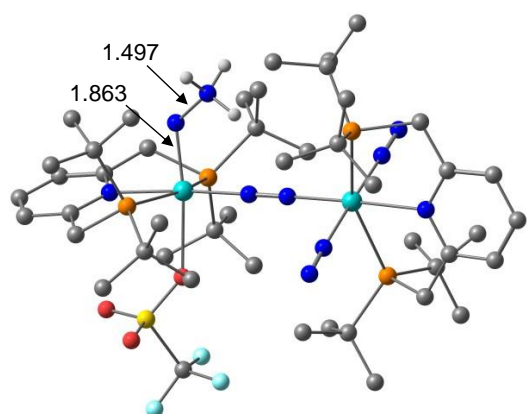
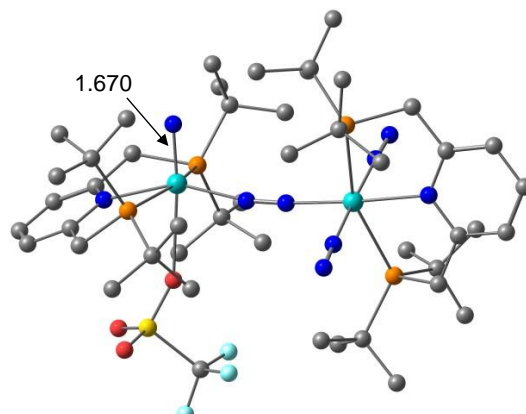


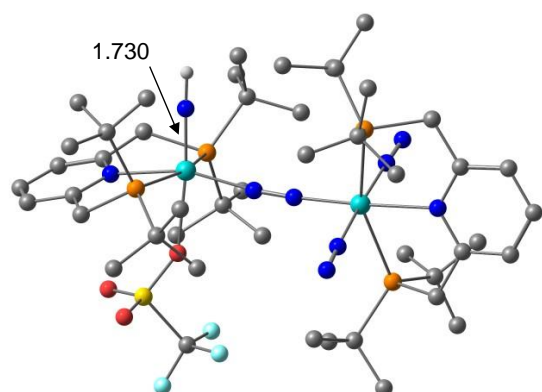
Figure S2-2. Optimized structures and selected geometric parameters of dinitrogen complex **1** and intermediates **II-XIII** (PNP). All hydrogen atoms attached to carbon atoms are omitted for clarity.



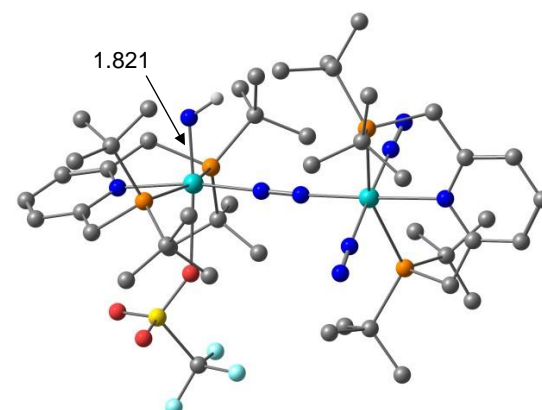
VI (PNP)



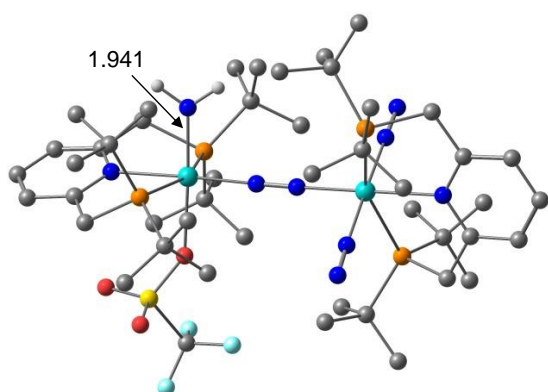
VII (PNP)



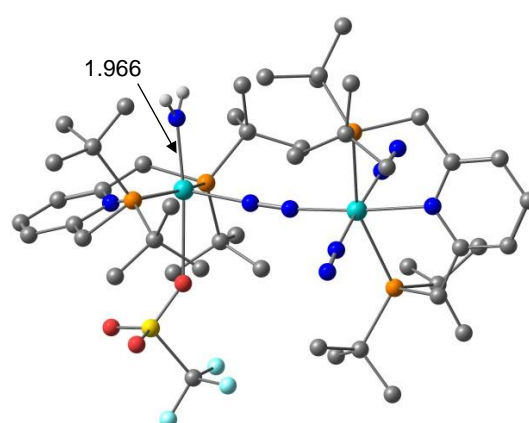
VIII⁺ (PNP)



VIII (PNP)

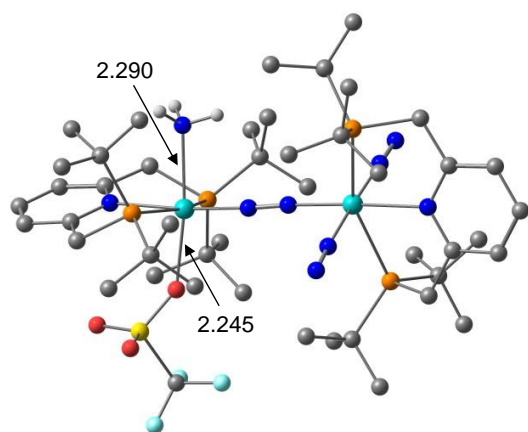


IX⁺ (PNP)

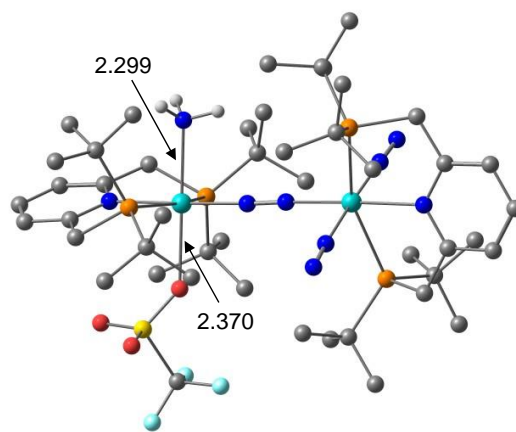


IX (PNP)

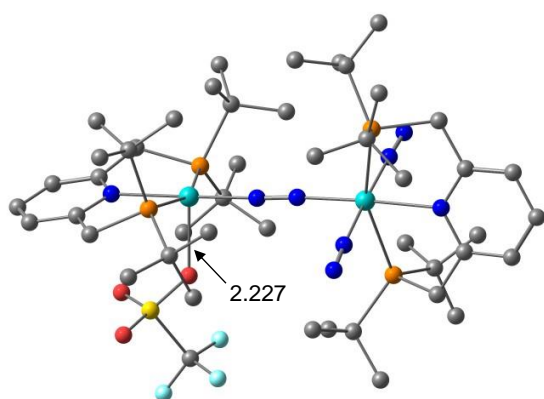
Figure S2-2. (Continued)



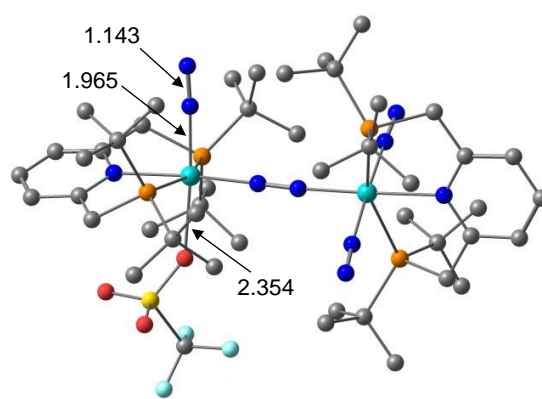
X⁺ (PNP)



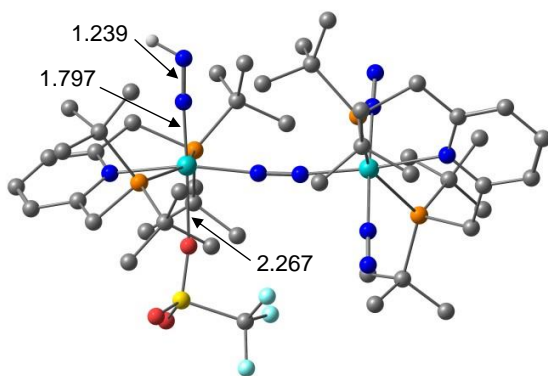
X (PNP)



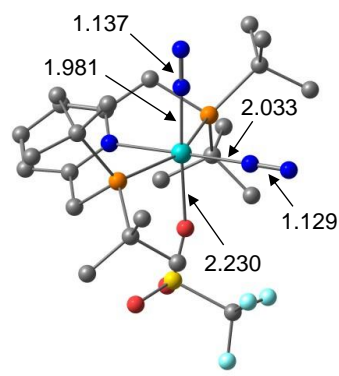
XI (PNP)



XII (PNP)



IV⁺ (PNP)



XIII (PNP)

Figure S2-2. (Continued)

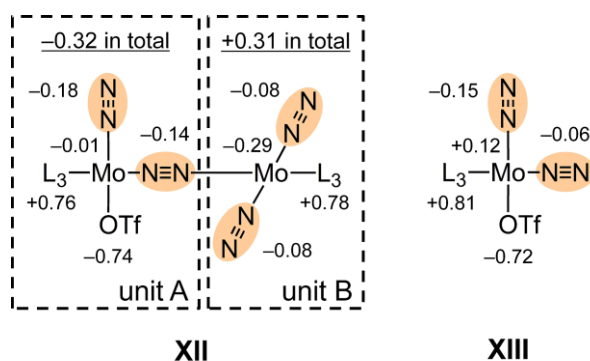
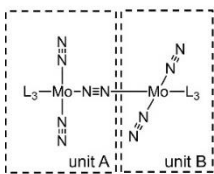
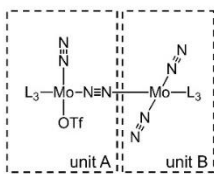


Figure S2-3. Distribution of the NPA atomic charge in **XII** and **XIII** ($L_3 = \text{PNP}$). The sum of atomic charges are separately obtained for the Mo atoms, the pincer ligand L_3 , the OTf group, the terminal (axial) N_2 ligands, and the bridging (equatorial) N_2 ligands.

Table S2-1. Differences in the NPA atomic charge (Δq) during the protonation of **1** and **XII** ($L_3 = \text{PNP}$)

Δq (II-I)		Δq (IV ⁺ -XII)		Δq (II-I)		Δq (IV ⁺ -XII)		
				unit A	unit B	unit A	unit B	
	1		XII	Mo	+0.37	+0.12	+0.37	+0.12
				NNH	-0.05	–	-0.04	–
				NN _{ter} ^[a]	+0.16	+0.06 ^[c]	–	+0.10 ^[c]
				NN _{br} ^[b]	-0.07	–	+0.02	–
				OTf	–	–	+0.03	–
				L ₃	+0.24	+0.17	+0.23	+0.17
				Total	+0.65	+0.35	+0.61	+0.39

Chapter 3

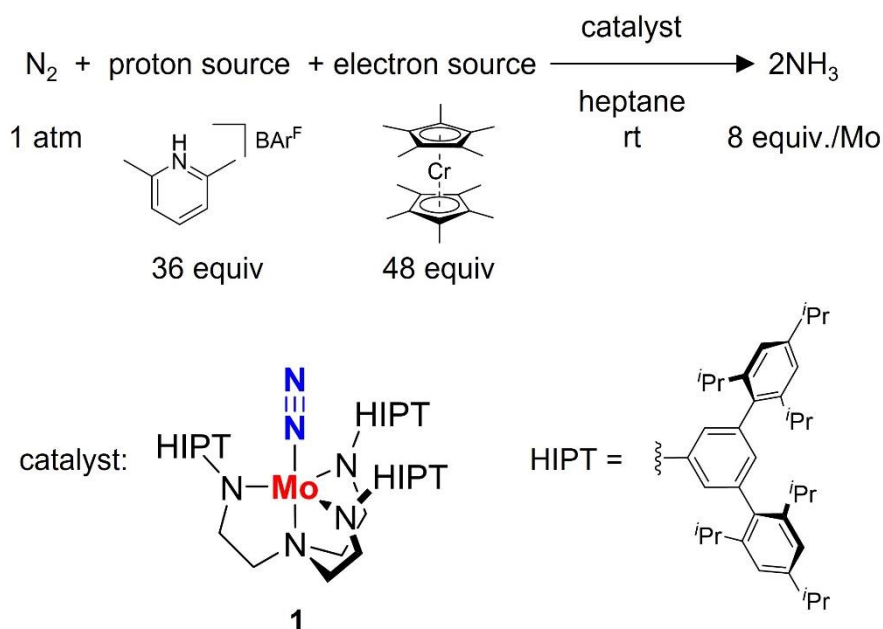
Relationship between Electronic Structure and Nitrogen Fixation Reaction Pathway of Dimolybdenum Complexes

3.1. Introduction

Nitrogen fixation converts ammonia (NH_3) from dinitrogen (N_2) and is regarded as an important process chemically and biologically. In industrial process, NH_3 is produced using the Haber-Bosch process. However, the molecule of N_2 is chemically inert; therefore, the Haber-Bosch process employs an iron-based catalyst under harsh reaction conditions of high temperature (300–500 °C) and high pressure (100–200 atm).¹ On the other hand, in natural process, the catalytic conversion of NH_3 from atmospheric N_2 proceeds on $\text{MoFe}_7\text{S}_9\text{C}$ iron-sulfur cluster, called FeMo-cofactor, in the active sites of certain bacterial metalloenzymes ($\text{N}_2 + 8\text{H}^+ + 8\text{e}^- \rightarrow 2\text{NH}_3 + \text{H}_2$).² The FeMo-cofactor structure is considered an attractive model for molecular catalysts for nitrogen fixation. In 2003, Yandulov and Schrock reported the first example of a metal-dinitrogen molecular complex as a catalyst for the conversion of NH_3 from N_2 in the presence of a proton source and an electron source under mild reaction conditions.³ They used the monomeric Mo(III)-N_2 complex $[\text{HIPTN}_3\text{N}]\text{Mo}^{\text{III}}(\text{N}_2)$ **1** using a tetradentate cage-type triamidoamine ligand $[\text{HIPTN}_3\text{N}]^{3-}$ ($= (3,5-(2,4,6-i\text{-Pr}_3\text{C}_6\text{H}_2)_2\text{C}_6\text{H}_3\text{NCH}_2\text{CH}_2)_3\text{N}^{3-}$) and demonstrated a catalytic reaction using **1** under mild reaction conditions in the presence of $[\text{LutH}]\text{BAr}^{\text{F}}_4$ as a proton source and CrCp^*_2 as an electron source ($\text{Lut} = 2,6$ -dimethylpyridine, $\text{BAr}^{\text{F}}_4 = \text{B}(3,5-(\text{CF}_3)_2\text{C}_6\text{H}_3)_4$, $\text{Cp}^* = \eta^5\text{-C}_5(\text{CH}_3)_5$) (Scheme 3-1), where up to 8 equiv. of NH_3 were produced based on the Mo center. The catalytic mechanism, deduced from the isolation and characterization of reaction intermediates, has been named the Yandulov-Schrock cycle (Figure 3-1, left).³ The cycle describes that stepwise protonation and reduction proceed on the Mo module $[\text{HIPTN}_3\text{N}]\text{Mo}$ for the conversion. Since this report, much experimental and theoretical work has been conducted on artificial

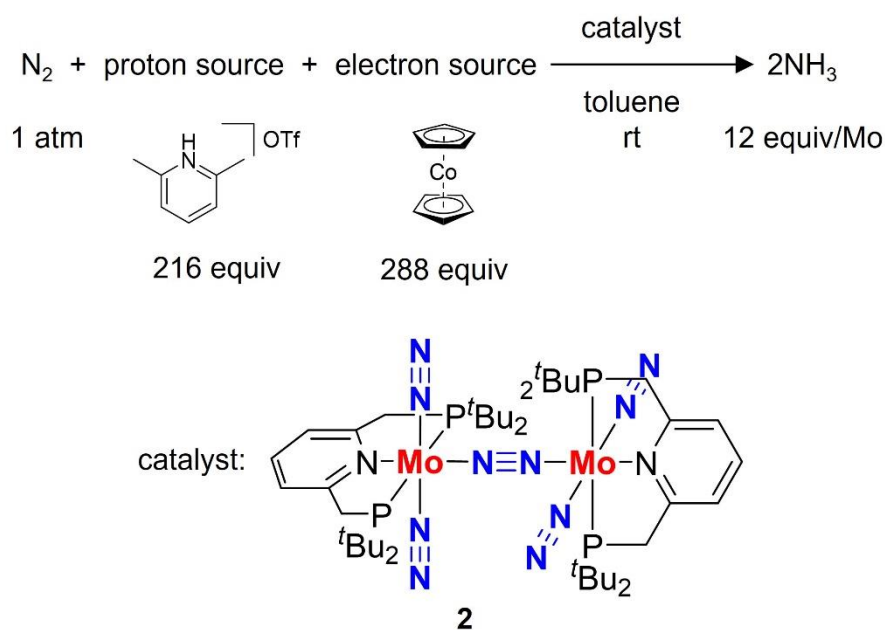
nitrogen fixation systems using molecular catalysts. The conversion of N_2 from N_2 catalyzed by transition metal– N_2 complexes proceeds in the presence of proton sources and electron sources ($\text{N}_2 + 6\text{H}^+ + 6\text{e}^- \rightarrow 2\text{NH}_3$). Complexes containing titanium,⁴ vanadium,⁵ iron,⁶⁻¹³ molybdenum,¹⁴⁻²³ ruthenium,²⁴ osmium,²⁴ cobalt,²⁵ and rhenium²⁶ as transition metals have been reported to catalyze the NH_3 production. Among these complexes, N_2 -bridged dimolybdenum complexes have presented excellent catalytic activity.

Scheme 3-1. Catalytic formation of ammonia from dinitrogen using **1** as a catalyst.



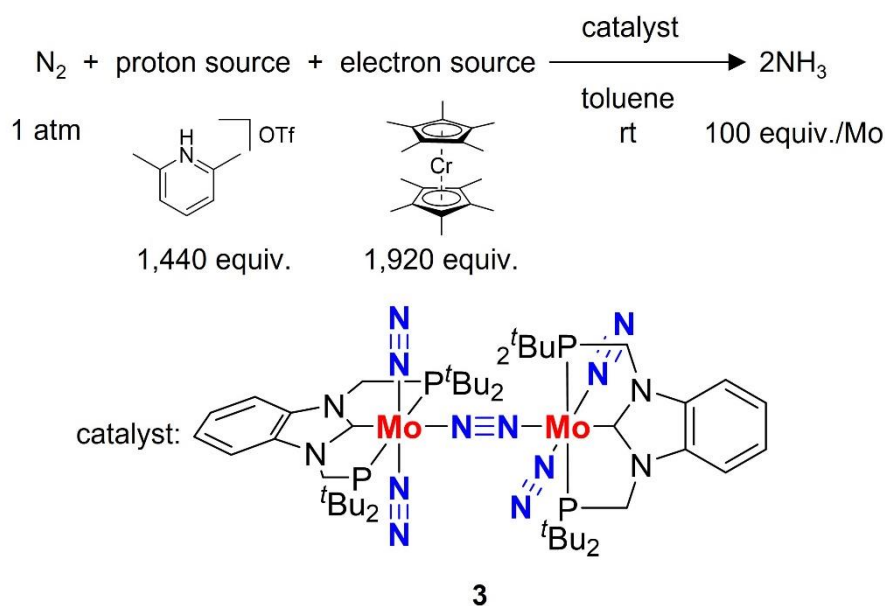
In 2011, Nishibayashi and coworkers succeeded in preparing an N₂-bridging Mo(0)Mo(0)–N₂ complex bearing a phosphine- and pyridine-based PNP-type tridentate pincer ligand [$\{\text{Mo}^0(\text{PNP})(\text{N}_2)_2\}_2(\mu\text{-N}_2)$] **2** (PNP = 2,6-bis(di-*tert*-butylphosphinomethyl)pyridine), and demonstrated the catalytic conversion of up to 12 equiv. of ammonia based on the Mo center using **2** (Scheme 3-2).¹⁴ The N₂ ligands of complex **2** can be recognized as two types from the coordination pattern: terminal (η^1) and bridging ($\mu\text{-}\eta^1\text{:}\eta^1$). Complex **2** has four terminal and one bridging dinitrogen ligands. In a proposed catalytic cycle using **2** describes the conversion of two equiv. of NH₃ from one of the terminal N₂ ligand following the Yandulov-Schrock cycle. The first protonation of the terminal N₂ ligand is considered the hardest step to proceed due to the chemical inactivity of the N₂ ligand in the catalytic cycle. The Mo–N≡N–Mo core of **2** should be important to promote the first protonation.

Scheme 3-2. Catalytic formation of ammonia from dinitrogen using dinitrogen-bridging dimolybdenum complex **2** as a catalyst.



Nishibayashi and coworkers further engineered phosphine- and *N*-heterocyclic carbene (NHC)-based PCP pincer ligand to prepare N₂-bridging Mo(0)Mo(0)-N₂ complex [{Mo⁰(PCP)(N₂)₂}₂(μ-N₂)] **3** (PCP = 1,3-((di-*tert*-butylphosphino)methyl)benzimidazole-2-ylidene). Complex **3** has a higher catalytic activity to produce up to 100 equiv. of NH₃ based on the Mo center under mild reaction conditions in the presence of [LutH]OTf as a proton source and CrCp*₂ as a reductant (Scheme 3-3).¹⁶ In general, the NHC moiety of the PCP ligands serves a stronger σ-donating ability than the pyridine moiety of the PNP ligand. In addition, density functional theory (DFT) calculations revealed that the NHC moiety has also π-backdonating ability from the Mo center.¹⁶ Therefore, about the PCP ligand, the combination of strong σ-donating and π-accepting abilities create a solid Mo-C bond to enhance its catalytic activity.

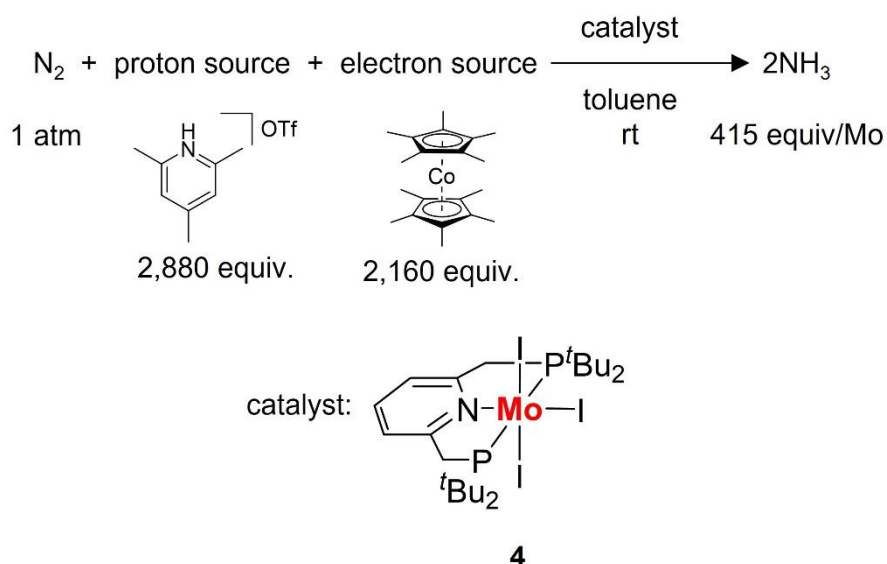
Scheme 3-3. Catalytic formation of ammonia from dinitrogen using dinitrogen-bridging dimolybdenum complex **3** as a catalyst.



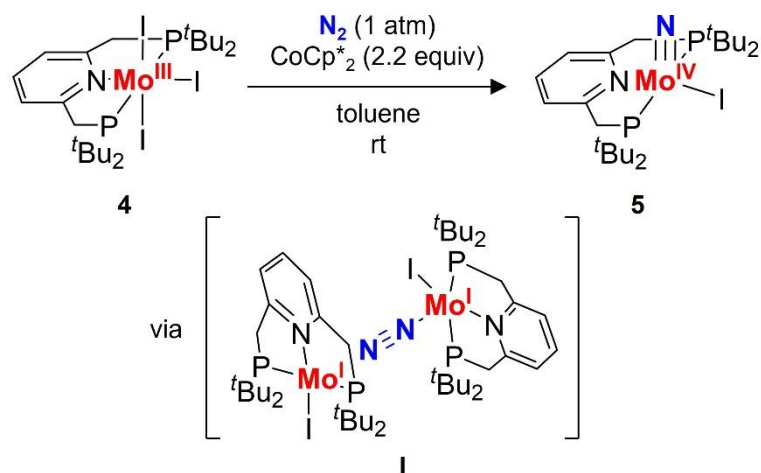
Subsequently, Nishibayashi and coworkers claimed that significant amount of NH₃ was afforded catalytically using the molybdenum-triiodide complex bearing the PNP ligand, [Mo^{III}I₃(PNP)] **4** (Scheme 3-4) under mild conditions in the presence of [ColH]OTf as a proton source and CoCp*₂ as an electron source (Col = 2,4,6-trimethylpyridine), in which up to 415 equiv. of NH₃ were produced.¹⁷ In this catalytic

reaction, the two-electron reduction of **4** with atmospheric N₂ is able to afford Mo(IV)–nitride complex, [Mo^{IV}(PNP)I(≡N)] **5** (Scheme 3-5). This stoichiometric experiment suggested that **5** may be formed via dinitrogen-bridging dimolybdenum intermediate, [{Mo^II(PNP)}₂(μ-N₂)] **I**. It is an unique point that the bridging N≡N bond of **I** is allowed to cleave. The conventional Yandulov-Schrock cycle do not include the N≡N bond cleavage. The N≡N bond cleavage should shorten the Yandulov-Schrock cycle, improving the catalytic activity of **4** (Figure 3-1; right).

Scheme 3-4. Catalytic formation of ammonia from dinitrogen using complex **4** as a catalyst.

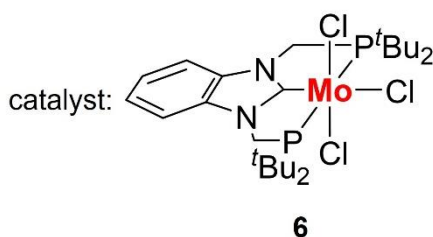
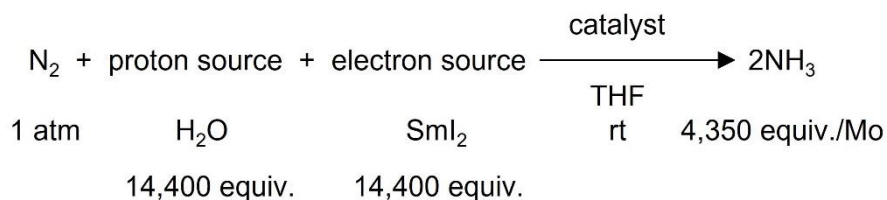


Scheme 3-5. Reduction of **4** with CoCp*₂.



Recently, a significant increase in the catalytic activity was documented using Mo(III)–trichloride complex, $[\text{Mo}^{\text{III}}\text{Cl}_3(\text{PCP})]$ **6**, in the presence of H_2O as a proton source and $\text{Sm}(\text{II})$ –diiodide (SmI_2) as an electron source, in which up to 4,350 equiv. of NH_3 were produced based on Mo center of **6** (Scheme 3-6).¹⁹ Compared to the previous catalytic reaction system using **4** shown in Scheme 3-4, the combination of proton and electron sources has changed from that of pyridine-conjugated acids, such as $[\text{LutH}]\text{OTf}$, and metallocenes. Therefore, the new combination of proton and electron sources may have led to a significant improvement in catalytic reaction.

Scheme 3-6. Catalytic formation of ammonia from dinitrogen using complex **6** as a catalyst in the presence of SmI_2 and H_2O .



The Mo–N≡N–Mo central structure in the dimolybdenum complexes or intermediates is thought to have an essential role in the activation of the N₂ ligands, such as protonation and reduction of a terminal N₂ ligand (Figure 3-1, left), and the direct N–N bond cleavage of a bridging N₂ ligand (Figure 3-1, right).¹⁷ The electronic property of Mo–N≡N–Mo structure should dominate the catalytic reaction pathway. Fryzuk and coworkers have qualitatively discussed that the orbital interactions of the end-on binding N₂ ligands to Mo centers.²⁷ Their discussion is helpful for qualitatively understanding the electronic property of Mo–N≡N–Mo structure. In this chapter, the author would like to firstly discuss the molecular orbitals (MOs) of the molecule of N₂. Next, the author will explain the interaction between Mo center and N₂ ligand about monomeric and dimeric Mo complexes and its role that varies with the electron number in Mo–N≡N–Mo structure. Finally, the author will describe the Yandulov-Schrock cycle (Figure 3-1; right) and its shortcut cycle (Figure 3-1; left) based on the results obtained by DFT calculations.

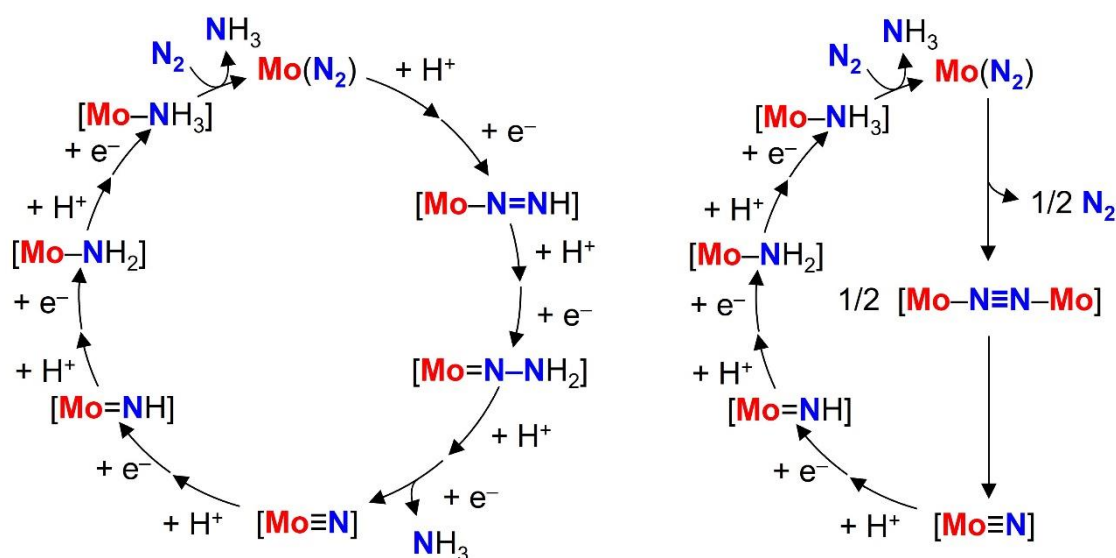


Figure 3-1. Proposed reaction intermediates for the conversion of dinitrogen to ammonia catalyzed by molybdenum complexes in the Yandulov–Schrock cycle (left) and in a shortcut cycle by direct N≡N bond cleavage of the bridging dinitrogen ligand (right).

3.2. Molecular Orbital of Dinitrogen (N₂)

Firstly, let us consider the N₂ molecule from the perspective of MO theory. MOs of N₂ are composed of two atomic orbitals (AOs) of N atom (mainly 2s and 2p as valence orbitals). The neutral N atom has a total of five electrons occupying the 2s and 2p orbitals. As a result of the interaction of the AOs of two N atoms, 10 MOs of N₂ molecule can be considered as shown in Figure 3-2. The electron configuration of the ground state N₂ molecule with 10 valence electrons is described as $(1\sigma_g)^2(2\sigma_u^*)^2(1\pi_u)^4(3\sigma_g)^2$, in which the asterisk * marks the antibonding orbitals of the N≡N bond. In particular, the $4\sigma_u^*$ orbital contributes to the σ -antibonding interaction of the N≡N bond and has a very high orbital energy. This is one of the reasons why the N₂ molecule is chemically stable from a viewpoint of the MO theory. The bond order of the N₂ molecule is easily counted to be $(8 - 2)/2 = 3$, where 8 is the number of electrons occupying bonding orbitals ($1\sigma_g$, $1\pi_u$, and $3\sigma_g$) and 2 is the number of electrons occupying an antibonding orbital ($2\sigma_u^*$). If the unoccupied $2\pi_g^*$ and $4\sigma_u^*$ orbitals are fully occupied by the 6 additional electrons, then the bond order is equal to 0, i.e., the chemical bond of N₂ is broken completely, yielding 2 equiv. of nitride (N³⁻).

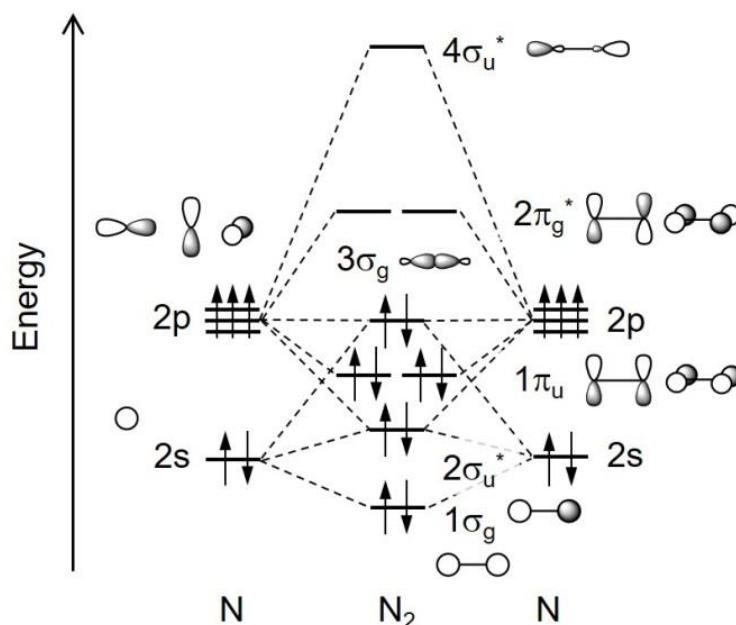


Figure 3-2. Qualitative orbital interaction diagram of N₂ constructed by atomic orbitals of two N atoms.

3.3. Orbital Interaction between Terminal N₂ Ligand and Mo Center

When the N₂ ligand coordinates to one low-valent Mo(0) or Mo(I) center in the η^1 style, π -backdonation from the d orbital of the Mo center to the $2\pi_g^*$ orbitals of the N₂ ligand and σ -donation from the $3\sigma_g$ orbital of the N₂ ligand to the d orbital of the Mo center are performed. The N₂ ligand plays as a σ -donor and a π -acceptor due to the occupied $3\sigma_g$ and unoccupied $2\pi_g^*$ orbitals. The π -backdonation strengthens the coordination bond of the Mo–N₂ moiety and weakens the N≡N triple bond. As a result, the N₂ ligand is reductively activated due to the negative charge on the N₂ ligand of Mo–N₂ and the longer N≡N bond than those of N₂ molecule.

The degree of reductive activation depends on the number of the π -accepting N₂ ligands sharing d orbitals of an Mo center. Figure 3-3 depicts a qualitative orbital interaction diagram highlighting the π -interactions between the Mo center and one or two N₂ ligands of Mo–N₂ and N₂–Mo–N₂ structure. Here, we are able to decompose the π -orbitals of the former Mo–N₂ structure to the d orbital of the Mo center and $2\pi_g^*$ orbital of the N₂ ligand. About the later N₂–Mo–N₂ structure, the π -orbitals are similarly decomposed to the π -orbitals of N₂–Mo, which is equal to the former Mo–N₂ structure, and $2\pi_g^*$ of the N₂ ligand. In the Mo–N₂ core structure, strong π -backdonation occurs because of the small energy gap ΔE between the π -donor and π -acceptor orbitals, as shown in Figure 3-3. On the other hand, in the N₂–Mo–N₂ core structure, weak π -backdonation to each N₂ ligand because of the large energy gap ΔE . The orbital energy of the π -donor fragment, N₂–Mo, is lower than that of a bare Mo atom. The effect of the π -backdonation from one Mo center to two and more terminal N₂ ligands will be smaller than that to only one terminal N₂ ligand. Therefore, to achieve strong π -backdonation to the only one terminal N₂ ligand, it is necessary to detach the other N₂ ligands.

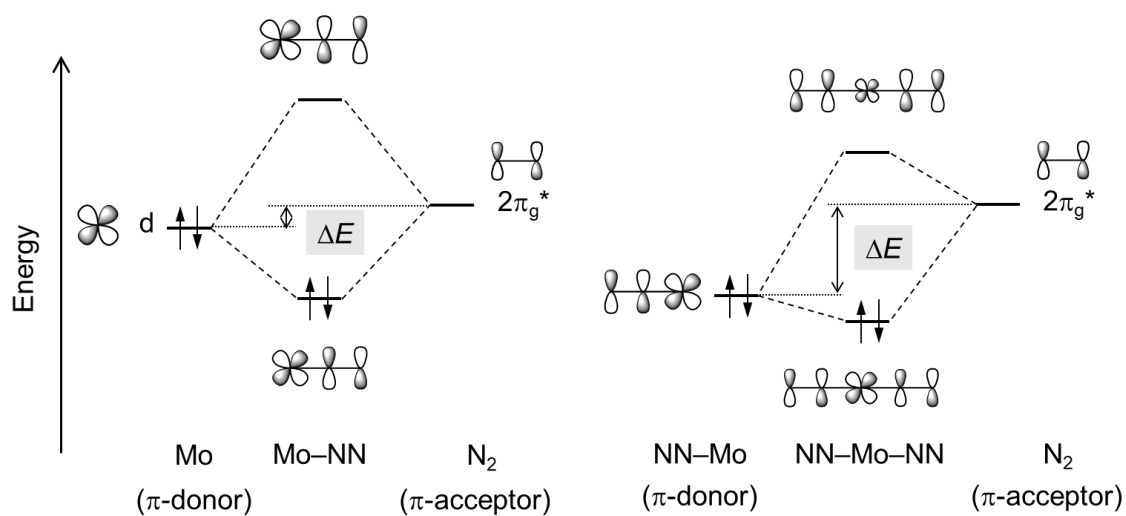


Figure 3-3. Qualitative orbital interaction diagrams focused on the π -interaction between the molybdenum center and the terminal dinitrogen ligand of Mo–NN (right) and NN–Mo–NN (left) core structures. ΔE is equal to the energy gap between the π -donor orbital of the metal center and the π -acceptor $2\pi_g^*$ orbital of the dinitrogen ligand.

3.4. Orbital Interaction between Bridged N₂ Ligand and Two Mo Centers

The straight Mo–N≡N–Mo moiety of the dinuclear molybdenum complexes exhibits important functions for the catalytic conversion of NH₃ from N₂. Focusing on its π -interaction, we see that two Mo centers cooperate effectively with a bridging N₂ ligand in the straight Mo–N≡N–Mo moiety. Orbital interactions between the bridging N₂ ligand and two Mo centers of the straight Mo–N≡N–Mo moiety has been the subject of discussion by Fryzuk and coworkers.²⁷ Mo(0)Mo(0)–N₂ complexes, [$\{\text{Mo}^0(\text{L}_3)(\text{N}_2)_2\}_2(\mu\text{-N}_2)$] ($\text{L}_3 = \text{PNP}$ for **2** and $\text{L}_3 = \text{PCP}$ for **3**), containing six-coordinate Mo(0) centers are constructed from two MoL₅ fragments and one bridging N₂ fragment, in which L describes a scaffold of ligands, such as pincer ligands and N₂ ligand. Using the same procedure, Mo(I)Mo(I) intermediate, [$\{\text{Mo}^{\text{I}}(\text{PNP})\text{I}\}_2(\mu\text{-N}_2)$] **I**, containing five-coordinate Mo(I) centers is constructed from two MoL₄ fragments and one bridging N₂ fragment. In the square pyramidal MoL₅ and square planar MoL₄ fragments, assuming the z-axis equal to the direction of bond of the straight Mo–N≡N–Mo moiety, the valence electrons occupy the d_{xy} , d_{yz} , and d_{zx} orbitals of the Mo centers. In particular, the d_{yz} and d_{zx} orbitals effectively overlap with the $1\pi_u$ and $2\pi_g^*$ orbitals of the bridging N₂ ligand as shown in Figure 3-4. Because both MoL₄–N≡N–MoL₄ and MoL₅–N≡N–MoL₅ are attributed in the fourfold geometry, four degenerate π -orbitals of $1e_u$, $1e_g$, $2e_u$, and $2e_g$ are provided.¹² The $1e_u$ and $1e_g$ orbitals are responsible for Mo–N bonding and the $2e_u$ and $2e_g$ orbitals are responsible for Mo–N antibonding. All four orbitals seem to be delocalized over the straight Mo–N≡N–Mo moiety. Widely delocalized π -orbital could provide for intermetallic electron transfer between two Mo centers. The d_{xy} orbital cannot interact with the bridging N₂ ligand and is characterized as a δ/δ^* orbital interacting with the other Mo center. The other d orbitals of the Mo centers, d_{z^2} and $d_{x^2-y^2}$, contribute to the σ -bonding MOs for Mo–L and M–N₂.

The complexes **2** and **3** with the straight Mo⁰–N≡N–Mo⁰ structure exhibit a $\pi^{12}\delta^4$ configuration of $(1e_u)^4(1e_g)^4(\delta)^2(\delta^*)^2(2e_u)^4(2e_g)^0$. The Energy of $2e_u$ orbital can be higher than the δ and δ^* orbitals. Therefore, π -backdonation from the Mo⁰–N≡N–Mo⁰ moiety to a terminal N₂ ligand is considered stronger than that of the corresponding monomeric Mo(0)–N₂ complex. On the other hand, the complex **I** with the straight Mo^I–N≡N–Mo^I

structure exhibits a $\pi^{10}\delta^4$ configuration of $(1e_u)^4(1e_g)^4(\delta)^2(\delta^*)^2(2e_u)^2(2e_g)^0$. The half occupation of the degenerated $2e_u$ orbital is crucial for the $N\equiv N$ bond breaking of the bridging N_2 ligand. When the $N\equiv N$ bond is stretched, the orbital energy of the σ -antibonding $4\sigma_u^*$ orbital of the bridging N_2 ligand becomes lowered. In the timing of the orbital energy of $4\sigma_u^*$ equal to that of $2e_u$ of the $Mo-N\equiv N-Mo$ moiety, two-electron transfer occurs from $2e_u$ to $4\sigma_u^*$. Here, $2e_u$ orbital that contributes to π -bonding of the $N\equiv N$ bond becomes unoccupied. The occupied $4\sigma_u^*$ and unoccupied $2e_u$ orbitals allow the bridging $N\equiv N$ bond breaking. On the other hand, if the $N\equiv N$ bond of the $Mo^0-N\equiv N-Mo^0$ moiety with the $\pi^{12}\delta^4$ configuration is completely broken, two electrons remain in the $2e_u$ orbital after the two-electron transfer from $2e_u$ to $4\sigma_u^*$. Therefore, direct $N\equiv N$ bond cleavage of the $Mo^0-N\equiv N-Mo^0$ moiety with the $\pi^{12}\delta^4$ configuration cannot proceed because of the effect of $2e_u$ orbital bonding $N\equiv N$. These two different roles of the $Mo^{I/0}-N\equiv N-Mo^{I/0}$ structure rely on the orbital interaction and the number of electrons on its π -orbitals.

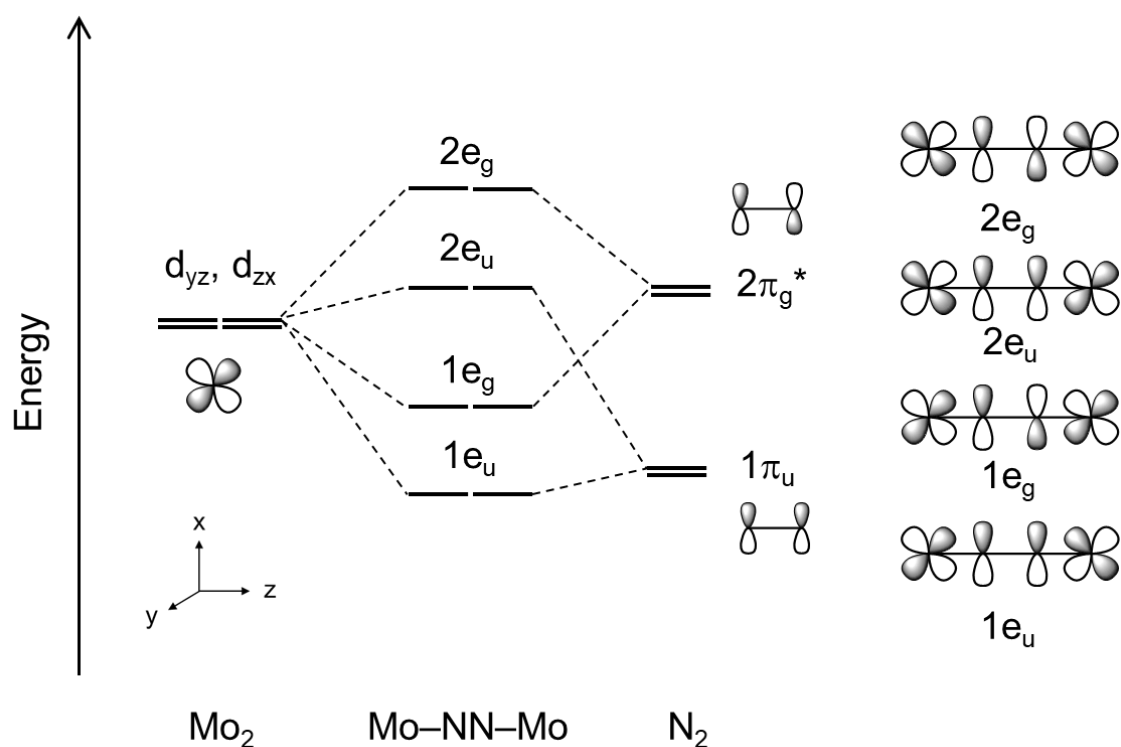


Figure 3-4. Qualitative orbital interaction diagram focused on the π -interaction between two Mo centers and a bridging dinitrogen ligand of a linear $Mo-NN-Mo$ core structure.

3.5. Conversion of Terminal N₂ Ligand of Dimolybdenum Complex to NH₃

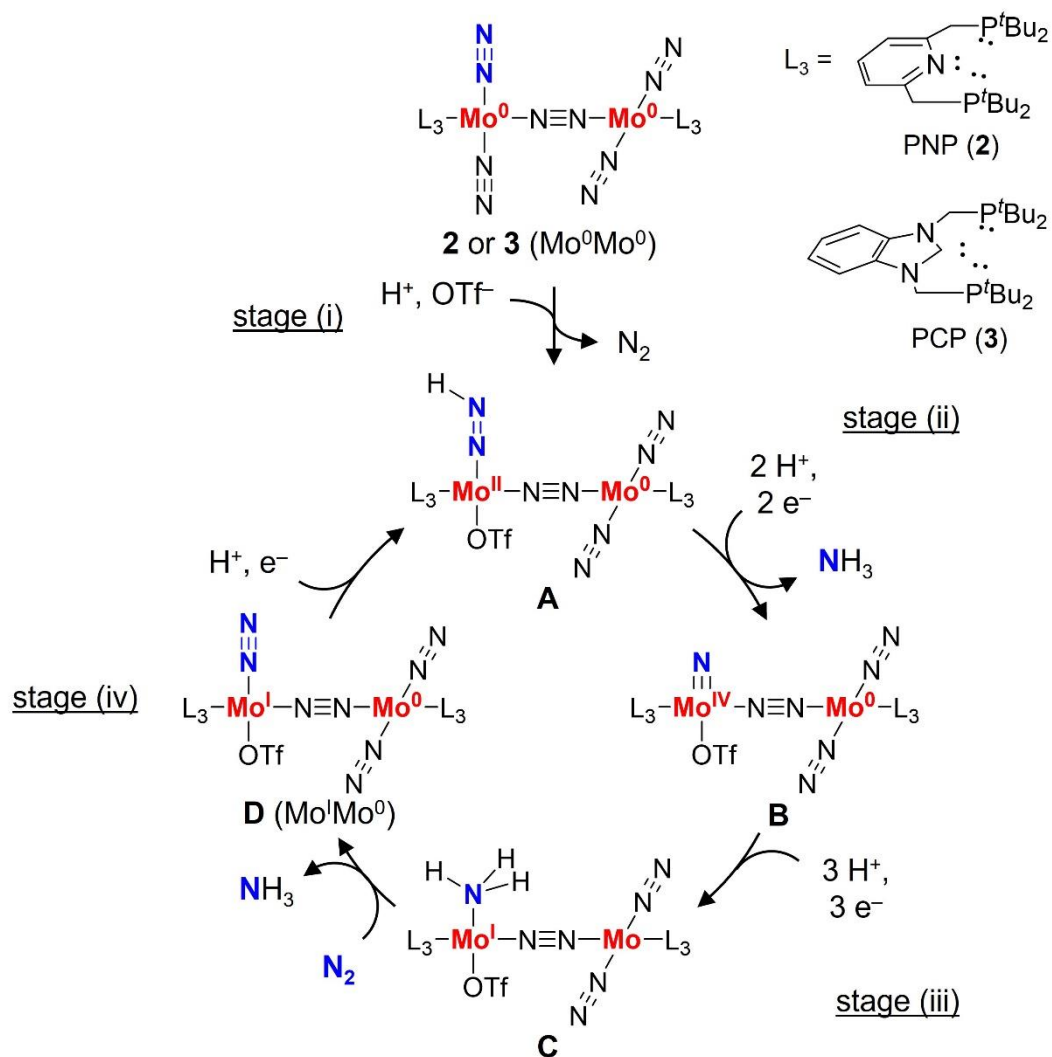
In N₂-bridged dinuclear Mo(0)Mo(0)–N₂ complexes **2** and **3**, the N≡N bond cleavage of the bridging dinitrogen ligand is not allowed due to its electronic structure. Complexes **2** and **3** has four terminal N₂ ligands. One of the terminal N₂ ligand is catalytically converted to 2 equiv. of NH₃ in the presence of [LutH]OTf (Lut = 2,6-dimethylpyridine, OTf = CF₃SO₃) as a proton source and Cp₂Co or Cp*₂Cr as an electron source.

DFT calculations were performed at the B3LYP-D3²⁹⁻³³ level of theory to propose an entire nitrogen fixation mechanism catalyzed by Mo(0)Mo(0)–N₂ complexes bearing PCP and PNP ligands [$\{\text{Mo}^0(\text{L}_3)(\text{N}_2)_2\}_2(\mu\text{-N}_2)$] **2** and **3**, in which L₃ represents the PNP ligand for **2** or the PCP ligand for **3**.²² Scheme 3-7 shows the plausible catalytic pathway and it can be divided into four stages (i)–(iv). In stage (i), protonation of a terminal N₂ ligand in **3** (**2**) induces exchange of the dinitrogen ligand *trans* to the protonated N₂ for OTf[–], the counter anion of LutH⁺. As a result, the Mo(II)Mo(0)–diazene complex, $[\text{Mo}^{\text{II}}(\text{L}_3)(\text{OTf})(\text{N}=\text{NH})-\text{N}\equiv\text{N}-\text{Mo}^0(\text{L}_3)(\text{N}_2)_2]$ **A**, is generated. In stage (ii), two sequential protonation/reduction reactions of **A** achieves the production of the first NH₃ and Mo(IV)Mo(0)–nitride complex, $[\text{Mo}^{\text{IV}}(\text{L}_3)(\text{OTf})(\equiv\text{N})-\text{N}\equiv\text{N}-\text{Mo}^0(\text{L}_3)(\text{N}_2)_2]$ **B**. In stage (iii), three of sequential protonation and reduction of **B** afford Mo(I)Mo(0)–NH₃ complex, $[\text{Mo}^{\text{I}}(\text{L}_3)(\text{OTf})(\text{NH}_3)-\text{N}\equiv\text{N}-\text{Mo}^0(\text{L}_3)(\text{N}_2)_2]$ **C**. In stage (iv), the NH₃ ligand in **C** is replaced by an incoming N₂ molecule to form Mo(I)Mo(0)–N₂ complex, $[\text{Mo}^{\text{I}}(\text{L}_3)(\text{OTf})(\text{N}_2)-\text{N}\equiv\text{N}-\text{Mo}^0(\text{L}_3)(\text{N}_2)_2]$ **D**. The alternating protonation and reduction of **D** provides **A** again. Owing to the reaction pathway, regeneration of the initial Mo(0)Mo(0)–N₂ complex **2** or **3** is not required to start the next catalytic cycle. Therefore, stages (ii)–(iv) compose the substantive catalytic cycle for nitrogen fixation.

The catalytic pathway shown in Scheme 3-7 includes two types of dinuclear Mo–N₂ complexes, the initial Mo(0)Mo(0)–N₂ complex [$\{\text{Mo}^0(\text{L}_3)(\text{N}_2)_2\}_2(\mu\text{-N}_2)$] **2** and **3**, and the Mo(I)Mo(0)–N₂ complex, $[\text{Mo}^{\text{I}}(\text{L}_3)(\text{N}_2)(\text{OTf})-\text{N}\equiv\text{N}-\text{Mo}^0(\text{L}_3)(\text{N}_2)_2]$ **D**, on the catalytic cycle. Protonation of the Mo–N₂ complex with LutH⁺ is regarded as the slowest reaction in the catalytic cycle. In the case of L₃ = PCP, for example, the reaction free energy ΔG₂₉₈ of the protonation of the terminal N₂ ligand of **D** (3.1 kcal mol^{–1}) was

computed to be more exergonic than that of **3** (6.5 kcal mol⁻¹). This comparison indicates that the N₂ ligand in **D** is more activated in the Mo^I-N≡N-Mo⁰ structure than that in the Mo⁰-N≡N-Mo⁰ structure of **3**. The bridging N≡N bond length was measured and a natural population analysis (NPA) was performed to evaluate the structural and electronic properties of the N₂ ligand in **3** and **D**.³⁴ The terminal N₂ ligand at the Mo^I center of **D** has a more negative NPA charge of -0.19 and a longer distance of N-N bond of 1.142 Å than those of the terminal N₂ ligand in **3** (-0.09 and 1.132 Å, respectively). The π-backdonation from a Mo center to the antibonding 2π_g* orbital of the N₂ ligand shows up as a negative NPA charge and the N≡N bond elongation. Despite of the coordination of OTf⁻, generally known as a strong electron-withdrawing group, the terminal N₂ ligand becomes more negative and the N≡N bond length of the terminal N₂ ligand in **D** is 0.010 Å longer than that in **3**. Figure 3-5 shows that the HOMO-1 of monomeric Mo(0)-N₂ complex, [Mo⁰(L₃)(N₂)₃] **E**, and HOMO of monomeric Mo(I)-N₂ complex, [Mo^I(L₃)(OTf)(N₂)₂] **F**, describe π-backdonation from the *d* orbital of the Mo center to the 2π_g* orbital of coordinated N₂ ligands, resulting in N≡N bond activation. In complex **E**, the electron given by π-backdonation is shared by two axial N₂ ligands, whereas in complex **D**, due to the low π-acceptability of the OTf group in the *trans* position to the axial N₂ ligand, the only one of terminal N₂ ligand at the Mo(I) center accepts more electrons. The HOMOs of **2** and **D** shows a π-orbital (2e_u) in the Mo-N≡N-Mo site, indicating that intermetallic electron transfer between two Mo centers is possible. The anionic OTf group coordinating to the Mo(I) center also triggers a formal charge imbalance between the Mo(I) and Mo(0) centers. The Mo(0) center in **D** is considered an electron-donation group and supports the protonation of Mo(I)-NN. Table 3-1 describes that both coordination of the OTf group to the Mo^I center and Mo^I-N≡N-Mo⁰ moiety are required for activate the terminal N₂ ligand. It is found that complex **D** with the Mo^I-N≡N-Mo⁰ moiety further stimulates the terminal N₂ ligand on the Mo(I) center.

Scheme 3-7. A plausible catalytic ammonia conversion cycle from the dinitrogen molecule using dimolybdenum complexes bearing pincer ligands as catalysts.



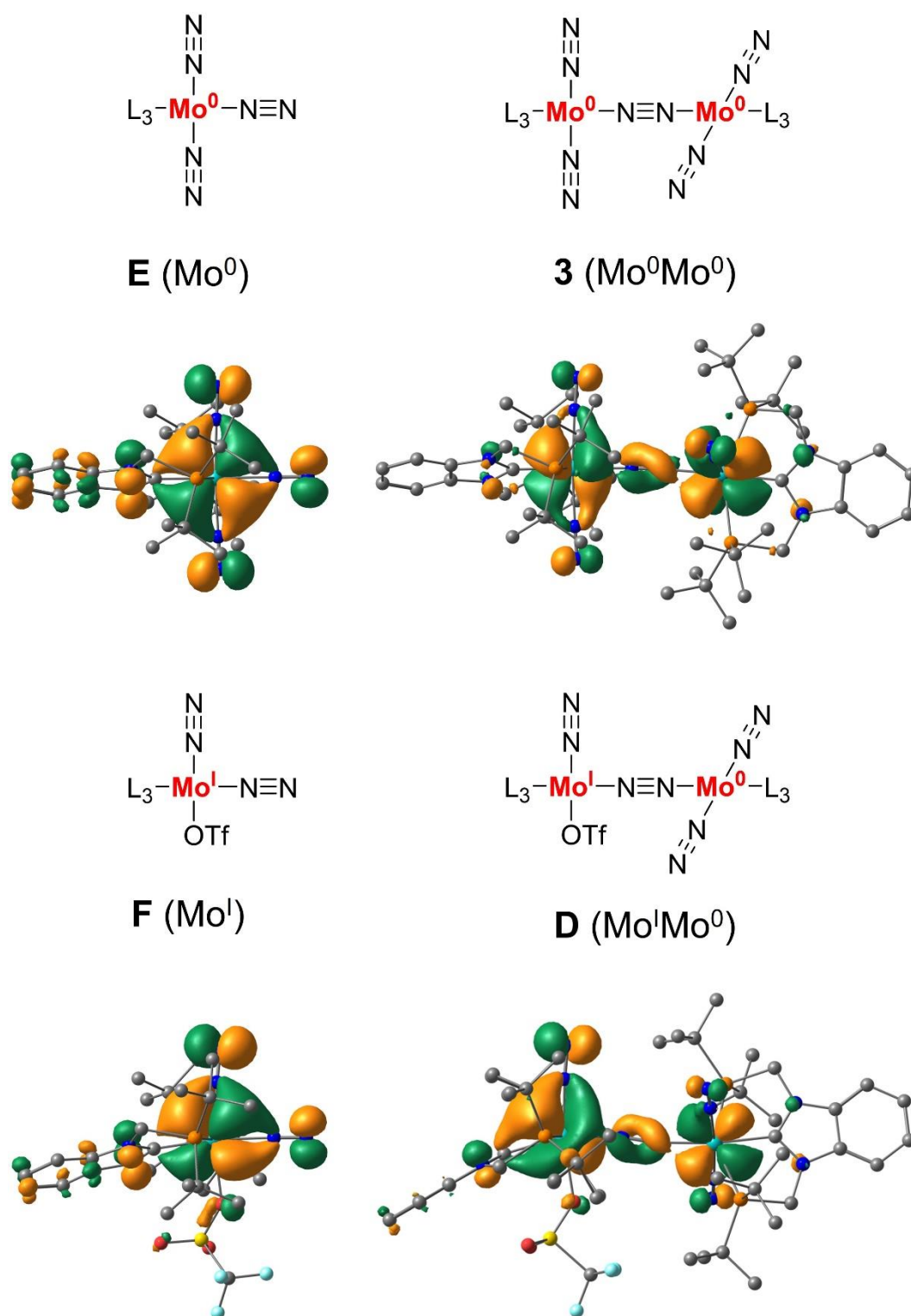
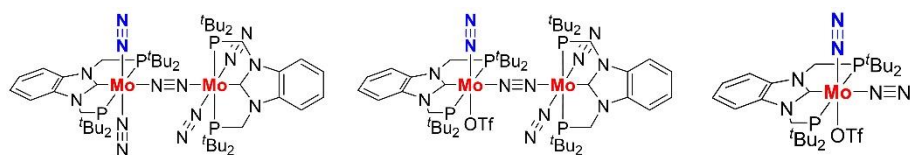


Figure 3-5. Spatial distributions of the HOMO-1 (**E**) and HOMO (**3**, **D**, and **F**).

Table 3-1. Free energy changes at 298 K (ΔG_{298}) for the protonation of the dinitrogen ligand of **3**, **D**, and **F**, and geometric and electronic properties of the complexes

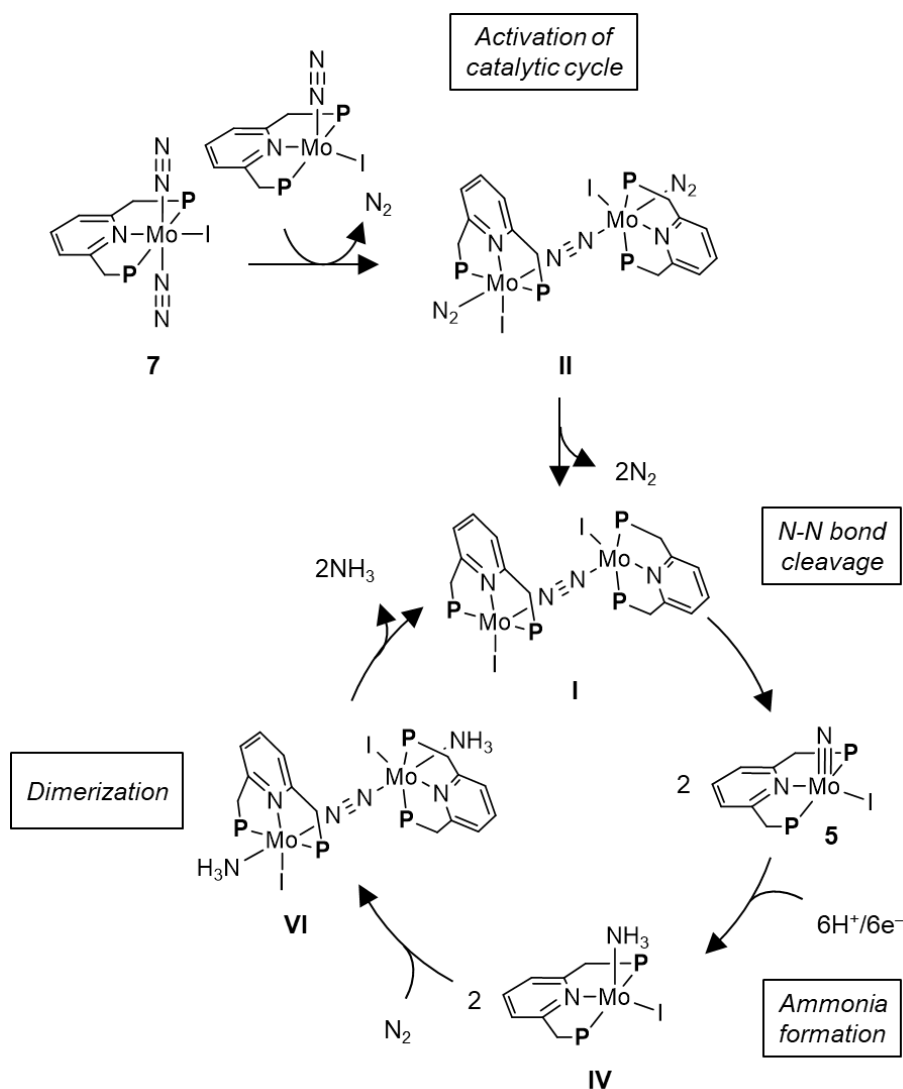
			
1 (Mo ⁰ Mo ⁰)	D (Mo ^I Mo ⁰)	F (Mo ^I)	
	1 (Mo ⁰ Mo ⁰)	D (Mo ^I Mo ⁰)	F (Mo ^I)
ΔG_{298} of protonation of the N₂ ligand [kcal/mol]	6.5	3.1	12.0
Mo- N₂ distance [Å]	2.039	1.971	1.995
N-N distance [Å]	1.132	1.142	1.135
N-N bond order	2.40	2.28	2.35
NPA charge of N₂	-0.09	-0.19	-0.14

3.6. Conversion of Bridging N₂ Ligand of Dimolybdenum Complex to NH₃

Two electron reduction of the Mo(III)–triiodide complex, [Mo^{III}(PNP)I₃] **4**, yields Mo(IV)–nitride complex, [Mo^{IV}(PNP)I(≡N)] **5**.^{7d} The conversion of Mo–(N₂)₂ complex, *trans*-[Mo^I(PNP)I(N₂)₂] **7**, formed by a two-electron reduction of Mo(IV)–nitride complex [Mo^{IV}(PNP)I(≡N)] **5** also occurs stoichiometrically under 1 atm of N₂.²³ This reaction is also determined to proceed the second-order with respect to concentration of **4** by experimental kinetic experiments. The experimental results indicate that the N≡N bond cleavage occurs in N₂-bridging Mo(I)Mo(I) complex, [{Mo^I(PNP)(I)}₂(μ-N₂)] **I**.

Yoshizawa group conducted DFT calculations at the B3LYP-D3²⁹⁻³³ level of theory and predicted a total catalytic reaction pathway using **7** based on obtained free energy profiles at 298 K.²³ Scheme 3-8 shows a plausible reaction pathway. The reaction pathway is divided into four stages. In the first stage, dimerization of **7** yields the Mo(I)Mo(I)–N₂ complex [{Mo^I(PNP)(I)(N₂)}₂(μ-N₂)] **II**. Liberation of two terminal N₂ ligands yields **I** (**II**→**III**→**I**). In the second stage, direct N≡N bond cleavage of the bridging N₂ ligand of **I** provides 2 equiv. of [Mo^{IV}(PNP)I(≡N)] **7**. In the third stage, three sequential protonation and reduction steps of **7** lead to the Mo(I)–NH₃ complex, [Mo^I(PNP)I(NH₃)] **IV**. In the fourth stage, coordination of an N₂ ligand to **IV** produces [Mo^I(PNP)I(N₂)(NH₃)] **V**. Dimerization of **V** yields the Mo(I)Mo(I) complex, [Mo^I(PNP)(I)(NH₃)–N≡N–Mo^I(PNP)(I)(NH₃)] **VI**. Finally, Liberation of two NH₃ ligands affords **I** (**VI**→**VII**→**I**).

Scheme 3-8. A plausible catalytic ammonia conversion cycle from the dinitrogen molecule using dimolybdenum complexes bearing a PNP ligand for the catalyst.



Following the exergonic $\text{N}\equiv\text{N}$ bond cleavage reaction of a bridging N_2 ligand of **I** yields two molecules of **5** with an activation energy of $21.8 \text{ kcal mol}^{-1}$ (Figure 3-6).¹⁷ The optimized structure of the transition state (**TS**) has a zigzag $\text{Mo}-\text{N}\equiv\text{N}-\text{Mo}$ moiety. The ground state of **8** is assigned to the triplet state by DFT calculations and that of **TS** and **7** is the closed-shell singlet via an intersystem crossing. The free energy profile indicates that the $\text{Mo}^0-\text{N}\equiv\text{N}-\text{Mo}^0$ moiety of **2** yields 2 equiv. of extremely endergonic *trans*- $[\text{Mo}^{\text{III}}(\text{PNP})(\text{N}_2)_2(\equiv\text{N})]$ **VIII**.¹⁷ The difference in these reaction free energies of the $\text{N}\equiv\text{N}$ bond cleavage is rationalized by the orbital interactions and electron number of the

fourfold geometrical Mo–N≡N–Mo moiety. Figure 3-7 describes the electron configuration focusing on the σ - and π -interactions of the linear (D_{4h} symmetry) Mo–N≡N–Mo structure and 2 equiv. of Mo≡N structures after N≡N bond breaking via the zigzag (C_{2h} symmetry) Mo–N≡N–Mo structure at **TS**.³⁵ The energy level of the $1a_{2u}$ orbital contributing to the σ -antibonding of the N≡N bond becomes lowered along N≡N elongation. Complex **I** with the Mo^I–N≡N–Mo^I moiety provides two stable Mo≡N moieties of **5**. On the other hand, in the case of complex **2** with Mo⁰–N≡N–Mo⁰ moiety, the excess two electrons occupy the π -antibonding orbitals of the Mo≡N cores of **VIII** after N≡N bond breaking. Therefore, unstable Mo(III)–nitride complex, *trans*-[Mo^{III}(PNP)(N₂)₂(≡N)] **VIII**, are generated. In other words, the electron number on the Mo–N≡N–Mo moiety dominates whether the N≡N bond can be cleaved or not. Scheme 3-9 describes the series of reactions from precursor **7** to the key dinuclear molybdenum complex **I** with the Mo^I–N≡N–Mo^I moiety, which are computed to be endergonic by 12.6 kcal mol⁻¹. It is considered that π -backdonation between the Mo^I–N≡N–Mo^I fragment and terminal N₂ ligands stabilizes important π -orbitals of **II**. Liberation of the two terminal N₂ ligand may be regarded as an activation of the bridging N₂ ligand. The formation of NH₃ from **5** to **IV** in the presence of ColH⁺ and CoCp*₂ is calculated to be endergonic in total by 9.5 kcal mol⁻¹. Dimerization of Mo(I)–NH₃ complexes **IV** and **V** to the key complex **I** is calculated to be exergonic in total by 31.1 kcal mol⁻¹. In contrast to the activation step from precursor **7** to **I**, the dimerization step from Mo(III)–NH₃ complex **IV** proceeds more readily in the catalytic cycle. The author has therefore proposed the importance of the Mo^I–N≡N–Mo^I moiety for N≡N bond cleavage of the bridging N₂ ligand and shortcut the conventional Yandulov-Schrock cycle.

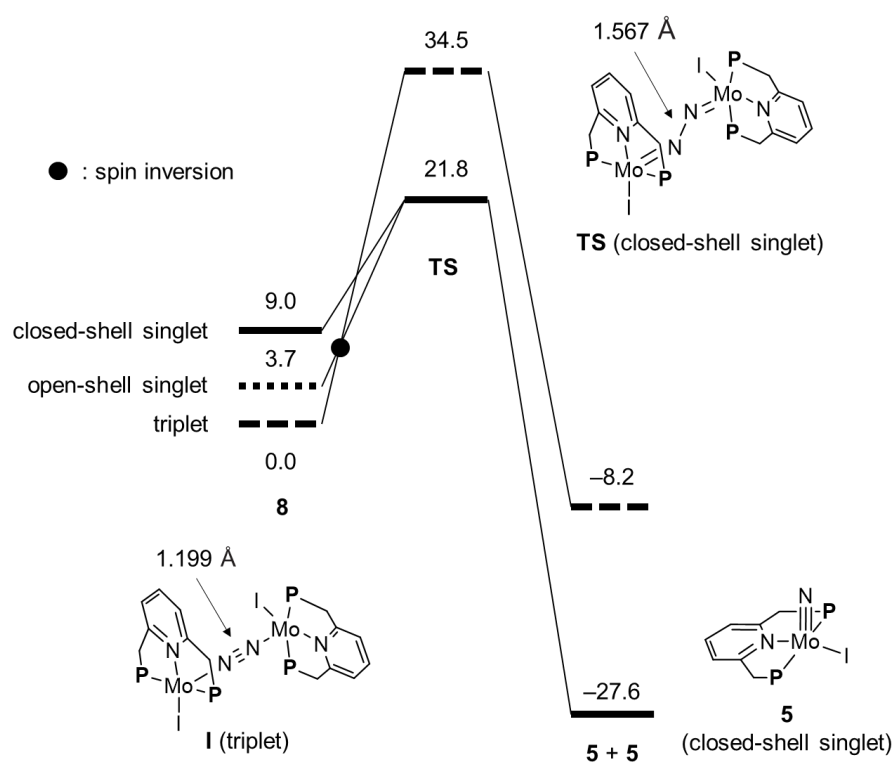


Figure 3-6. Free energy diagram for the direct N-N bond cleavage reaction of the bridging dinitrogen ligand of **I**, which yields two equivalents of **5** at 298 K.

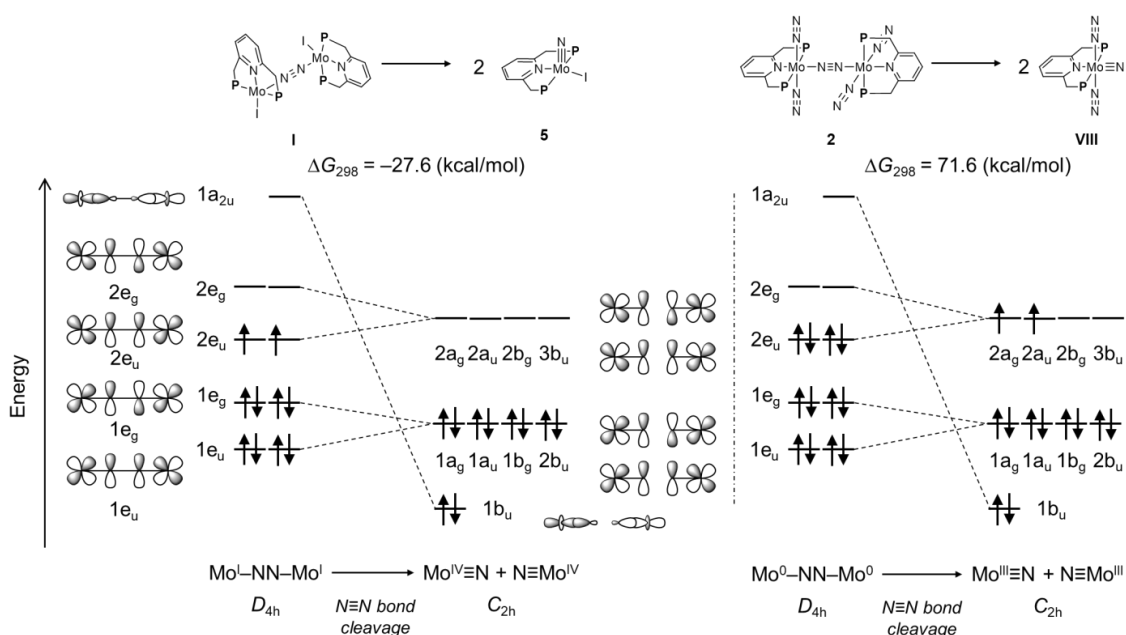
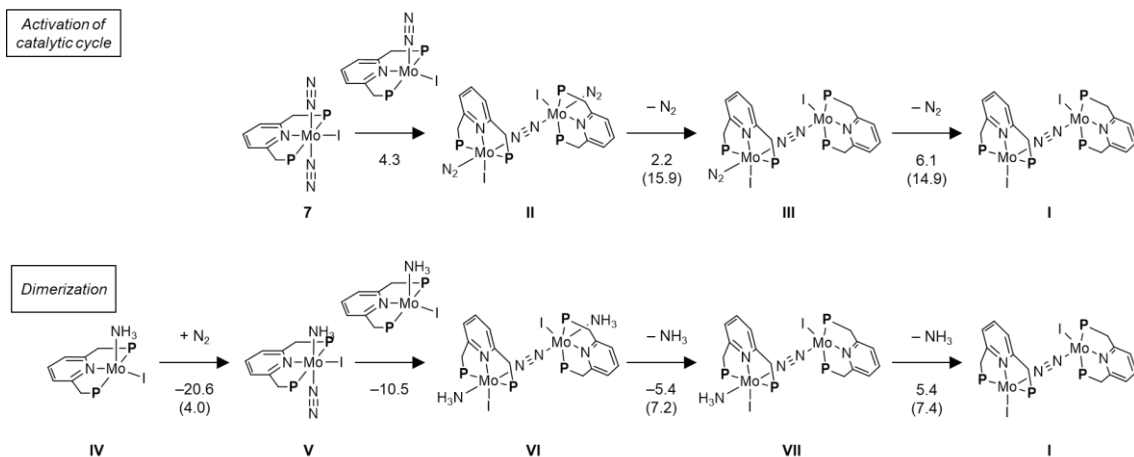


Figure 3-7. Reaction free energies for $\text{N}\equiv\text{N}$ bond cleavage of the bridging dinitrogen ligand and the electron configuration of the $\text{Mo}-\text{N}\equiv\text{N}-\text{Mo}$ moiety.

Scheme 3-9. Activation of catalytic Cycle from **7** and dimerization of **IV** to the dinuclear $\text{Mo}^{\text{I}}\text{Mo}^{\text{I}}$ intermediate **I**.



3.7. Conclusions

The author has summarized the development of catalytic nitrogen fixation using N_2 -bridged dimolybdenum complexes and two different pathways depending on the electronic property of $\text{Mo}-\text{N}\equiv\text{N}-\text{Mo}$ moiety of the N_2 -bridged dimolybdenum complexes. In the conventional Yandulov-Schrock cycle, NH_3 is generated by stepwise protonation and reduction of the terminal N_2 ligand on the Mo center. Both $\text{Mo}^0-\text{N}\equiv\text{N}-\text{Mo}^0$ and $\text{Mo}^{\text{I}}-\text{N}\equiv\text{N}-\text{Mo}^0$ core moieties allow intermetallic electron transfer between two Mo centers through the bridging N_2 ligand to promote protonation of the terminal dinitrogen ligand. On the other hand, the $\text{Mo}^{\text{I}}-\text{N}\equiv\text{N}-\text{Mo}^{\text{I}}$ moiety affords extremely stable Mo(IV)-nitride species via direct $\text{N}\equiv\text{N}$ bond cleavage to shortcut the Yandulov-Schrock cycle. The author expects that the shortcut significantly improves the catalytic activity. The different role of the $\text{Mo}-\text{N}\equiv\text{N}-\text{Mo}$ moiety is dominated by its electronic properties. The author has thought essential orbital interactions between the Mo centers and the N_2 ligand to qualitatively elucidate the electronic properties of the $\text{Mo}-\text{N}\equiv\text{N}-\text{Mo}$ moiety. Finally, the author has presented plausible catalytic reaction pathways along to both Yandulov-Schrock cycle and its shortcut cycle inferred from DFT calculations. The DFT calculations proved the validity of our qualitative discussion using orbital interactions.

References

1. Liu, H. *Ammonia Synthesis Catalysts, Innovation and Practice*; Chemical Industry Press and World Scientific: Singapore and Beijing, **2013**.
2. (a) Einsle, O.; Tezcan, F. A.; Andrade, S. L. A.; Schmid, B.; Yoshida, M.; Howard, J. B.; Rees, D. C. Nitrogenase MoFe-Protein at 1.16 Å Resolution: A Central Ligand in the FeMo-Cofactor. *Science* **2002**, *297*, 1696–1700. (b) Lancaster, K. M.; Roemelt, M.; Ettenhuber, P.; Hu, Y.; Ribbe, M. W.; Neese, F.; Bergmann, U.; DeBeer, S. X-ray Emission Spectroscopy Evidences a Central Carbon in the Nitrogenase Iron-Molybdenum Cofactor. *Science* **2011**, *334*, 974–977. (c) Hoffman, B. M.; Lukoyanov, D.; Yang, Z.-Y.; Dean, D. R.; Seefeldt, L. C. Mechanism of Nitrogen Fixation by Nitrogenase: The Next Stage. *Chem. Rev.* **2014**, *114*, 4041–4062.
3. Yandulov, D. V.; Schrock, R. R. Catalytic Reduction of Dinitrogen to Ammonia at a Single Molybdenum Center. *Science* **2003**, *301*, 76–78.
4. Doyle, L. R.; Wooles, A. J.; Jenkins, L. C.; Tuna, F.; McInnes, E. J. L.; Liddle, S. T. Catalytic Dinitrogen Reduction to Ammonia at a Triamidine-Titanium Complex. *Angew. Chem. Int. Ed.* **2018**, *57*, 6314–6318; *Angew. Chem.* **2018**, *130*, 6422–6426.
5. Sekiguchi, Y.; Arashiba, K.; Tanaka, H.; Eizawa, A.; Nakajima, K.; Yoshizawa, K.; Nishibayashi, Y. Catalytic Reduction of Molecular Dinitrogen to Ammonia and Hydrazine Using Vanadium Complexes. *Angew. Chem. Int. Ed.* **2018**, *57*, 9064–9068; *Angew. Chem.* **2018**, *130*, 9202–9206.
6. Anderson, J. S.; Rittle, J.; Peters, J. C. Catalytic Conversion of nitrogen to ammonia by an iron model complex. *Nature* **2013**, *501*, 84–87.
7. Creutz, S. E.; Peters, J. C. Catalytic Reduction of N₂ to NH₃ by an Fe–N₂ complex Featuring a C-Atom Anchor. *J. Am. Chem. Soc.* **2014**, *136*, 1105–1115.
8. Ung, G.; Peters, J. C. Low-Temperature N₂ to Two-Coordinate L₂Fe⁰ Enables Reductive Trapping of L₂FeN₂[–] and NH₃ Generation. *Angew. Chem. Int. Ed.* **2015**, *54*, 532–535; *Angew. Chem.* **2015**, *127*, 542–545.

9. Del Castillo, T. J.; Thompson, N. B.; Peters, J. C. A Synthetic Single-Site Fe Nitrogenase: High Turnover, Freeze-Quench ^{57}Fe Mossbauer Data, and a Hydride Resting State. *J. Am. Chem. Soc.* **2016**, *138*, 5341–5350.
10. Kuriyama, S.; Arashiba, K.; Nakajima, K.; Matsuo, Y.; Tanaka, H.; Ishii, K.; Yoshizawa, K.; Nishibayashi, Y. Catalytic Transformation of Dinitrogen into Ammonia and Hydrazine by Iron–Dinitrogen Complexes Bearing Pincer Ligand. *Nat. Commun.* **2016**, *7*, 12181.
11. Hill, P. J.; Doyle, L. R.; Crawford, A. D.; Myers, W. K.; Ashley, A. E. Selective Catalytic Reduction of N_2 to N_2H_4 by a Simple Fe Complex. *J. Am. Chem. Soc.* **2016**, *138*, 13521–13524.
12. Chalkley, M. J.; Del Castillo, T. J.; Matson, B. D.; Roddy, J. P.; Peters, J. C. Catalytic N_2 -to- NH_3 Conversion by Fe at Lower Driving Force: A Proposed Role for Metallocene-Mediated PCET. *ACS Cent. Sci.* **2017**, *3*, 217–223.
13. Buscagan, T. M.; Oyala, P. H.; Peters, J. C. N_2 -to- NH_3 Conversion by a Triphos–Iron Catalyst and Enhanced Turnover under Photolysis. *Angew. Chem. Int. Ed.* **2017**, *56*, 6921–6926; *Angew. Chem.* **2017**, *129*, 7025–7030.
14. Arashiba, K.; Miyake, Y.; Nishibayashi, Y. A Molybdenum Complex Bearing PNP-Type Pincer Ligands Leads to the Catalytic Reduction of Dinitrogen into Ammonia. *Nat. Chem.* **2011**, *3*, 120–125.
15. Arashiba, K.; Kinoshita, E.; Kuriyama, S.; Eizawa, A.; Nakajima, K.; Tanaka, H.; Yoshizawa, K.; Nishibayashi, Y. Catalytic Reduction of Dinitrogen to Ammonia by Use of Molybdenum–Nitride Complexes Bearing a Tridentate Triphosphine as Catalysts. *J. Am. Chem. Soc.* **2015**, *137*, 5666–5669.
16. Eizawa, A.; Arashiba, K.; Tanaka, H.; Kuriyama, S.; Matsuo, Y.; Nakajima, K.; Yoshizawa, K.; Nishibayashi, Y. Remarkable Catalytic Activity of Dinitrogen-Bridged Dimolybdenum Complexes Bearing NHC-Based PCP-Pincer Ligands toward Nitrogen Fixation. *Nat. Commun.* **2017**, *8*, 14874.

17. Arashiba, K.; Eizawa, A.; Tanaka, H.; Nakajima, K.; Yoshizawa, K.; Nishibayashi, Y. Catalytic Nitrogen Fixation via Direct Cleavage of Nitrogen–Nitrogen Triple Bond of Molecular Dinitrogen under Ambient Reactions. *Bull. Chem. Soc. Jpn.* **2017**, *90*, 1111–1118.
18. Eizawa, A.; Arashiba, K.; Egi, A.; Tanaka, H.; Nakajima, K.; Yoshizawa, K.; Nishibayashi, Y. Catalytic Reactivity of Molybdenum–Trihalide Complexes Bearing PCP-Type Pincer Ligands. *Chem. Asian J.* **2019**, *14*, 2091–2096.
19. Ashida, Y.; Arashiba, K.; Tanaka, H.; Egi, A.; Nakajima, K.; Yoshizawa, K.; Nishibayashi, Y. Molybdenum-Catalyzed Ammonia Formation Using Simple Monodentate and Bidentate Phosphines as Auxiliary Ligands. *Inorg. Chem.* **2019**, *58*, 8927–8932.
20. Ashida, Y.; Kondo, S.; Arashiba, K.; Kikuchi, T.; Nakajima, K.; Kakimoto, S.; Nishibayashi, Y. A Practical Synthesis of Ammonia from Nitrogen Gas, Samarium Diiodide and Water Catalyzed by a Molybdenum–PCP Pincer Complex. *Synthesis* **2019**, *51*, 3792–3795.
21. Ashida, Y.; Arashiba, K.; Nakajima, K.; Nishibayashi, Y. Molybdenum-Catalyzed Ammonia Production with Samarium Diiodide and Alcohols or Water. *Nature* **2019**, *568*, 536–540.
22. Egi, A.; Tanaka, H.; Konomi, A.; Nishibayashi, Y.; Yoshizawa, K. Nitrogen Fixation Catalyzed by Dinitrogen-Bridged Dimolybdenum Complexes Bearing PCP- and PNP-Type Pincer Ligands: A Shortcut Pathway Deduced from Free Energy Profile. *Eur. J. Inorg. Chem.* **2020**, 1490–1498.
23. Arashiba, K.; Tanaka, H.; Yoshizawa, K.; Nishibayashi, Y. Cycling between Molybdenum–Dinitrogen and –Nitride Complexes to Support the Reaction Pathway for Catalytic Formation of Ammonia from Dinitrogen. *Chem. Eur. J.* **2020**, *26*, 13383–13389.
24. Fajardo, Jr., J.; Peters, J. C. Catalytic Nitrogen-to-Ammonia Conversion by Osmium and Ruthenium Complexes. *J. Am. Chem. Soc.* **2017**, *139*, 16105–16108.

25. Kuriyama, S.; Arashiba, K.; Tanaka, H.; Matsuo, Y.; Nakajima, K.; Yoshizawa, K.; Nishibayashi, Y. Direct Transformation of Molecular Dinitrogen into Ammonia Catalyzed by Cobalt Dinitrogen Complexes Bearing Anionic PNP Pincer Ligands. *Angew. Chem. Int. Ed.* **2016**, *55*, 14291–14293; *Angew. Chem.* **2016**, *128*, 14503–14507.
26. Meng, F.; Kuriyama, S.; Tanaka, H.; Egi, A.; Yoshizawa, K.; Nishibayashi, Y. Ammonia Formation Catalyzed by a Dinitrogen-Bridged Dirhenium Complex Bearing PNP-Pincer Ligands under Mild Reaction Conditions. *Angew. Chem. Int. Ed.* **2021**, *60*, 13906–13912; *Angew. Chem.* **2021**, *133*, 14025–14031.
27. Fryzuk, M. D.; Haddad, T. S.; Mylvaganam, M.; McConville, D. H.; Rettig, S. J. End-On Versus Side-On Bonding of Dinitrogen to Dinuclear Early Transition-Metal Complexes. *J. Am. Chem. Soc.* **1993**, *115*, 2782–2792.
28. *Nitrogen Fixation—Topics in Organometallic Chemistry* (Ed.: Nishibayashi, Y.), Springer, **2017**.
29. Grimme, S.; Antony, J.; Ehrlich, S.; Krieg, H. A Consistent and Accurate *Ab Initio* Parameterization of Density Functional Dispersion Correlation (DFT-D) for the 94 Elements H-Pu. *J. Chem. Phys.* **2010**, *132*, 154104.
30. Becke, A. D. Density-Functional Exchange-Energy Approximation with Correct Asymptotic Behavior. *Phys. Rev. A* **1988**, *38*, 3098–3100.
31. Becke, A. D. Density-Functional Thermochemistry. III. The Role of Exact Exchange. *J. Chem. Phys.* **1993**, *98*, 5648–5652.
32. Lee, C.; Yang, W.; Parr, R. G. Development of the Colle-Salvetti Correlation-Energy Formula into a Functional of the Electron Density. *Phys. Rev. B* **1988**, *37*, 785–789.
33. Vosko, S. H.; Wilk, L.; Nusair, M. Accurate Spin-Dependent Electron Liquid Correlation Energies for Local Spin Density Calculation: A Critical Analysis. *Can. J. Phys.* **1980**, *58*, 1200–1211.
34. NBO 6.0. Glendening, E. D.; Badenhoop, J. K.; Reed, A. E.; Carpenter, J. E.; Bohmann, J. A.; Morales, C. M.; Landis, C. R.; Weinhold, F. (Theoretical Chemistry Institute, University of Wisconsin, Madison, WI, 2013); <http://nbo6.chem.wisc.edu/>.

35. Laplaza, C. E.; Johnson, M. J. A.; Peters, J. C.; Odom, A. L.; Kim, E.; Cummins, C. C.; George, G. N.; Pickering, I. J. Dinitrogen Cleavage by Three-Coordinate Molybdenum(III) Complexes: Mechanistic and Structural Data. *J. Am. Chem. Soc.* **1996**, *118*, 8623–8638.

Chapter 4

Computational Design of Pincer Ligand for Mo-Catalyzed Nitrogen Fixation

4.1. Introduction

Nitrogen fixation, the conversion of dinitrogen (N_2) into ammonia (NH_3), is an industrially and biologically important reaction. An industrial nitrogen fixation process, the Haber-Bosch process, requires very harsh reaction conditions of high temperature (350–550°C) and high pressure (150–350 atm), employing heterogeneous catalysts.¹ In contrast to the industrial process, a biological process requires mild reaction conditions, such as room temperature and atmospheric pressure, employing enzyme nitrogenase. The active site of nitrogenase is the unique FeMo-cofactor, $\text{Fe}_7\text{MoS}_9\text{C}$, containing transition metals.^{2–5} Achievement of artificial nitrogen fixation under mild conditions is considered one of the challenging topics. One of the promising ways for it is to develop molecular catalysts with Mo centers, which are contained in FeMo-cofactor.

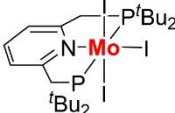
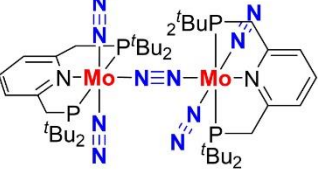
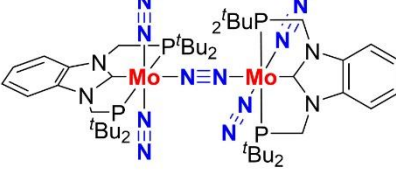
In 2003, Yandulov and Schrock achieved the first catalytic ammonia production under mild reaction conditions, where 8 equiv. of NH_3 per Mo center, using Mo(III)– N_2 complex with a tetradentate triamide-monoamine ligand, as shown in Figure 4-1.⁶ Moreover, Tuzek has also achieved the catalytic or overstoichiometric ammonia production using molybdenum complexes under mild conditions.^{7,8} In 2011, Nishibayashi and coworkers found that an N_2 -bridged dimolybdenum(0) complex bearing pyridine-based pincer ligand called as PNP ligand due to its ligand scaffolds, $[\{\text{Mo}(\text{PNP})(\text{N}_2)_2\}_2(\mu\text{-N}_2)]$ **1** (PNP = 2,6-bis(di-*tert*-butylphosphinomethyl)pyridine) (Figure 4-1), has higher catalytic activity for ammonia formation under mild reaction conditions, where 12 equiv. of NH_3 were produced based on the Mo atom of the catalyst in the presence of $[\text{LutH}]\text{OTf}$ ($\text{LutH}^+ = 2,6\text{-lutidin-1-ium}$, $\text{OTf}^- = \text{trifluoromethane sulfonate}$) as a proton

source and Cp_2Co ($\text{Cp} = \eta^5\text{-C}_5\text{H}_5$).^{9–11} In addition, introducing an electron-donating OCH_3 group to the PNP ligand in **1** increased a larger amount of NH_3 , where up to 26 equiv. of NH_3 were formed based on the Mo center of the catalyst.¹²

In most cases, using reasonably designed ligands such as the tridentate PNP ligand are essential to convert dinitrogen to ammonia under mild reaction conditions. In general, tridentate pincer ligands provide robustness and variability for molecular catalysts.¹³ Since finding the efficient Mo(0)-N_2 complex **1** bearing the PNP ligand toward catalytic nitrogen fixation,⁹ Nishibayashi and coworkers have developed various molybdenum complexes bearing tridentate pincer-type ligands and further enhanced their catalytic activity, where up to 60,000 equiv. of NH_3 were produced per the Mo center of catalysts.

As shown in Figure 4-1, Nishibayashi and coworkers designed an *N*-heterocyclic carbene- (NHC-)based pincer ligand (PCP ligand) and prepared an N_2 -bridged dimolybdenum(0) complex bearing the PCP ligand, $[\{\text{Mo}(\text{PCP})(\text{N}_2)_2\}_2(\mu\text{-N}_2)]$ **2** (PCP = 1,3-bis(di-*tert*-butylphosphinomethyl)benzimidazole-2-ylidene).¹⁴ When **2** was used as a catalyst in the presence of $[\text{LutH}]\text{OTf}$ as a proton source and Cp^*_2Cr ($\text{Cp}^* = \eta^5\text{-C}_5(\text{CH}_3)_5$) as an electron source, 100 equiv. of NH_3 were produced based on the Mo center of the catalyst. While the PNP ligand in **1** serves as a σ -donor to the Mo center, the PCP ligand in **2** serves as not only a strong σ -donor but also a π -acceptor.¹⁴ These electronic properties of the PCP ligand are responsible for a stiff bond between the Mo center and the carbene C atom of the PCP ligand, leading to the improvement of the catalytic activity. Recently, Nishibayashi and coworkers found that an Mo(III)-trihalide complex bearing the PNP ligand, $[\text{Mo}(\text{PNP})\text{I}_3]$ **3** (Figure 4-1), further improves the catalytic activity.^{15,16} Using **3** as a catalyst, they achieved the catalytic activity in the presence of $[\text{ColH}]\text{OTf}$ ($\text{ColH} = 2,4,6\text{-colidinium}$) as a proton source and Cp^*_2Co as an electron source under mild reaction conditions, where up to 415 equiv. of NH_3 were produced based on the Mo atom of the complex.¹⁵ In 2019, the Mo(III)-trihalide complex bearing the PCP ligand in place of the PNP ligand in **3**, $[\text{Mo}(\text{PCP})\text{Cl}_3]$ **4** (Figure 4-1), exhibited further higher catalytic activity in the presence of a combination of H_2O as a proton source and SmI_2 as an electron source under mild reaction conditions, where 4,350 equiv. of NH_3 were produced based on the Mo atom of the complex.¹⁷ In addition, quite recently, introducing

the electron-withdrawing CF₃ group into the PCP ligand of **4** has been found the catalytic activity to produce up to 60,000 equiv. of NH₃ based on the Mo atom of the complex.¹⁸

cat.			
	3 (2017) 415 equiv./Mo	1 (2011) 12 equiv./Mo	2 (2017) 100 equiv./Mo
proton source	[LutH]OTf	[LutH]OTf	[LutH]OTf
electron source	Cp* ₂ Co	Cp ₂ Co	Cp* ₂ Cr

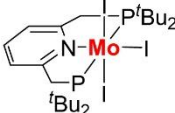
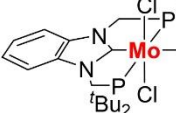
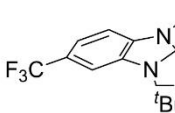
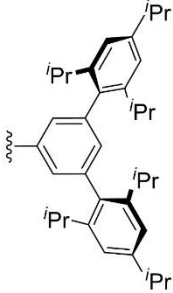
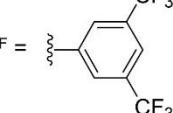
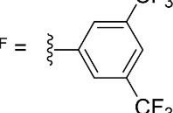
cat.				 HIPT =  Ar ^F = 
	3 (2017) 415 equiv./Mo	4 (2019) 4,350 equiv./Mo	CF₃-substituted 4 (2021) 60,000 equiv./Mo	
proton source	[CoH]OTf	H ₂ O	H ₂ O	
electron source	Cp* ₂ Co	Sml ₂	Sml ₂	

Figure 4-1. Mo-based molecular catalysts (cat.), proton sources, and electron sources of catalytic systems for nitrogen fixation.

As the author mentioned above, the molecular catalytic system of Mo-pincer ligand, which Nishibayashi and his coworkers have developed since 2011, has undergone three major innovations in the reaction mechanism and dramatically improved the catalytic activity of nitrogen fixation. The first innovation is passing through a catalytic cycle of **3** (Figure 4-2(c)) with the cleavage of the N≡N bond of the dinitrogen molecule. For the nitrogen fixation catalyzed by N₂-bridged dimolybdenum(0) complexes **1** (L₃ = PNP) and **2** (L₃ = PCP), our density functional theory (DFT) calculations proposed a theoretically-plausible catalytic cycle as shown in Figure 4-2(b).^{10,11,19} In the catalytic cycle, Mo(I)Mo(0)–N₂ complex, [Mo(L₃)(OTf)(N₂)–N≡N–Mo(L₃)(N₂)₂] **D**, is converted

to Mo(IV)Mo(0)-nitride complex, $[\text{Mo}(\text{L}_3)(\text{OTf})(\equiv\text{N})-\text{N}\equiv\text{N}-\text{Mo}(\text{L}_3)(\text{N}_2)_2]$ **B**, via alternating three protonations and three reductions. After that, **D** is regenerated by three more pairs of protonation and reduction. On the other hand, for the nitrogen fixation catalyzed by **3**, the catalytic cycle shown in Figure 4-2(c) has been investigated thoroughly from both theoretical and experimental viewpoints.^{15,16} Figure 4-2(c) sharply differs from Figure 4-2(b) in the cleavage of the N–N bond of an Mo–N≡N–Mo moiety of **E** to yield directly the corresponding Mo(IV)-nitride complex, $[\text{Mo}^{\text{IV}}(\text{L}_3)(\text{I})(\equiv\text{N})]$ **5**.¹⁵ As a result, only three pairs of protonation and reduction to **5** occur in the catalytic cycle, promoting ammonia formation. The second innovation was employing water (H₂O) as a proton source and SmI₂ as an electron source in the catalytic system of **4** as shown in Figure 4-1.^{17,20} In the catalytic system of **1**, **2**, and **3**, combinations of conjugate acids of pyridine derivative and metallocene have been used as proton and electron sources, respectively. These combinations provide an alternating protonation and reductions to **1**, **2**, and **5** (L₃ = PNP). On the other hand, in the catalytic system of **4**, a combination of H₂O and SmI₂ is proposed to achieve proton-coupled electron transfer (PCET) from an H₂O–SmI₂ complex with a weak O–H bond to Mo-nitride complex **5** (L₃ = PCP).²¹ Thus, **4** exhibits more significant catalytic activity than **3**, because of the change from a two-step alternating protonation and reduction to a one-step PCET process (simultaneous proton and electron transfer). If the catalytic cycle of **4** is like that of the analogous complex **3**, the Mo(III)-imide (**I**) and Mo(II)-amide (**II**) complexes are intermediates in the conversion of **5** to Mo(I)-ammine complex, $[\text{Mo}^{\text{I}}(\text{PCP})(\text{I})(\text{NH}_3)]$ **III**, as shown in Figure 4-2(d).¹⁸ The third innovation is introducing electron-withdrawing substituents into the PCP ligand to make the PCET process more effective.¹⁸ In the catalytic system of **4**, the energy level of the LUMO of **5**(PCP) should be focused on, since an electron from an H₂O–SmI₂ complex is expected to occupy the LUMO of the **5**(PCP). The author has expected that introducing electron-withdrawing groups, such as F, Cl, and CF₃ to the PCP ligand lowers the energy level of the LUMO of **5**(PCP) and improves the catalytic activity for nitrogen fixation using DFT calculations.¹⁸ In fact, Nishibayashi group has synthesized substituted Mo(PCP)-trihalide complexes and experimentally confirmed to improve the catalytic activity, where up to 60,000 equiv. of NH₃ based on the Mo atom of them.¹⁸

This success of DFT predictions showed the utility of theory-based ligand design. In this study, the author investigates electronic influences and trends in introducing substituents into the PCP ligand. The goal is to find substituents that should improve the catalytic activity over the CF₃ group. Moreover, the author will obtain a promising strategy for ligand design based on this theoretical analysis.

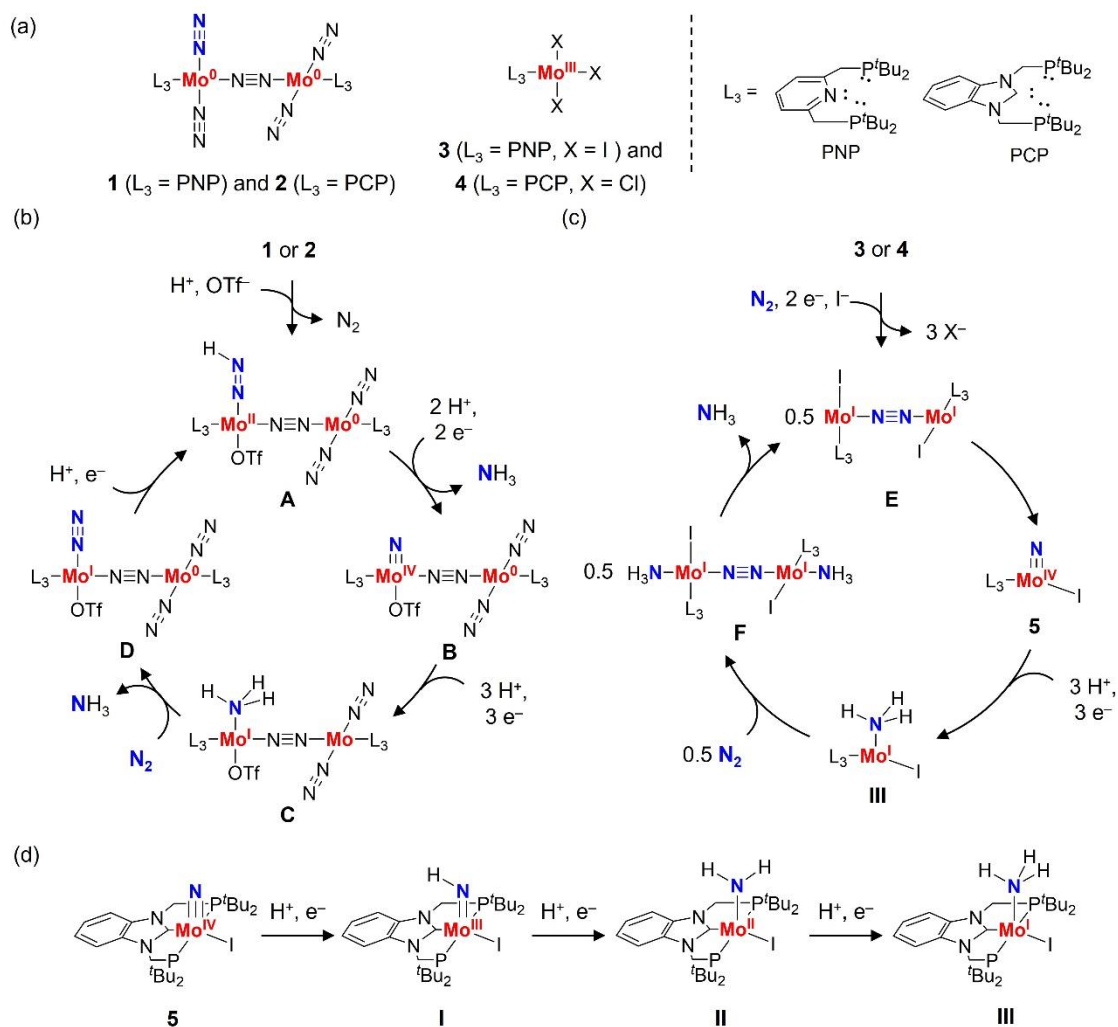
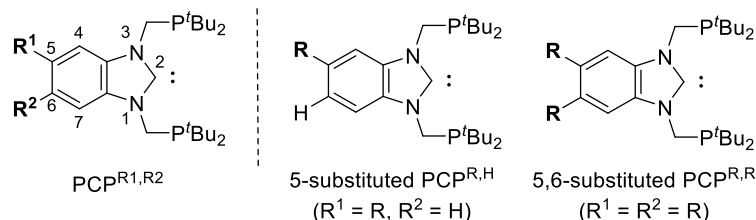


Figure 4-2. Proposed catalytic cycles of the conversion of ammonia from dinitrogen using Mo–PNP and –PCP complexes. (a) Schematic structures of N₂-bridged dimolybdenum complexes **1** and **2** and molybdenum-trihalide complexes **3** and **4** bearing tridentate pincer ligand (L_3). (b) The proposed catalytic cycle in the presence of **1** or **2** as a catalyst. (c) The proposed catalytic cycle in the presence of **3** or **4** as a catalyst. (d) Successive N–H bond formation via PCET process from **5** to **III** in the presence of H₂O as a proton source and SmI₂ as an electron source.

4.2. Computational Methods

Introducing substituents into the PCP ligand is a promising way to control the electronic properties of the Mo–PCP complexes and improve the catalytic activity of the molybdenum-trihalide complex for nitrogen fixation. Very recently, the author has successfully demonstrated that introducing electron-withdrawing groups, such as -F, -Cl, and -CF₃, into the PCP ligand dramatically improved the catalytic activity.¹⁸ The CF₃ group with the strongest electron-withdrawing ability of these groups achieved the highest catalytic activity for nitrogen fixation. Therefore, the author predicts that introducing electron-withdrawing groups stronger than the CF₃ group can further improve the catalytic activity. In this study, the author has designed substituted PCP ligands having various electron-donating/withdrawing groups to control electronic properties of the Mo–PCP complexes shown in Figure 4-2(d). In the substituted PCP ligands, the substituents (R) were introduced at the 5 (R¹) and 6 (R²) positions of the benzimidazole moiety of the PCP ligand along to the atomic numbering protocol in Scheme 4-1. As a result, the author modeled 5-substituted (R¹ = R, R² = H) and 5,6-substituted (R¹ = R² = R) PCP ligands. The Hammett substituent constant σ_p is widely known as a quantitative indicator for evaluating the electron-donating/withdrawing ability of substituents.²² Based on the Hammett substituent constant,²² the author selected 20 substituents containing 4 electron-donating substituents, -OH (σ_p = -0.37), -OCH₃ (-0.27), -CH₃ (-0.27), and -Ph (-0.01), and 16 electron-withdrawing substituents, -F (0.06), -Br (0.23), -Cl (0.23), -OCF₃ (0.35), -CCl₃ (0.46), -NC (0.49), -SCF₃ (0.50), -CF₃ (0.54), -CN (0.66), -SF₅ (0.68), -SiF₃ (0.69), -SO₂CH₃ (0.72), -PF₄ (0.80), -SO₂CF₃ (0.96), -SO₂F (0.91), and -SO₂Cl (1.11). Totally, 40 substituted PCP ligands as well as the unsubstituted PCP ligand (R¹ = R² = H) were modeled in this study.

Scheme 4-1. Atomic numbering protocol of the benzimidazole moiety of PCP ligand and schematic structure of two type of substituted PCP ligands.



DFT calculations were performed with the Gaussian09 program (Rev. E.01).²³ Geometry optimizations were carried out with the B3LYP-D3 functional, which is the B3LYP hybrid functional²⁴⁻²⁷ combined with an empirical dispersion correction developed by Grimme.²⁸ In this study, the SDD (Stuttgart/Dresden pseudopotentials) basis sets^{29,30} are employed for the molybdenum and iodine atoms. The 6-31G(d) basis sets³¹⁻³⁴ are employed for the other atoms. All optimized structures were confirmed to have no imaginary frequency by vibrational analysis. To determine energy profiles, single-point energy calculations were performed at the optimized geometries by using the 6-311+G(d,p) basis sets³⁵⁻³⁷ instead of 6-31G(d). In the single-point calculations, the solvation effects of tetrahydrofuran (THF; $\epsilon = 7.4257$) were considered by using the polarizable continuum model (PCM),³⁸ because the author would like to simulate catalytic reactions using **4** and its substituted derivatives in THF as a solvent.^{17,18}

The reactivity of the 40 substituted models of the Mo(IV)–nitride complex **5** was discussed from the N–H bond strength of Mo(III)–imide (–NH), Mo(II)–amide (–NH₂), and Mo(I)–ammine (–NH₃) group in [Mo(PCP^{R1,R2})(I)(NH_x)] ($x = 1-3$), in which PCP^{R1,R2} presents a substituted PCP ligand. The N–H bond strength was evaluated as the bond dissociation free energy (BDFE) and bond dissociation enthalpy (BDE) at 298 K, which were calculated based on homolysis of the N–H bond, [Mo(PCP^{R1,R2})(I)(NH_x)] → [Mo(PCP^{R1,R2})(I)(NH_{x-1})] + H ($x = 1-3$).¹⁸ The BDFE_{N-H} and BDE_{N-H} have been utilized for evaluating the reactivity of various transition metal–nitrogen complexes with hydrogen (H⁺/e[−]) sources via PCET involving a concerted transfer of a single proton and a single electron.^{18,20,39-41}

4.3. Results and Discussion

4.3.1. Effect on LUMO energy of Mo-nitride complex

Our previous kinetic study¹⁸ revealed that the transformation of the nitride N atom of **5** into ammonia via PCET is the rate-determining in the proposed catalytic cycle as shown in Figure 4-2(c). DFT calculations on the $BDFE_{N-H}$ of $[Mo(PCP)(I)(NH_x)]$ ($x = 1-3$) demonstrated that the N–H bond strength of the Mo(III)–imide complex **I** ($x = 1$; 33.8 kcal mol⁻¹) is much weaker than those of Mo(II)–amide complex **II** ($x = 2$; 52.7 kcal mol⁻¹) and Mo(I)–ammine complex **III** ($x = 3$; 41.2 kcal mol⁻¹). Thus, the PCET to the Mo(IV)–nitride complex **5** is a key elementary reaction step to be improved. The reactivity of **5** with a coupled H^+/e^- donor (an H_2O/SmI_2 complex) can be improved by increasing the electron affinity of **5**, because the PCET involves a concerted transfer of a proton and an electron. As shown in Figure 4-3(a), the LUMO of **5** is delocalized over the imidazole ring of the PCP ligand. Therefore, the electron affinity of **5** is tunable by introducing electron-donating/withdrawing groups to the PCP ligand. In this study, the author designed PCP ligands substituted with $-CH_3$, $-F$, $-Cl$, and $-CF_3$ groups to compare the LUMO energies of the corresponding Mo(IV)–nitride complexes.¹⁸ As the author predicted, the calculated LUMO energies strongly correlated with the Hammett constant σ_p of the substituents, and **5-CF₃-5** complex had the lowest LUMO energy. The author here expands our scope to 20 models of substituted PCP ligands (including 4 substituted PCP ligands mentioned above) and aim to obtain deeper insight into the relationship between the electron-donating/withdrawing ability of the substituents and the LUMO energies of the substituted Mo(IV)–nitride complexes.

Tables 4-1 and 4-2 list calculated LUMO energies of the 5- and 5,6-substituted **5**, respectively, together with the Hammett constant of the corresponding substituent (R). Entry numbers are given in ascending order of the σ_p values except for H (entry 1). The author can find two trends in Tables 4-1 and 4-2. First, the larger the Hammett constant of a substituent on the PCP ligand (i.e. the stronger the electron-withdrawing ability of a substituent), the lower the LUMO energy of the corresponding Mo(IV)–nitride complex. Second, comparing PCP ligands with the same substituent, the LUMO energy of a doubly(5,6)-substituted Mo(IV)–nitride complex is lower than that of a singly(5)-

substituted one. Figure 4-4 plots the LUMO energies of (a) 5-substituted and (b) 5,6-substituted Mo(IV)–nitride complexes versus the Hammett constant of the substituent. In both substituted models, the LUMO energies of the Mo(IV)–nitride complexes show a good linear correlation with the Hammett constants, where $R^2 = 0.89$ for the 5-substituted model and 0.94 for the 5,6-substituted model. It should be noted that the energies of the LUMO+1 were plotted instead of the LUMO for entry 21 (-SO₂Cl) in Figure 4-4(a) and entries 30 (-CCl₃), 35 (-SF₅), 37 (-PF₄), 39 (-SO₂CF₃), 40 (-SO₂F), and 41 (-SO₂Cl) in Figure 4-4(b). This is because spatial distribution of the LUMO of the Mo(IV)–nitride complexes substituted with these groups is strongly localized in the vicinity of the substituents. For example, as shown in Figure 4-3(b), the LUMO of the 5-SO₂Cl-substituted Mo-nitride complex 5-SO₂Cl-**5** (-2.68 eV) is localized at the SO₂Cl group, while the spatial distribution of the LUMO+1 (-1.92 eV) is similar to that of the LUMO of the **5** as shown in Figure 4-3(a). From these results, the author can expect that the electron affinity of the Mo(IV)–nitride complex is further improved by introducing stronger electron-withdrawing substituents than the CF₃ group. In summary, the DFT calculations for 40 models complexes show that introducing electron-withdrawing groups into the PCP ligand significantly lowers the LUMO energies of the Mo(IV)–nitride complexes. The lowering of the LUMO energy enhances the electron affinity of **5**, which is important for electron transfer to **5** in the PCET process. Mo(III)–trihalide complexes bearing PCP ligand substituted with strong electron-withdrawing groups such as -SF₅ are expected to have higher catalytic activity than CF₃-substituted Mo(III)–trihalide complex, which have been reported to have the highest catalytic activity.¹⁸

Interestingly, the LUMO energies of Ph-substituted Mo(IV)–nitride complexes (-1.50 eV for 5-Ph-**5** and -1.46 eV for 5,6-Ph-**5**) are lower than that of the **5** (-1.41 eV), although the Ph group is classified as a weak electron-donating group ($\sigma_p = -0.01$).²² In particular, the LUMO energy of 5-Ph-**5** is comparable to that of the 5-F-substituted Mo-nitride complex 5-F-**5** (-1.53 eV). The author will discuss later how the Ph group affects the electronic structure of **5**.

Table 4-1. LUMO energy of 5-substituted Mo-nitride complexes and $\Delta\delta_{\text{calc}}$ and $\Delta\delta_{\text{exp}}$ values of the corresponding PCP–Se adducts

entry	Substituent group R	Hammett constant σ_p	LUMO energy (eV)	$\Delta\delta_{\text{calc}}$ (ppm)	$\Delta\delta_{\text{exp}}^a$ (ppm)
1	-H	0.00	-1.41 ^a	0.00	0.00
2	-OH	-0.37	-1.37	-5.82	
3	-OCH ₃	-0.27	-1.31	-9.10	
4	-CH ₃	-0.17	-1.34	-7.86	
5	-Ph	-0.01	-1.50	7.57	
6	-F	0.06	-1.53	25.14	
7	-Br	0.23	-1.61	34.64	
8	-Cl	0.23	-1.61	32.64	
9	-OCF ₃	0.35	-1.65	29.37	
10	-CCl ₃	0.46	-1.82	60.90	
11	-NC	0.49	-1.85	64.07	
12	-SCF ₃	0.50	-1.76	52.50	
13	-CF ₃	0.54	-1.71 ^a	48.16	27.2
14	-CN	0.66	-1.99	83.69	
15	-SF ₅	0.68	-1.88	72.50	
16	-SiF ₃	0.69	-1.80	48.83	
17	-SO ₂ CH ₃	0.72	-1.88	63.49	
18	-PF ₄	0.80	-1.88	81.67	
19	-SO ₂ CF ₃	0.91	-2.13	93.39	
20	-SO ₂ F	0.96	-2.14	105.83	
21	-SO ₂ Cl	1.11	-2.68(-1.92) ^b	115.69	

^aref 18.

^bLUMO+1 energy in parenthesis.

Table 4-2. LUMO energy of 5,6-substituted Mo-nitride complexes and $\Delta\delta_{\text{calc}}$ and $\Delta\delta_{\text{exp}}$ values of the corresponding PCP–Se adducts

entry	Substituent group R	Hammett constant σ_p	LUMO energy (eV)	$\Delta\delta_{\text{calc}}$ (ppm)	$\Delta\delta_{\text{exp}}^a$ (ppm)
1	-H	0.00	-1.41 ^a	0.00	0.00
22	-OH	-0.37	-1.31	-22.91	
23	-OCH ₃	-0.27	-1.19	-39.04	
24	-CH ₃	-0.17	-1.29 ^a	-27.78	
25	-Ph	-0.01	-1.46	4.40	
26	-F	0.06	-1.64 ^a	41.63	23.1
27	-Br	0.23	-1.77	49.61	
28	-Cl	0.23	-1.78 ^a	51.26	30.2
29	-OCF ₃	0.35	-1.84	75.65	
30	-CCl ₃	0.46	-2.17(-2.06) ^b	109.25	
31	-NC	0.49	-2.16	115.71	
32	-SCF ₃	0.50	-1.96	81.06	
33	-CF ₃	0.54	-1.94 ^b	86.97	49.5
34	-CN	0.66	-2.33	149.90	
35	-SF ₅	0.68	-2.58(-2.15) ^b	140.98	
36	-SiF ₃	0.69	-2.03	85.48	
37	-SO ₂ CH ₃	0.72	-2.08	101.90	
38	-PF ₄	0.80	-2.20(-2.15) ^b	120.38	
39	-SO ₂ CF ₃	0.91	-2.38(-2.35) ^b	157.84	
40	-SO ₂ F	0.96	-2.51(-2.42) ^b	171.72	
41	-SO ₂ Cl	1.11	-3.11(-2.64) ^b	178.02	

^aref 18.

^bLUMO+1 energy in parenthesis.

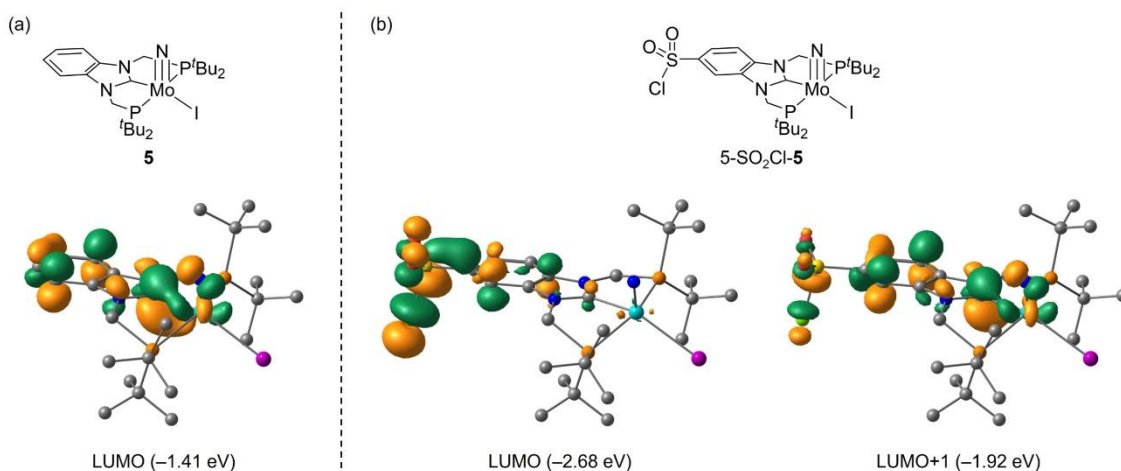


Figure 4-3. Spatial distributions of LUMO and LUMO+1 of (a) **5** and (b) 5-SO₂Cl-**5**.

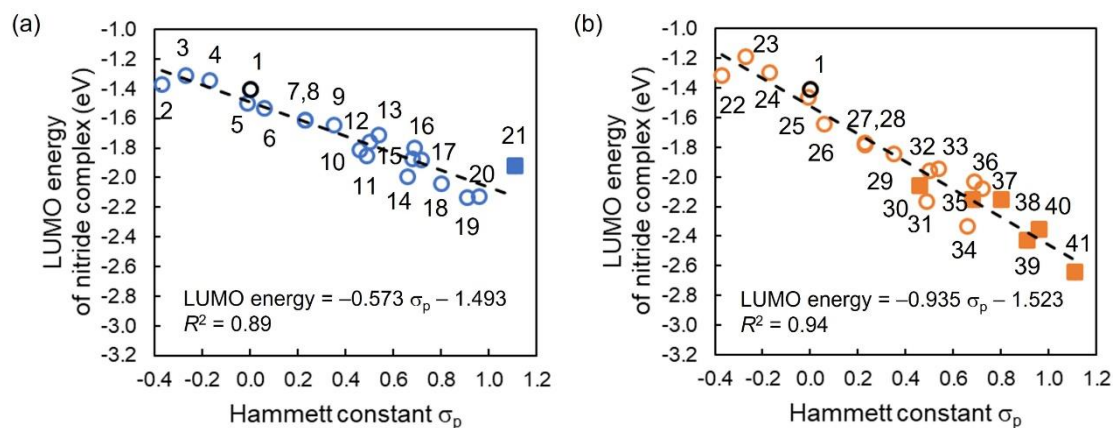


Figure 4-4. LUMO energies of (a) 5-substituted and (b) 5,6-substituted Mo-nitride complexes as a function of Hammett constant σ_p of the introduced substituent. Entry numbers of substituted models in Tables 4-1 and 4-2 are marked near their plots. In models of entry 21, 29, 35, 37, 38, 39, 40, and 41, the LUMO+1 energy is plotted as a square symbol.

4.3.2. Effect on π -accepting ability of PCP ligand

In this study, the empirical Hammett substituent constant is employed as a numerical index of the electron-donating/withdrawing ability of substituents on the *N*-heterocyclic carbene (NHC)-based PCP ligand. When an NHC-based ligand is coordinating to a *d*-metal center, it can serve as a π -acceptor as well as a strong σ -donor.⁴²⁻⁴⁴ The author previously demonstrated that the high nitrogen fixation ability of dimolybdenum(0)–PCP complex **2** can be rationalized by a rigid Mo–C bond between the Mo(0) center and carbene C atom of the PCP ligand.¹⁴ Therefore, in the Mo(PCP)–nitride complex, the strength of the π -accepting ability should also affect the catalytic activity for nitrogen fixation. In 2015, Cavallo and coworkers reported that ⁷⁷Se-NMR chemical shift of NHC–Se adducts with a C=Se bond is a useful quantitative indicator of the π -accepting ability of NHCs.⁴⁵ They observed that various NHC–Se adducts showed an excellent correlation between the experimental ⁷⁷Se-NMR chemical shifts and the calculated ⁷⁷Se-NMR shielding values. The calculated ⁷⁷Se-NMR shielding values also correlated with the energy gap between a filled *p* orbital of the Se atom and the vacant π^* orbital of the NHC moiety in the NHC–Se shown in Figure 4-5(a). In our Mo–PCP system shown in Figure 4-3(a), the LUMO of Mo(IV)–nitride complex **5** contains the π^* orbital of the NHC-based PCP ligand as a main component. The author would like to calculate ⁷⁷Se-NMR shielding values of substituted PCP ligands to evaluate the π -accepting ability of the substituted PCP^{R1,R2} ligand. At first, the author investigated a correlation between experimental ⁷⁷Se-NMR chemical shifts and calculated ⁷⁷Se-NMR shielding values of the C=Se moiety about six synthesized PCP–Se adducts as shown in Figure 4-5(b) (unsubstituted one and five substituted ones containing CH₃, F, Cl, and CF₃ groups). The optimization of structures of the substituted PCP^{R1,R2}–Se adducts was carried out by the B3LYP-D3/6-31G(d) procedure of DFT calculation.^{24-28,31-34} After that, the author carried out the ⁷⁷Se-NMR shielding calculations with the gauge-independent atomic orbital (GIAO) method⁴⁶⁻⁵⁰ using the 6-311+G(d,p) basis set³⁵⁻³⁷ instead of the 6-31G(d) and obtained the isotropic shielding constant σ_{calc} . The PCM model was employed to evaluate the solvent effect of THF.³⁸ To evaluate relative ⁷⁷Se-NMR chemical shifts of PCP^{R1,R2}–Se adducts to that of the unsubstituted PCP–Se adduct, the author here defined $\Delta\delta(\text{PCP}^{\text{R1,R2}}\text{--Se})$ value as follows:

$$\Delta\delta(\text{PCP}^{\text{R1,R2}}\text{-Se}) = \delta(\text{PCP}^{\text{R1,R2}}\text{-Se}) - \delta(\text{PCP-Se}) \quad (1)$$

where $\delta(\text{PCP}^{\text{R1,R2}}\text{-Se})$ and $\delta(\text{PCP-Se})$ are the ^{77}Se -NMR chemical shift of the substituted $\text{PCP}^{\text{R1,R2}}\text{-Se}$ adduct and the unsubstituted PCP-Se adduct, respectively. Positive experimental $\Delta\delta$ ($\Delta\delta_{\text{exp}}$) and calculated $\Delta\delta$ ($\Delta\delta_{\text{calc}}$) values indicate that introducing substituents into the PCP ligand enhances the π -accepting ability of the PCP ligand. In particular, in the case of $\Delta\delta_{\text{calc}}$, the author can obtain it from the ^{77}Se -NMR shielding value σ_{calc} of the $\text{PCP}^{\text{R1,R2}}\text{-Se}$ and the unsubstituted PCP-Se adducts instead of $\delta_{\text{calc}}(\text{PCP}^{\text{R1,R2}}\text{-Se})$ and $\delta_{\text{calc}}(\text{PCP-Se})$. In general, the NMR chemical shift of a sample ($\delta(\text{sample})$) is defined using NMR shielding values of the sample ($\sigma(\text{sample})$) and a reference ($\sigma(\text{reference})$) as follows:

$$\delta(\text{sample}) = \sigma(\text{reference}) - \sigma(\text{sample}) \quad (2)$$

Following this eq. (2), the $\delta_{\text{calc}}(\text{PCP}^{\text{R1,R2}}\text{-Se})$ and $\delta_{\text{calc}}(\text{PCP-Se})$ values are rewritten as follows:

$$\delta_{\text{calc}}(\text{PCP}^{\text{R1,R2}}\text{-Se}) = \sigma_{\text{calc}}(\text{reference}) - \sigma_{\text{calc}}(\text{PCP}^{\text{R1,R2}}\text{-Se}) \quad (3)$$

$$\delta_{\text{calc}}(\text{PCP-Se}) = \sigma_{\text{calc}}(\text{reference}) - \sigma_{\text{calc}}(\text{PCP-Se}) \quad (4)$$

where $\sigma_{\text{calc}}(\text{reference})$, $\sigma_{\text{calc}}(\text{PCP}^{\text{R1,R2}}\text{-Se})$, and $\sigma_{\text{calc}}(\text{PCP-Se})$ are the calculated NMR shielding values of the reference, the substituted $\text{PCP}^{\text{R1,R2}}\text{-Se}$ adduct, and the unsubstituted PCP-Se adduct, respectively. Therefore, using eq. (3) and (4), the author can rewrite eq. (1) as follows:

$$\Delta\delta_{\text{calc}}(\text{PCP}^{\text{R1,R2}}\text{-Se}) = \sigma_{\text{calc}}(\text{PCP-Se}) - \sigma_{\text{calc}}(\text{PCP}^{\text{R1,R2}}\text{-Se}) \quad (5)$$

The $\sigma_{\text{calc}}(\text{PCP}^{\text{R1,R2}}\text{-Se})$ and $\sigma_{\text{calc}}(\text{PCP-Se})$ values are in the Supporting Information. Tables 4-1 and 4-2 show the $\Delta\delta_{\text{exp}}$ value of the C=Se moiety of the synthesized $\text{PCP}^{\text{R1,R2}}\text{-Se}$ adducts. The larger the Hammett constant of the substituent, the larger the $\Delta\delta_{\text{exp}}$ value of the $\text{PCP}^{\text{R1,R2}}\text{-Se}$ adducts. Figure 4-5(c) plots the $\Delta\delta_{\text{exp}}$ value versus the $\Delta\delta_{\text{calc}}$ value, and is in an excellent correlation ($R^2 = 1.00$), although the slope equals 0.54. Therefore, the author confirmed that the $\Delta\delta_{\text{calc}}$ value is useful as a qualitative indicator to evaluate the π -accepting ability of the PCP ligand in our PCP-Se system.

Next, the author calculated $\Delta\delta_{\text{calc}}$ values of 40 substituted PCP–Se adducts in Tables 4-1 and 4-2 and investigated a correlation between the $\Delta\delta_{\text{calc}}$ value and the LUMO energy of the corresponding Mo(IV)–nitride complex $[\text{Mo}^{\text{IV}}(\text{PCP}^{\text{R1,R2}})(\text{I})(\equiv\text{N})]$. The larger the Hammett constant σ_{p} of the substituent, the larger the $\Delta\delta_{\text{calc}}$ value of the substituted PCP–Se adduct tends to be. Figure 4-6 plots the LUMO energy of the substituted Mo(IV)–nitride complex versus the $\Delta\delta_{\text{calc}}$ value of the corresponding PCP–Se adduct. The correlation between the LUMO energy and the $\Delta\delta_{\text{calc}}$ value ($R^2 = 0.97$) is better than the correlation between the LUMO energy and the Hammett substituent constant σ_{p} ($R^2 = 0.89$ for Figure 4-3(a), 0.94 for Figure 4-3(b)). The following discussion will evaluate the electron-donating/withdrawing abilities of the substituted PCP ligands with the $\Delta\delta_{\text{calc}}$ values instead of the Hammett substituent constants. Notably, the $\Delta\delta_{\text{calc}}$ value enables us to compare the effect of the number of substituents numerically. As a result, for the same substituent, the magnitude of the $\Delta\delta_{\text{calc}}$ value of the doubly-substituted PCP–Se adducts tends to be larger than that of the singly-substituted ones. Interestingly, the $\Delta\delta_{\text{calc}}$ values of Ph-substituted PCP–Se adducts, where the Ph group is classified in a weak electron-donating group ($\sigma_{\text{p}} = -0.01$), were calculated to be 7.57 and 4.40 for the single- and double-substituted models. The positive $\Delta\delta_{\text{calc}}$ values indicate that introducing Ph groups into the PCP ligand enhances the π -accepting ability of the PCP ligand, like an electron-withdrawing substituent.

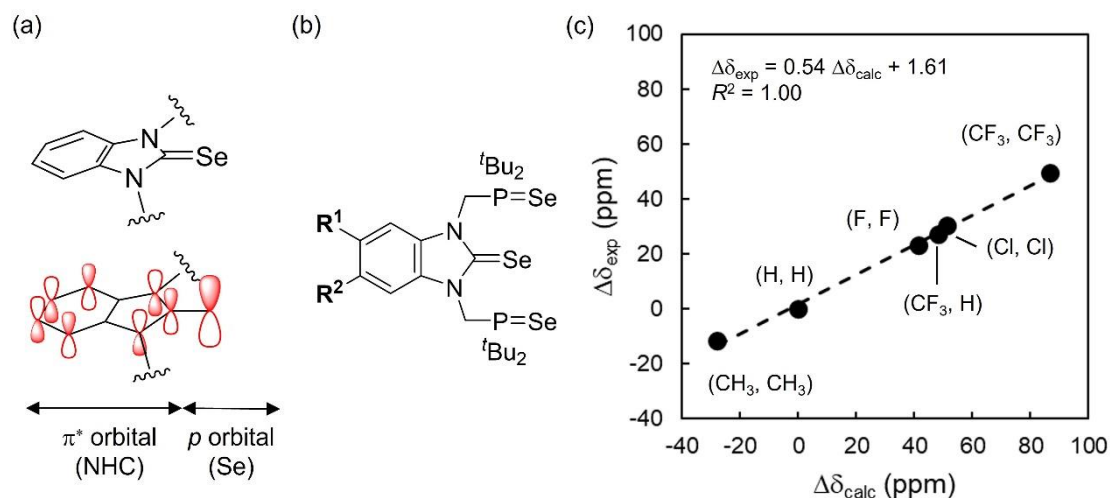


Figure 4-5. (a) A schematic distribution of p interaction between the Se atom and the benzimidazole moiety of the PCP ligand, (b) a calculated structure of the substituted PCP-Se adduct, and (c) a relationship between $\Delta\delta_{exp}$ and $\Delta\delta_{calc}$ values for synthesized PCP^{R^1,R^2} -Se adducts.

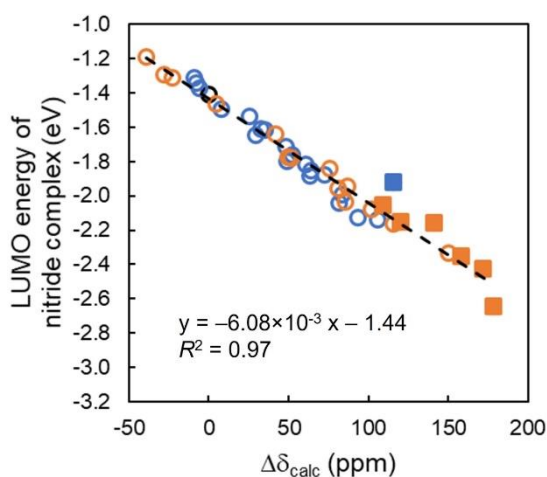


Figure 4-6. LUMO energy of the nitride complex bearing 5- (blue circle) and 5,6-substituted PCP ligands (orange circle) versus $\Delta\delta_{calc}$ value of the corresponding PCP-Se adduct. The LUMO+1 energy is plotted as a square symbol.

4.3.3 Thermodynamic strength of N-H bond for prediction of the catalytic activity

The author next investigated how the introduction of electron-donating/withdrawing substituents to the PCP ligand affected the N-H bond strength of $[\text{Mo}(\text{PCP}^{\text{R1,R2}})(\text{I})(\text{NH}_x)]$ ($x = 1-3$) based on the bond dissociation free energy (BDFE) and bond dissociation enthalpy (BDE). As shown in the proposed catalytic mechanism in Figure 4-2(d), three successive PCET processes transform the nitride N atom of $[\text{Mo}(\text{PCP})(\text{I})(\equiv\text{N})]$ **5** into NH_3 via three intermediates, Mo(III)-imide complex, $[\text{Mo}(\text{PCP})(\text{I})(=\text{NH})]$ **I**, Mo(II)-amide complex, $[\text{Mo}(\text{PCP})(\text{I})(\text{NH}_2)]$ **II**, and Mo(I)-ammine complex, $[\text{Mo}(\text{PCP})(\text{I})(\text{NH}_3)]$ **III**. The values of $\text{BDFE}_{\text{N-H}}$ and $\text{BDE}_{\text{N-H}}$ calculated for $[\text{Mo}(\text{PCP}^{\text{R1,R2}})(\text{I})(\text{NH}_x)]$, which correspond to the hydrogen atom affinity of the substituted complexes of **I-III**, provide useful information on substituent effects on the formation of ammonia via PCET. Chirik and coworkers utilized the $\text{BDFE}_{\text{N-H}}$ values in discussing the photo-induced PCET-driven reductions of different transition-metal-nitrogen complexes, such as Mn-nitride,^{39,40} Ti-amide,⁴¹ and Co-imide complexes.⁴¹ The author also theoretically evaluated the hydrogen affinity of an Mo(I)-NNH complex from the $\text{BDFE}_{\text{N-H}}$ value, where PCET formed the Mo(I)-NNH complex from an $\text{SmI}_2/\text{H}_2\text{O}$ complex to $[\text{Mo}(\text{N}_2)(\text{PMePh}_2)_4]$.²⁰

Tables 4-3 and 4-4 summarize the values of $\text{BDFE}_{\text{N-H}}$ and $\text{BDE}_{\text{N-H}}$ calculated for the Mo(III)-imide, Mo(II)-amide, and Mo(I)-ammine complexes bearing 5- and 5,6-substituted PCP ligands, $[\text{Mo}(\text{PCP}^{\text{R1,R2}})(\text{I})(\text{NH}_x)]$ ($x = 1-3$), respectively. Figure 4-7 plots (a) $\text{BDFE}_{\text{N-H}}$ and (b) $\text{BDE}_{\text{N-H}}$ values computed for the three intermediates versus $\Delta\delta_{\text{calc}}$ representing the π -accepting ability of the substituted PCP ligands. The author can point out some trends in Figure 4-7. (1) The $\text{BDFE}_{\text{N-H}}$ and $\text{BDE}_{\text{N-H}}$ values of the unsubstituted and substituted complexes exhibit the following order, imide ($x = 1$) < ammine ($x = 3$) < amide ($x = 2$), which is the same trend reported in our previous study. (2) The stronger electron-withdrawing substituents that are introduced to the PCP ligand, the larger the $\text{BDFE}_{\text{N-H}}$ and $\text{BDE}_{\text{N-H}}$ values. For example, the $\text{BDFE}_{\text{N-H}}$ and $\text{BDE}_{\text{N-H}}$ values of 5,6-substituted and unsubstituted imide complexes are calculated to be 32.1 and 40.0 kcal mol⁻¹ for -OCH₃ (entry 23, $\Delta\delta_{\text{calc}} = -39.04$), 33.8 and 41.3 kcal mol⁻¹ for -H (entry 1, $\Delta\delta_{\text{calc}} = 0.00$), and 37.8 and 46.0 kcal mol⁻¹ for -SO₂Cl (entry 41, $\Delta\delta_{\text{calc}} = 178.02$). Thus, the thermodynamic stability of the substituted Mo(III)-imide complexes should depend

on the π -accepting ability of the substituted PCP ligands. Since the BDFE value of an O–H bond of an $\text{SmI}_2/\text{H}_2\text{O}$ complex is estimated to be 34 kcal mol^{-1} in THF solvent,²¹ the introduction of strongly electron-withdrawing substituents to the PCP ligand can promote the PCET reaction to yield the substituted Mo-imide complex. (3) The introduction of the electron-withdrawing groups effectively strengthens the N–H bond of the Mo-imide complexes compared to that of the amide and ammine complexes. As shown in Figure 4-7(a), the slopes fitted to the 41 plots of $\text{BDFE}_{\text{N-H}}$ value of $[\text{Mo}(\text{PCP}^{\text{R1,R2}})(\text{I})(\text{NH}_x)]$ were 2.83×10^{-2} for Mo(III)–imide, 1.82×10^{-2} for Mo(II)–amide, and 9.83×10^{-3} for Mo(I)–ammine. The smallest $\text{BDFE}_{\text{N-H}}$ values of the Mo(III)–imide complexes and the steepest slope fitted for the imide complexes indicate that the formation of imide complexes should be focused on as a key reaction step in the proposed catalytic cycle for nitrogen fixation. The author also found that the correlation between $\text{BDE}_{\text{N-H}}$ and $\Delta\delta_{\text{calc}}$ was better than that for $\text{BDFE}_{\text{N-H}}$ ($R^2 = 0.95$ vs. 0.67). Therefore, in the following discussion, the author will adopt the $\text{BDE}_{\text{N-H}}$ value as an index of the N–H bond strength in the substituted imide complexes $[\text{Mo}(\text{PCP}^{\text{R1,R2}})(\text{I})(=\text{NH})]$.

Table 4-3. BDFE_{N-H} and BDE_{N-H} of Mo-imide, -amide, and -amine complexes bearing 5-substituted PCP ligands

entry	substituent R	BDFE _{N-H} value (kcal mol ⁻¹)			BDE _{N-H} value (kcal mol ⁻¹)		
		imide	amide	amine	imide	amide	amine
		(I)	(II)	(III)	(I)	(II)	(III)
1	-H	33.8	52.7	41.2	41.3	60.6	47.7
2	-OH	33.3	51.7	41.4	40.8	60.1	48.2
3	-OCH ₃	33.0	52.0	41.0	40.7	60.1	47.9
4	-CH ₃	33.3	51.8	41.6	40.8	60.2	48.3
5	-Ph	34.1	52.3	41.9	41.7	60.3	48.5
6	-F	34.0	52.3	41.9	41.5	60.8	48.6
7	-Br	35.4	51.8	42.5	42.3	60.6	48.6
8	-Cl	34.8	52.2	42.4	42.1	60.8	48.7
9	-OCF ₃	36.0	54.9	45.8	42.3	61.2	51.8
10	-CCl ₃	37.4	37.4	44.9	42.6	61.7	48.0
11	-NC	35.7	52.8	42.7	42.9	61.4	49.1
12	-SCF ₃	36.1	54.6	43.4	42.6	61.4	48.8
13	-CF ₃	35.8	52.3	42.8	42.8	61.1	48.8
14	-CN	36.4	53.1	42.7	43.5	61.7	49.1
15	-SF ₅	38.0	53.9	44.6	43.6	61.7	49.2
16	-SiF ₃	37.4	53.8	44.2	43.1	61.3	49.0
17	-SO ₂ CH ₃	35.3	51.8	39.1	42.7	59.2	46.5
18	-PF ₄	38.4	53.7	45.0	44.1	61.8	49.4
19	-SO ₂ CF ₃	35.6	52.5	41.1	43.5	59.6	48.1
20	-SO ₂ F	37.4	53.1	43.5	44.3	62.1	49.5
21	-SO ₂ Cl	37.8	53.7	43.6	44.9	53.7	50.1

Table 4-4. BDFE_{N-H} and BDE_{N-H} values of imide, amide, and ammine intermediates bearing 5,6-substituted PCP ligands

entry	substituent R	BDFE _{N-H} value (kcal mol ⁻¹)			BDE _{N-H} value (kcal mol ⁻¹)		
		imide	amide	ammine	imide	amide	ammine
		(I)	(II)	(III)	(I)	(II)	(III)
1	-H	33.8	52.7	41.2	41.3	60.6	47.7
22	-OH	32.7	52.0	41.0	40.5	59.9	47.6
23	-OCH ₃	32.1	51.8	40.7	40.0	59.4	47.4
24	-CH ₃	32.8	52.1	42.1	40.6	60.0	47.5
25	-Ph	34.5	52.8	41.2	41.7	60.9	48.0
26	-F	33.6	53.6	41.4	41.8	61.4	48.2
27	-Br	34.8	54.8	41.4	42.6	62.1	48.5
28	-Cl	33.7	54.7	41.4	42.3	62.0	48.4
29	-OCF ₃	35.8	55.0	43.9	42.7	62.3	48.7
30	-CCl ₃	38.1	52.3	43.7	43.5	59.6	48.0
31	-NC	35.4	55.4	41.3	43.8	63.0	48.6
32	-SCF ₃	38.4	54.2	43.9	43.4	62.5	49.0
33	-CF ₃	35.1	50.9	42.3	43.1	59.6	48.2
34	-CN	36.6	55.9	41.9	44.8	63.6	49.0
35	-SF ₅	39.3	56.9	44.7	45.1	64.7	49.6
36	-SiF ₃	38.1	57.1	43.2	44.2	63.2	49.1
37	-SO ₂ CH ₃	36.6	51.5	42.3	43.6	60.2	48.5
38	-PF ₄	37.4	53.8	44.2	45.0	63.7	49.6
39	-SO ₂ CF ₃	37.4	52.7	42.3	45.1	60.2	49.7
40	-SO ₂ F	38.5	57.1	43.0	45.9	64.5	49.9
41	-SO ₂ Cl	37.8	57.4	43.2	46.0	64.5	50.2

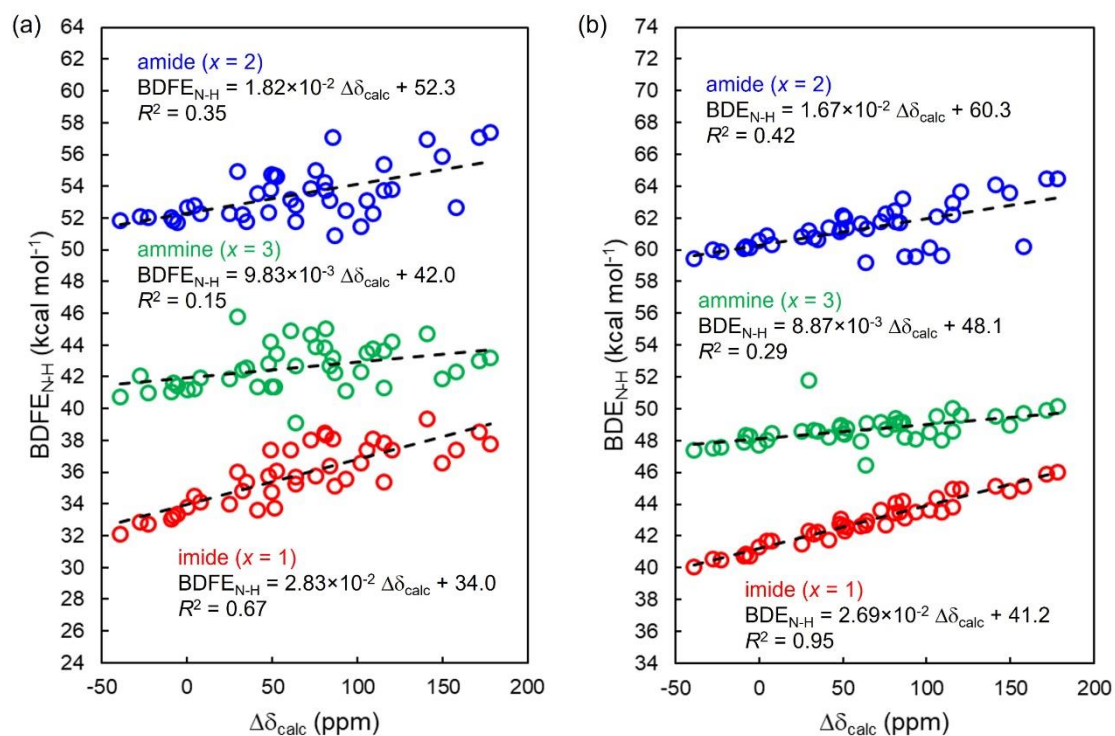


Figure 4-7. (a) $\text{BDFE}_{\text{N-H}}$ and (b) $\text{BDE}_{\text{N-H}}$ plots of substituted Mo-imide (red), -amide (blue), and -amine (green) complexes versus $\Delta\delta_{\text{calc}}$ value of the corresponding PCP–Se adducts. Each broken line is fitted to the 41 plots of $\text{BDFE}_{\text{N-H}}$ or $\text{BDE}_{\text{N-H}}$ in Table 4-3 or Table 4-4.

4.3.4. New design of PCP ligand with fused benzene rings

While the Ph group is classified as a weak electron-donating substituent based on the Hammett constant ($\sigma_p = -0.01$),²² the Ph group introduced to the PCP ligand works as an electron-withdrawing substituent based on the π -accepting ability of Ph-substituted PCP ligands ($\Delta\delta_{\text{calc}} = 7.57$ for 5-substitution and $\Delta\delta_{\text{calc}} = 4.40$ for 5,6-substitution). Moreover, introducing the Ph group to the PCP ligand lowered the LUMO energy of Mo-nitride complex **5** and slightly increased the $\text{BDE}_{\text{N-H}}$ value of Mo(III)–imide complex, $[\text{Mo}^{\text{III}}(\text{PCP})(\text{I})(=\text{NH})]$ **I**. Focusing on the LUMO energy, for example, the LUMO energy of 5-substituted Mo-nitride complex 5-Ph-**5** (−1.50 eV) is lower than that of **5** (−1.41 eV). This result can be explained by looking at the spatial distribution of the LUMO of 5-Ph-**5**. Figure 4-8(a) shows the optimized structure of 5-Ph-**5** with $\phi = 140.2^\circ$ and its spatial distribution of LUMO, where ϕ is defined as a C₁–C₂–C₃–C₄ dihedral angle. The LUMO, which is attributed to a π^* orbital, extends over the Ph group and the neighboring benzimidazole moiety, stabilizing its energy. Next, the author investigated a relationship between the LUMO energy of 5-Ph-**5** and ϕ , as shown in Figure 4-8(b). This obtained curve of the LUMO energy has a symmetrical shape with respect to ϕ in the range 0 to 180° . It shows minimum energy (−1.59 eV) at $\phi = 0^\circ$ and maximum energy (−1.41 eV) at $\phi = 90^\circ$. When $\phi = 0^\circ$ that means the introduced Ph group and the imidazole moiety of the PCP ligand in the same plane, the spatial distribution of the LUMO exhibits the effective π conjugated system. On the other hand, $\phi = 90^\circ$ means that the plane of the Ph group is orthogonal to that of the imidazole moiety. Therefore, the distribution of the LUMO is not found on the Ph group, and this distribution is similar to that of **5**. Certainly, the LUMO energy of 5-Ph-**5** at $\phi = 90^\circ$ is the same as that of **5**. In summary, the author can control the electronic properties of 5-Ph-**5** by ϕ . Notably, at $\phi = 0^\circ$, 5-Ph-**5** should achieve higher catalytic activity for nitrogen fixation than the optimized structure ($\phi = 140.2^\circ$).

This result encouraged us to propose a new design of PCP ligands to introduce benzene rings in the same plane as the benzimidazole moiety of the PCP ligand. The author newly designed two PCP ligands with n -fused benzene rings; naphtho[2,3-*d*]imidazole-based PCP ($n = 2$; entry 42) and naphtho[2,3-*f*]benzimidazole-based PCP ligands ($n = 3$; entry 43) as shown in Figure 4-9. About the PCP ligands with n -fused

benzene rings, Table 4-5 lists the LUMO energy of Mo-nitride complex **5**, $\Delta\delta_{\text{calc}}$ values of the PCP-Se adducts, and the $\text{BDE}_{\text{N-H}}$ of the Mo-imide complexes **I** about the PCP ligands. As the author expected, the LUMO energies of the Mo-nitride complexes with n -fused benzene rings (-1.83 eV for $n = 2$ and -2.17 eV for $n = 3$) is lower than that of **5** (-1.41 eV for $n = 1$) because of the effective delocalization of the LUMO orbital of **5** as shown in Figure 4-10. Moreover, they are also lower than the LUMO energy of **5-Ph-5** at $\phi = 0^\circ$ (-1.50 eV). Owing to $\Delta\delta_{\text{calc}}$, the π -accepting ability of the PCP ligands is enhanced by fused benzene rings. The $\text{BDE}_{\text{N-H}}$ of the Mo-imide complexes with n -fused benzene rings are calculated to be $42.9 \text{ kcal mol}^{-1}$ ($n = 2$) and $44.2 \text{ kcal mol}^{-1}$ ($n = 3$). These values are comparable to or greater than the $\text{BDE}_{\text{N-H}}$ of 5- CF_3 -substituted Mo-imide complex ($42.8 \text{ kcal mol}^{-1}$) that exhibited the highest catalytic activity among substituted PCP ligands synthesized previously.¹⁸ Figure 4-11 plots the $\text{BDE}_{\text{N-H}}$ of **I** and Mo-imide complexes with π -extended PCP ligands versus $\Delta\delta_{\text{calc}}$ of the corresponding PCP-Se adducts with the regression line fitted by 41 plots in Figure 4-7(b). Because these plots nicely fit the broken line, $\Delta\delta_{\text{calc}}$ is an excellent indicator to predict the catalytic activity not only in the substituted models but also in this n -fused model. In summary, Our DFT calculations have shown that the catalytic activity can also be enhanced by extending π -conjugated system of **5** through fused benzene rings.

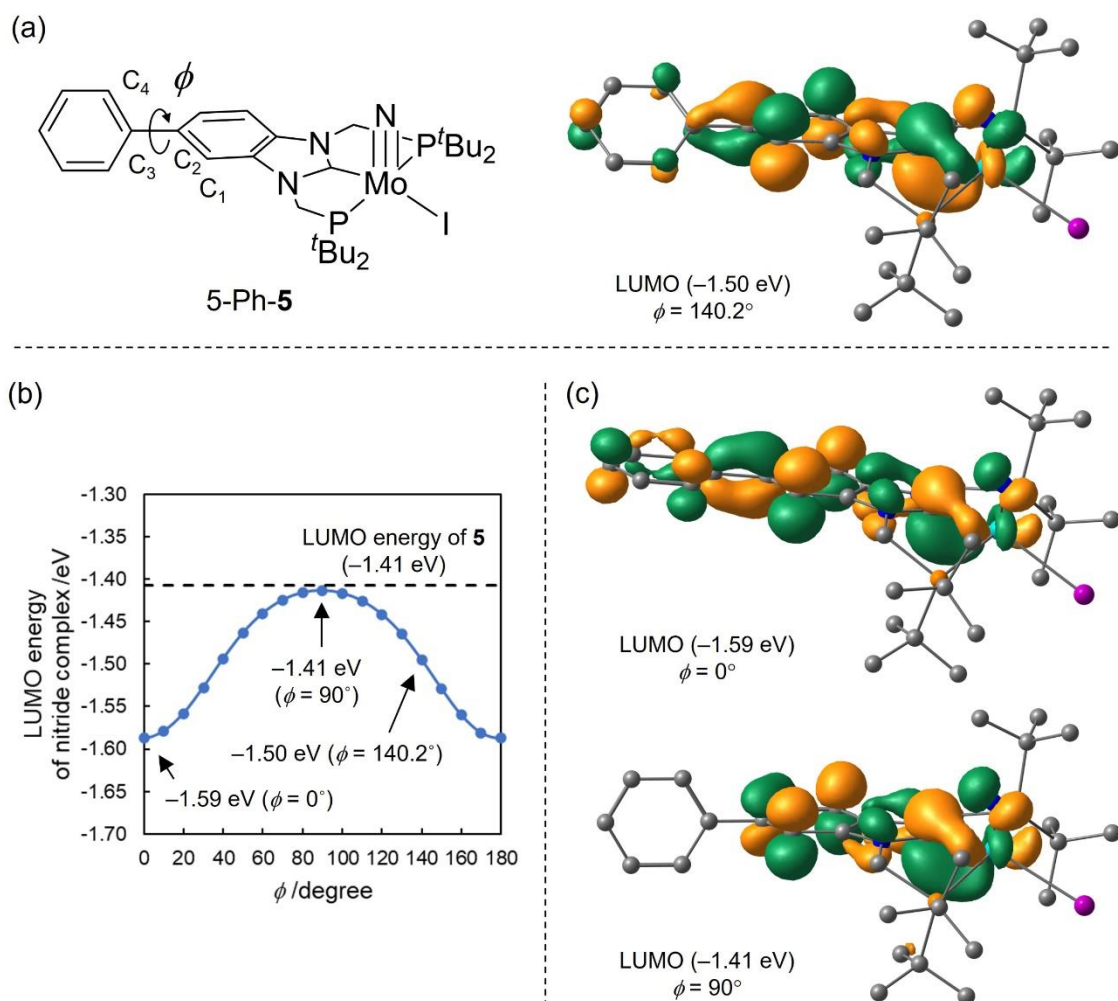


Figure 4-8. (a) Schematic structure of 5-Ph-**5** with C_1 - C_2 - C_3 - C_4 dihedral angle ϕ and spatial distribution of LUMO for the optimized structure of 5-Ph-**5** with $\phi = 140.2^\circ$. (b) LUMO energy of 5-Ph-**5** depending on ϕ . The broken line represents the LUMO energy of **5**. (c) Spatial distributions of the LUMO of 5-Ph-**5** with $\phi = 0$, and 90° .

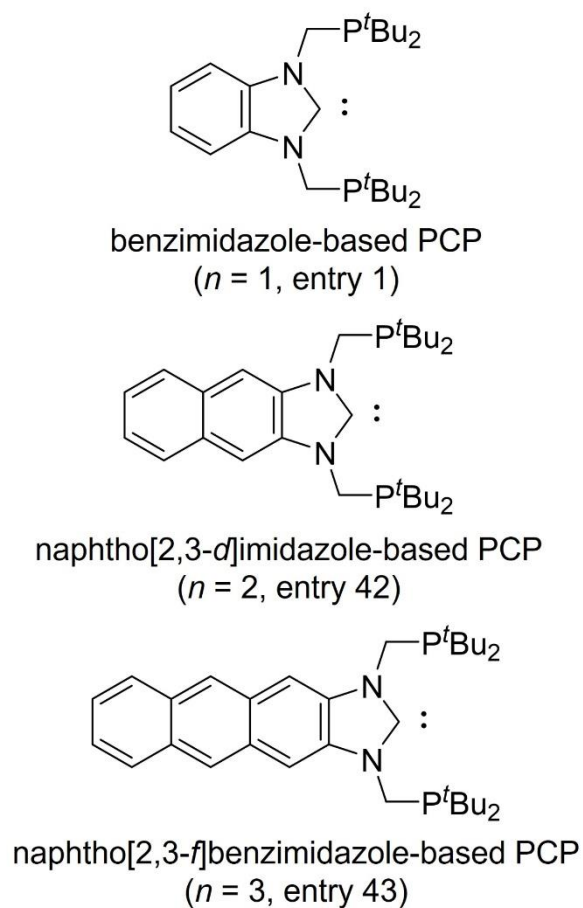


Figure 4-9. PCP ligands containing n fused benzene rings.

Table 4-5. Calculated values for PCP ligands containing n fused benzene rings

entry	fused benzene rings n	LUMO energy of Mo(IV)–nitride complex /eV	$\Delta\delta_{\text{calc}}$ (ppm)	BDE _{N-H} of Mo(III)–imide complex /kcal mol ⁻¹
1	1	-1.41	0.00	41.3
42	2	-1.83	69.7	42.9
43	3	-2.17	110.4	44.2

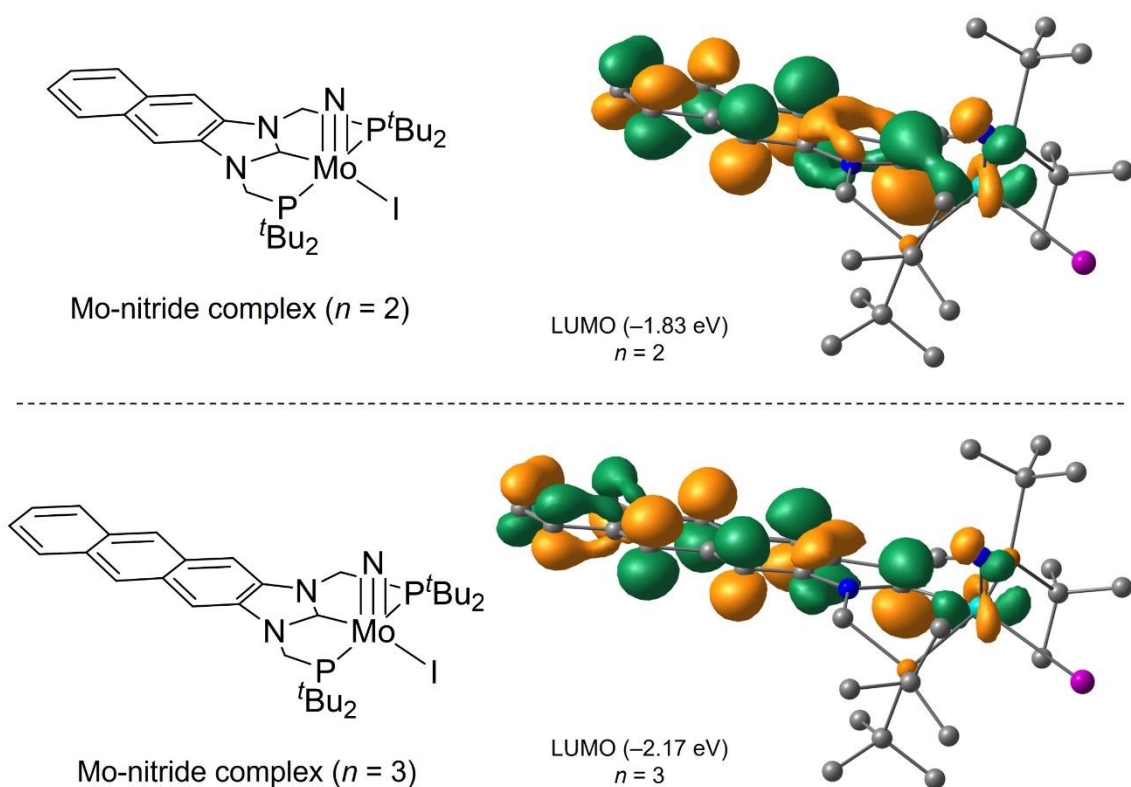


Figure 4-10. Schematic structures and spatial distributions of Mo-nitride complexes bearing PCP ligands with n -fused benzene rings.

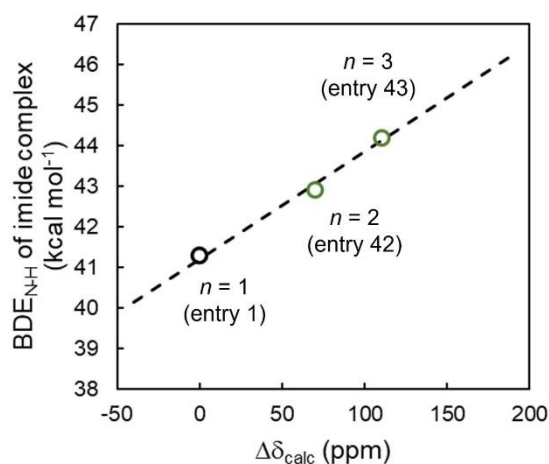


Figure 4-11. $\text{BDE}_{\text{N-H}}$ plot of imide complexes bearing π -extended PCP ligands versus $\Delta\delta_{\text{calc}}$ value of the corresponding PCP–Se adducts with n -fused benzene rings. The broken line is a linear correlation obtained by the 40 substituted Mo-imide complexes in Figure 4-5(b).

4.4. Conclusions

The author has designed substituted PCP ligands using a set of 20 substituents with a wide range of the Hammett substituent constant and performed DFT calculations for substituted Mo-PCP complexes and PCP–Se adducts to predict electronic properties and enhancement of catalytic activity for nitrogen fixation. To be an effective PCET process to an Mo-nitride complex, introducing electron-withdrawing substituents lowers the LUMO energy of the Mo-nitride complex. The LUMO energy of the Mo-nitride complex has an excellent correlation with $\Delta\delta_{\text{calc}}$ value based on the π -accepting ability of the substituted PCP ligand. A $\text{BDE}_{\text{N-H}}$ value of an Mo-imide complex, which should be relevant to the catalytic activity, is enhanced by introducing strongly electron-withdrawing substituents into the PCP ligand. In addition, the $\text{BDE}_{\text{N-H}}$ value correlates well with the $\Delta\delta_{\text{calc}}$ value. It should be noted that the $\Delta\delta_{\text{calc}}$ value indicated that the Ph group works as an electron-withdrawing group in this Mo-PCP system because it extends the π -conjugate system of the benzimidazole moiety of the PCP ligand. Furthermore, the author newly designed π -extended PCP ligands containing some fused benzene rings to enhance the π -accepting ability of the PCP ligand. As a result, the author expected the using Mo complex bearing the π -extended PCP ligand exhibits more significant catalytic activity than that of the CF_3 -substituted Mo complex. Thus, this study provides a new ligand design strategy for nitrogen fixation other than introducing substituents. In the near future, π -extended PCP ligands will be synthesized and exhibit the enhancement of the catalytic activity.

References

1. Shima, T.; Hu, S.; Luo, G.; Kang, X.; Luo, Y.; Hou, Z. Dinitrogen Cleavage and Hydrogenation by a Trinuclear Titanium Polyhydride Complex. *Science*, **2013**, *340*, 1549–1552.
2. Burgess, B. K.; Lowe, D. V. Mechanism of Molybdenum Nitrogenase. *Chem. Rev.* **1996**, *96*, 2983–3011.
3. Einsle, O.; Tezcan, F. A.; Andrade, S. L. A.; Schmid, B.; Yoshida, M.; Howard, J. B.; Rees, D. C. Nitrogenase MoFe-Protein at 1.16 Å Resolution: A Central Ligand in the FeMo-Cofactor. *Science* **2002**, *297*, 1696–1700.
4. Lancaster K. M.; Roemelt, M.; Ettenhuber, P.; Hu, Y.; Ribbe, M. W.; Neese, F.; Bergmann, U. Debeer, S. X-ray Emission Spectroscopy Evidences a Central Carbon in the Nitrogenase Iron-Molybdenum Cofactor. *Science* **2011**, *334*, 974–977.
5. Hoffman, B. M.; Lukoyanov, D.; Yang, Z.-Y.; Dean, D. R.; Seefeldt, L. C. Mechanism of Nitrogen Fixation by Nitrogenase: The Next Stage. *Chem. Rev.* **2014**, *114*, 4041–4062.
6. Yandulov, D. V.; Schrock, R. R. Catalytic Reduction of Dinitrogen to Ammonia at a Single Molybdenum Center. *Science* **2003**, *301*, 76–78.
7. Stucke, N.; Krahmer, J.; Näther, C.; Tucek, F. Molybdenum Complexes Supported by PN3P Pincer Ligands: Synthesis, Characterization, and Application to Synthetic Nitrogen Fixation. *Eur. J. Inorg. Chem.* **2018**, *2018*, 47, 5108–5116.
8. Engesser, T. A.; Kindjajev, A.; Junge, J.; Krahmer, J. Tucek, F. A Chatt-Type Catalyst with One Coordination Site for Dinitrogen Reduction to Ammonia. *Chem. Eur. J.* **2020**, *26*, 14807–14812.
9. Arashiba K.; Miyake, Y.; Nishibayashi, Y. A Molybdenum Complex bearing PCP-Type Pincer Ligands Leads to the Catalytic Reduction of Dinitrogen into Ammonia. *Nat. Chem.* **2011**, *3*, 120–125.

10. Tanaka, H.; Arashiba, K.; Kuriyama, S.; Sasada, A.; Nakajima, K.; Yoshizawa, K.; Nishibayashi, Y. Unique Behaviour of Dinitrogen-Bridged Dimolybdenum Complexes Bearing Pincer Ligand Towards Catalytic Formation of Ammonia. *Nat. Commun.* **2014**, *5*, 3737.
11. Tanaka, H.; Nishibayashi, Y.; Yoshizawa, K. Interplay between Theory and Experiment for Ammonia Synthesis Catalyzed by Transition Metal Complexes. *Acc. Chem. Res.* **2016**, *49*, 987–995.
12. Kuriyama, S.; Arashiba, K.; Nakajima, K.; Tanaka, H.; Kamaru, N.; Yoshizawa, K.; Nishibayashi, Y. Catalytic Formation of Ammonia from Molecular Dinitrogen by Use of Dinitrogen-Bridged Dimolybdenum-Dinitrogen Complexes Bearing PNP-Pincer Ligands: Remarkable Effect of Substituent at PNP-Pincer Ligand. *J. Am. Chem. Soc.* **2014**, *136*, 9719–9731.
13. van der Vulgt, J. I.; Reek, J. N. H. Neutral Tridentate PNP Ligands and Their Hybrid Analogues: Versatile Non-Innocent Scaffolds for Homogeneous Catalysis. *Angew. Chem. Int. Ed.* **2009**, *48*, 8832–8846.
14. Eizawa, A.; Arashiba, K.; Tanaka, H.; Kuriyama, S.; Matsuo, Y.; Nakajima, K.; Yoshizawa, K.; Nishibayashi, Y. Remarkable Catalytic Activity of Dinitrogen-Bridged Dimolybdenum Complexes Bearing NHC-Based PCP-Pincer Ligands toward Nitrogen Fixation. *Nat. Commun.* **2017**, *8*, 14874.
15. Arashiba, K.; Eizawa, A.; Tanaka, H.; Nakajima, K.; Yoshizawa, K.; Nishibayashi, Y. Catalytic Nitrogen Fixation via Direct Cleavage of Nitrogen-Nitrogen Triple Bond of Molecular Dinitrogen under Ambient Reaction Conditions. *Bull. Chem. Soc. Jpn.* **2017**, *90*, 1111–1118.
16. Arashiba, K.; Tanaka, H.; Yoshizawa, K.; Nishibayashi, Y. Cycling between Molybdenum-Dinitrogen and -Nitride Complexes to Support the Reaction Pathway for Catalytic Formation of Ammonia from Dinitrogen. *Chem. Eur. J.* **2020**, *26*, 13383–13389.

17. Ashida, Y.; Arashiba, K.; Nakajima, K.; Nishibayashi, Y. Molybdenum-Catalyzed Ammonia Production with Samarium Diiodide and Alcohols or Water. *Nature* **2019**, *568*, 536–540.
18. Ashida, Y.; Mizushima, T.; Arashiba, K.; Egi, A. Tanaka, H.; Yoshizawa, K.; Nishibayashi, Y. Catalytic Ammonia Production from dinitrogen with Molybdenum Complexes Bearing PCP-Type Pincer Ligands. *ChemRxiv* **2022** doi: 10.26434/chemrxiv-2022-jp6hz.
19. Egi, A.; Tanaka, H.; Konomi, A.; Nishibayashi, Y.; Yoshizawa, K. Nitrogen Fixation Catalyzed by Dinitrogen-Bridged Dimolybdenum Complexes Bearing PCP- and PNP-Type Pincer Ligands: A Shortcut Pathway Deduced from Free Energy Profile. *Eur. J. Inorg. Chem.* **2020**, *2020*, 1490–1498.
20. Ashida, Y.; Arashiba, K.; Tanaka, H.; Egi, A.; Nakajima, K.; Yoshizawa, K.; Nishibayashi, Y. Molybdenum-Catalyze Ammonia Formation Using Simple Monodentate and Bidentate Phosphines as Auxiliary Ligands. *Inorg. Chem.* **2019**, *58*, 8927–8932.
21. Bartulovich, C. O.; Flowers, R. A. Coordination-included O-H bond weakening in Sm(II)-water complexes. *Dalton Trans.* **2019**, *48*, 16142–16147.
22. Hansch, C.; Leo, A.; Taft, W. A Survey of Hammett Substituent Constants and Resonance and Field Parameters. *Chem. Rev.* **1991**, *91*, 165–195.
23. Gaussian 09, Revision E.01, Frisch, M. J.; Trucks, G. W.; Schlegel, H. B.; Scuseria, G. E.; Robb, M. A.; Cheeseman, J. R.; Scalmani, G.; Barone, V.; Mennucci, B.; Petersson, G. A.; Nakatsuji, H.; Caricato, M.; Li, X.; Hratchian, H. P.; Izmaylov, A. F.; Bloino, J.; Zheng, G.; Sonnenberg, J. L.; Hada, M.; Ehara, M.; Toyota, K.; Fukuda, R.; Hasegawa, J.; Ishida, M.; Nakajima, T.; Honda, Y.; Kitao, O.; Nakai, H.; Vreven, T.; Montgomery, J. A., Jr.; Peralta, J. E.; Ogliaro, F.; Bearpark, M.; Heyd, J. J.; Brothers, E.; Kudin, K. N.; Staroverov, V. N.; Keith, T.; Kobayashi, R.; Normand, J.; Raghavachari, K.; Rendell, A.; Burant, J. C.; Iyengar, S. S.; Tomasi, J.; Cossi, M.; Rega, N.; Millam, J. M.; Klene, M.; Knox, J. E.; Cross, J. B.; Bakken, V.; Adamo, C.; Jaramillo, J.; Gomperts, R.; Stratmann, R. E.; Yazyev, O.; Austin, A. J.; Cammi, R.; Pomelli, C.; Ochterski, J. W.; Martin, R. L.; Morokuma,

- K.; Zakrzewski, V. G.; Voth, G. A.; Salvador, P.; Dannenberg, J. J.; Dapprich, S.; Daniels, A. D.; Farkas, O.; Foresman, J. B.; Ortiz, J. V.; Cioslowski, J.; Fox, D. J. Gaussian, Inc., Wallingford CT, 2013.
24. Becke, A. D. Density-functional exchange-energy approximation with correct asymptotic behavior. *Phys. Rev. A* **1988**, 38, 3098–3100.
 25. Becke, A. D. Density-functional thermochemistry. III. The role of exact exchange. *J. Chem. Phys.* **1993**, 98, 5648–5652.
 26. Lee, C.; Yang, W.; Parr, R. G. Development of the Colle-Salvetti correlation-energy formula into a functional of the electron density. *Phys. Rev. B* **1988**, 37, 785–789.
 27. Vosko, S. H.; Wilk, L.; Nusair, M. J. Accurate spin-dependent electron liquid correlation energies for local spin density calculations: a critical analysis. *Can. J. Phys.* **1980**, 58, 1200–1211.
 28. Grimme, S.; Antony, J.; Ehrlich, S.; Krieg, H. A consistent and accurate ab initio parametrization of density functional dispersion correction (DFT-D) for the 94 elements H-Pu. *J. Phys. Chem.* **2010**, 132, 154104.
 29. Dolg, M.; Wedig, U.; Stoll, H.; Preuß, H. Energy-adjusted ab initio pseudopotentials for the first row transition elements. *J. Chem. Phys.* **1987**, 86, 866–872.
 30. Andrae, D.; Häußermann, U.; Dolg, M.; Stoll, H.; Preuß, H. Energy-adjusted ab initio pseudopotentials for the second and third row transition elements. *Theor. Chim. Acta.* **1990**, 77, 123–141.
 31. Ditchfield, R.; Hehre, W. J.; Pople, J. A. Self-consistent molecular-orbital methods. IX. An extended Gaussian-type basis for molecular-orbital studies of organic molecules. *J. Chem. Phys.* **1971**, 54, 724–728.
 32. Hehre, W. J.; Ditchfield, R.; Pople, J. A. Self-consistent molecular orbital methods. XII. Further extensions of Gaussian-type basis sets for use in molecular orbital studies of organic molecules. *J. Chem. Phys.* **1972**, 56, 2257–2261.

33. Hariharan, P. C.; Pople, J. A. The influence of polarization functions on molecular orbital hydrogenation energies. *Theor. Chem. Acc.* **1973**, *28*, 213–222.
34. Franci, M. M.; Pietro, W. J.; Hehre, W. J.; Binkley, J. S.; Gordon, M. S.; DeFrees, D. J.; Pople, J. A. Self-consistent molecular orbital methods. XXIII. A polarization-type basis set for second-row elements. *J. Chem. Phys.* **1982**, *77*, 3654–3665.
35. Krishnan, R.; Binkley, J. S.; Seeger, R.; Pople, J. A. Self-consistent molecular orbital methods. XX. A basis set for correlated wave functions. *J. Chem. Phys.* **1980**, *72*, 650–654.
36. McLean, A. D.; Chandler, G. S. Contracted Gaussian basis sets for molecular calculations. I. Second row atoms, $Z=11-18$. *J. Chem. Phys.* **1980**, *72*, 5639–5648.
37. Clark, T.; Chandrasekhar, J.; Spitznagel, G. W.; Schleyer, P. v. R. Efficient diffuse function-augmented basis sets for anion calculations. III. The 3-21+G basis set for first-row elements, Li–F. *J. Comput. Chem.* **1983**, *4*, 294–301.
38. Tomasi, J.; Mannucci, B.; Cammi, R. Quantum Mechanical Continuum Solvation Models. *Chem. Rev.* **2005**, *105*, 2999–3094.
39. Wang, D.; Loose, F.; Chirik, P. J.; Knowles, R. R. N-H Bond Formation in a Manganese(V) Nitride Yields Ammonia by Light-Driven Proton-Coupled Electron Transfer. *J. Am. Chem. Soc.* **2019**, *141*, 4795–4799.
40. Loose, F.; Wang, D.; Tian, L.; Scholes, G. D.; Knowles, R. R.; Chirik, P. J. Evaluation of Excited State Bond Weakening for Ammonia Synthesis from a Manganese Nitride: Stepwise Proton Coupled Electron Transfer is Preferred over Hydrogen Atom Transfer. *Chem. Commun.* **2019**, *55*, 5595–5598.
41. Park, Y.; Kim, S.; Tian, L.; Zhong, H.; Scholes, G. D.; Chirik, P. J. Visible Light Enables Catalytic Chemical Bonds with Molecular Hydrogen. *Nat. Chem.* **2021**, *13*, 969–976.
42. Jacobsen, H.; Correa, A.; Costabile, C.; Cavallo, L. π -Acidity and π -Basicity of N-Heterocyclic Carbene Ligands. A Computational Assessment. *J. Organomet. Chem.* **2006**, *691*, 4350–4358.

43. Jacobsen, H.; Correa, A.; Poater, A.; Costabile, C.; Cavallo, L. Understanding the M-(NHC) (NHC = N-Heterocyclic Carbene) Bond. *Coord. Chem. Rev.* **2009**, *253*, 687–703.
44. Tulloch, A. A. D.; Danopoulos, A. A.; Kleinhenz, S.; Light, M. E.; Hursthouse, M. B.; Eastham, G. Structural Diversity in Pyridine-*N*-Functionalized Carbene Copper(I) Complexes. *Organometallics* **2001**, *20*, 2027–2031.
45. Vummaleti, S. V. C.; Nelson, D. J.; Poater, A.; Gómez-Suárez, A.; Cordes, D. B.; Slawin, A. M. Z.; Nolan, S. P.; Cavallo, L. What Can NMR Spectroscopy of Selenoureas and Phosphinidenes Teach Us about the σ -Accepting Abilities of *N*-Heterocyclic Carbenes? *Chem. Sci.* **2015**, *6*, 1895–1904.

Supporting Information

Table S4-1. ^{77}Se -NMR magnetic shielding constants of substituted PCP-Se adduct for $\Delta\delta_{\text{calc}}$ value

substituent R	5-substituted model ($\text{R}^1 = \text{R}, \text{R}^2 = \text{H}$)		5,6-substituted model ($\text{R}^1 = \text{R}^2 = \text{R}$)	
	entry	^{77}Se -NMR magnetic shielding (ppm)	entry	^{77}Se -NMR magnetic shielding (ppm)
-H	1	1528.855	-	-
-OH	2	1534.674	22	1551.762
-OCH ₃	3	1536.957	23	1567.894
-CH ₃	4	1536.717	24	1556.708
-Ph	5	1521.281	25	1524.460
-F	6	1503.714	26	1487.228
-Br	7	1493.893	27	1479.243
-Cl	8	1496.216	28	1477.595
-OCF ₃	9	1499.486	29	1453.209
-CCl ₃	10	1467.957	30	141.608
-NC	11	1464.790	31	1413.15
-SCF ₃	12	1476.357	32	1447.800
-CF ₃	13	1480.693	33	1441.881
-CN	14	1445.161	34	1378.957
-SF ₅	15	1456.352	35	1387.873
-SiF ₃	16	1480.022	36	1443.371
-SO ₂ CH ₃	17	1465.366	37	1426.953
-PF ₄	18	1447.182	38	1408.470
-SO ₂ CF ₃	19	1435.461	39	1371.017
-SO ₂ F	20	1423.022	40	1357.137
-SO ₂ Cl	21	1413.161	41	1350.838

Chapter 5

General Conclusions

Nitrogen fixation, which converts chemically inert dinitrogen (N_2) to reactive ammonia (NH_3), is an important catalytic process in modern industrial chemistry. In industry, the Haber-Bosch process is energy-intensive, requiring harsh reaction conditions of high temperature and high pressure with synthesis gas (H_2). On the other hand, in nature, NH_3 is catalytically produced by the enzyme nitrogenase under mild conditions of room temperature and atmospheric pressure. Then, the eight-electron reduction of N_2 gas yields two equiv. of NH_3 on FeMo-cofactor, the active site containing transition metals in nitrogenase. By mimicking the catalytic function, it is possible to develop molecular catalysts for synthesizing useful NH_3 from the inert N_2 .

The author performed density functional theory (DFT) calculations for reaction analyses and ligand designs in this thesis. The ligand designs based on theoretical calculations prior to experiments is expected to inspire and accelerate the development of molecular catalysts.

In Chapter 2, the author has analyzed a reaction mechanism for nitrogen fixation catalyzed N_2 -bridged dimolybdenum- N_2 complexes bearing PNP and PCP-type pincer ligands [$\{MoL_3(N_2)_2\}_2(\mu-N_2)$] (L_3 = 2,6-bis((di-*tert*-butylphosphino)methyl)pyridine (PNP), 1,3-bis((di-*tert*-butylphosphino)methyl)benzimidazole-2-ylidene (PCP)) using DFT calculations. The author proposed a catalytic cycle that maintains an $Mo-N\equiv N-Mo$ moiety for converting a terminal N_2 ligand to NH_3 . The DFT calculations described the entire reaction pathway to proceed under mild reaction conditions. The electronic states of the $Mo-N\equiv N-Mo$ moiety was important for protonation of the terminal N_2 ligand, which is considered the most difficult reaction step in the catalytic cycle. The DFT calculations revealed that a formal charge imbalance between metal centers, such as $Mo^I-N\equiv N-Mo^0$ rather than $Mo^0-N\equiv N-Mo^0$, makes a stronger synergetic effect.

The N_2 -bridged dimolybdenum- N_2 complexes with $Mo^I-N\equiv N-Mo^0$ or Mo^0-

$\text{N}\equiv\text{N}-\text{Mo}^0$ moieties in Chapter 2 reductively activate a terminal N_2 ligand and undergo the catalytic cycle following the classical Yandulov-Schrock cycle. On the other hand, an N_2 -bridged dimolybdenum- N_2 complex with a more oxidative $\text{Mo}^{\text{I}}-\text{N}\equiv\text{N}-\text{Mo}^{\text{I}}$ moiety, which should be yielded by two-electron reduction of an $\text{Mo}(\text{III})$ -trihalide complex $[\text{Mo}^{\text{III}}(\text{PNP})\text{I}_3]$ or $[\text{Mo}^{\text{III}}(\text{PCP})\text{Cl}_3]$, promotes an $\text{N}-\text{N}$ bond cleavage of the bridging N_2 ligand, resulting in a shortcut of the Yandulov-Schrock cycle. Thus, each proposed catalytic cycle is quite different: the former converts the terminal N_2 ligand to NH_3 , whereas the latter converts the bridging N_2 ligand to NH_3 . In Chapter 3, this difference in the catalytic cycle was explained in terms of the electronic structure of the $\text{Mo}-\text{N}\equiv\text{N}-\text{Mo}$ moiety of the N_2 -bridged dimolybdenum complex. The more oxidative $\text{Mo}^{\text{I}}-\text{N}\equiv\text{N}-\text{Mo}^{\text{I}}$ moiety produces two equivalents of stable $\text{Mo}(\text{IV})$ -nitride complexes via the $\text{N}-\text{N}$ bond cleavage. On the other hand, the extra electrons in the $\text{Mo}^0-\text{N}\equiv\text{N}-\text{Mo}^0$ moiety occupy the π -antibonding $\text{Mo}\equiv\text{N}$ bond of the $\text{Mo}(\text{III})$ -nitride complex after the cleavage, thus prohibiting the cleavage reaction. It is theoretically explainable that the number of electrons in the $\text{Mo}-\text{N}\equiv\text{N}-\text{Mo}$ moiety controls whether the $\text{N}-\text{N}$ bond cleavage reaction of the bridging nitrogen proceeds.

In Chapter 4, the author designed PCP ligands based on DFT calculations. The excellent catalytic activity of the nitrogen fixation has been exhibited using an $\text{Mo}(\text{III})$ -trihalide complex bearing the PCP ligand $[\text{Mo}^{\text{III}}(\text{PCP})\text{Cl}_3]$ as a molecular catalyst in the presence of water as a proton source and SmI_2 as an electron source. Focusing on the PCET process to $\text{Mo}(\text{IV})$ -nitride complex $[\text{Mo}^{\text{IV}}(\text{PCP})(\text{I})(\equiv\text{N})]$ in the catalytic cycle, the author designed PCP ligands to control the electronic state of $\text{Mo}-\text{PCP}$ complexes by introducing substituents and fused benzene rings into the PCP ligand. The author estimated the catalytic activity from the strength of the formed $\text{N}-\text{H}$ bond of the corresponding $\text{Mo}(\text{III})$ -imide $[\text{Mo}^{\text{III}}(\text{PCP})(\text{I})(=\text{NH})]$. As a result, introducing electron-withdrawing substituents and fused benzene rings into the PCP ligand leads to the enhance in the strength of the $\text{N}-\text{H}$ bond, because of the enhancement of the p-accepting ability of the PCP ligand. Thus, the author succeeded in proposing a direction for ligand design for nitrogen fixation catalyzed by the molybdenum complex.

In this thesis, the author performed DFT calculations to develop molecular catalysts containing molybdenum atoms for nitrogen fixation. The molecular catalysts are

unique in that their catalytic cycle includes dimolybdenum intermediates with an Mo–N≡N–Mo moiety. The role of the Mo–N≡N–Mo moiety in the catalytic reaction is theoretically explained in this thesis. Focusing on the most important reaction step in the catalytic cycle, the author modified the PCP ligand by theoretical calculations. During the ligand design, the author proposed strategies and useful indicators obtained by DFT calculations. Finally, this thesis is unique in the author brought findings from the reaction analysis using the DFT calculations to the PCP ligand design.

In this study, while the author performed ligand design prior to experimental synthesis of the ligand using theoretical calculations on the assumption that the electronic structure of metal complexes can be controlled by containing ligands, the author strongly believes that the collaboration of the theoretical calculations and machine learning methods will accelerate the design of promising ligands for nitrogen fixation.

Acknowledgments

This thesis provides a summary of studies conducted by the author as a member of Yoshizawa laboratory at Department of Chemistry and Biochemistry, Kyushu University, from 2017 to 2022. The author's work is partially supported by project JPNP21020, commissioned by the New Energy and Industrial Technology Development Organization (NEDO).

The author could not have written the thesis without the support of many teachers, coworkers, and friends. The author was very grateful to them.

At first, the author would like to express his cordial gratitude to Professor Kazunari Yoshizawa and Associate Professor Yoshihito Shiota for leading me to theoretical chemistry. He also would like to express his sincere appreciation to Associate Professor Staykov Aleksandar and Yuta Tsuji, and Assistant Professor Yosuke Sumiya for their helpful advice and suggestions.

The author would like to acknowledge Program for Department of Chemistry and Biochemistry, Kyushu University. He thanks Dr. Yuta Hori, Dr. Tsukasa Abe, Dr. Masataka Yoshida, Dr. Amit Shrestha, Ms. Yoko Nishi, Mrs. Mayuko Miyanishi, and Mrs. Asuka Konomi for their generous support. The author wishes to thank to all other member of the Yoshizawa laboratory for their direct and indirect support.

The author would like to appreciate Professor Hiromasa Tanaka at School of Liberal Arts and Sciences, Daido University, for discussion with the author on theoretical study of molecular catalyst for nitrogen fixation over a prolonged period.

The author would like to appreciate Professor Yoshiaki Nishibayashi at Department Applied Chemistry, School of Engineering, The University of Tokyo, and his

coworkers for the collaboration in experiments.

The author would like to express his gratitude for the scholarship from Japan Chemical Industry Association for Chemistry Personnel Cultivation Program.

Finally, I would like to dedicate this thesis to my father, Shuji Egi, my mother, Setsuko Egi, and my sisters, Mizuki Egi and Yue Egi.

Fukuoka, December 2022

Akihito Egi

List of Publications

Chapter 2

“Nitrogen Fixation Catalyzed by Dinitrogen-Bridged Dimolybdenum Complexes Bearing PCP- and PNP-Type Pincer Ligands: A Shortcut Pathway Deduced from Free Energy Profiles.”

Akihito Egi, Hiromasa Tanaka, Asuka Konomi, Yoshiaki Nishibayashi, and Kazunari Yoshizawa.

European Journal of Inorganic Chemistry, 1490–1498, (2020).

Chapter 3

“Theoretical Views on Catalytic Reaction Pathways for Nitrogen Fixation by Dinitrogen-Bridging Dimolybdenum Complexes.”

Akihito Egi, Hiromasa Tanaka, and Kazunari Yoshizawa.

Journal of Synthetic Organic Chemistry, Japan, **79**, 1480–1489, (2021).

Chapter 4

“Computational Design and Evaluation of Substituted PCP-Type Pincer Ligands for Mo-Catalyzed Nitrogen Fixation.”

Akihito Egi, Hiromasa Tanaka, Yoshiaki Nishibayashi, and Kazunari Yoshizawa.

To be submitted.

The following papers are not included in this thesis

“Catalytic Reactivity of Molybdenum-Trihalide Complexes Bearing PCP-Type Pincer Ligands.”

Aya Eizawa, Kazuya Arashiba, **Akihito Egi**, Hiromasa Tanaka, Kazunari Nakajima, Kazunari Yoshizawa, and Yoshiaki Nishibayashi.

Chemistry - An Asian Journal, **14**, 2091-2096, (2019).

“Molybdenum-Catalyzed Ammonia Formation Using Simple Monodentate and Bidentate Phosphine as Auxiliary Ligands.”

Yuya Ashida, Kazuya Arashiba, Hiromasa Tanaka, **Akihito Egi**, Kazunari Nakajima, Kazunari Yoshizawa, and Yoshiaki Nishibayashi.

Inorganic Chemistry, **58**, 8927-8932, (2019).

“Ammonia Formation Catalyzed by a Dinitrogen-Bridged Dirhenium Complex Bearing PNP-Pincer Ligands under Mild Reaction Conditions.”

Fanqiang Meng, Shogo Kuriyama, Hiromasa Tanaka, **Akihito Egi**, Kazunari Yoshizawa, and Yoshiaki Nishibayashi.

Angewandte Chemie International Edition, **60**, 13906-13912, (2021).

“Catalytic Reduction of Dinitrogen into Ammonia and Hydrazine by Using Chromium Complexes Bearing PCP-Type Pincer Ligands.”

Yuya Ashida, **Akihito Egi**, Kazuya Arashiba, Hiromasa Tanaka, Taichi Mitsumoto, Shogo Kuriyama, Kazunari Yoshizawa, and Yoshiaki Nishibayashi.

Chemistry - A European Journal, **28**, e202200557, (2022).

“Direct Synthesis of Cyanate Anion from Dinitrogen Mediated by Molybdenum Complexes Bearing Pincer-Type Ligand.”

Takayuki Itabashi, Kazuya Arashiba, **Akihito Egi**, Hiromasa Tanaka, Keita Sugiyama, Shun Sugimoto, Shogo Kuriyama, Kazunari Yoshizawa, and Yoshiaki Nishibayashi.

Nature Communications, **13**, 6161 (2022).

“Preparation and Reactivity of Rhenium-Nitride Complexes Bearing PNP-Type Pincer Ligands toward Nitrogen Fixation.”

Fanqiang Meng, Shogo Kuriyama, **Akihito Egi**, Hiromasa Tanaka, Kazunari Yoshizawa, and Yoshiaki Nishibayashi.

Organometallics, doi: 10.1021/acs.organomet.2c00312 (2022).

“Catalytic Production of Ammonia from Dinitrogen Employing Molybdenum Complexes bearing *N*-Heterocyclic Carbene-Based PCP-Type Pincer Ligand.”

Yuya Ashida, Takuro Mizushima, Kazuya Arashiba, **Akihito Egi**, Hiromasa Tanaka, Kazunari Yoshizawa, and Yoshiaki Nishibayashi.

Nature Synthesis, *just accepted* (2023).